CELL MEDIATED THERAPEUTICS FOR CANCER TREATMENT: TUMOR HOMING CELLS AS THERAPEUTIC DELIVERY VEHICLES

by

SIVASAI BALIVADA

M.S., Kansas State University, 2009

AN ABSTRACT OF A DISSERTATION

submitted in partial fulfillment of the requirements for the degree

DOCTOR OF PHILOSOPHY

Department of Anatomy & Physiology
College of Veterinary Medicine

KANSAS STATE UNIVERSITY
Manhattan, Kansas

2013

Abstract

Many cell types were known to have migratory properties towards tumors and different research groups have shown reliable results regarding cells as delivery vehicles of therapeutics for targeted cancer treatment. Present report discusses proof of concept for 1. Cell mediated delivery of Magnetic nanoparticles (MNPs) and targeted Magnetic hyperthermia (MHT) as a cancer treatment by using *in vivo* mouse cancer models, 2. Cells surface engineering with chimeric proteins for targeted cancer treatment by using *in vitro* models. 1. **Tumor homing cells can carry MNPs specifically to the tumor site and tumor burden will decrease after alternating magnetic field (AMF) exposure.** To test this hypothesis, first we loaded Fe/Fe_3O_4 bi-magnetic NPs into neural progenitor cells (NPCs), which were previously shown to migrate towards melanoma tumors. We observed that NPCs loaded with MNPs travel to subcutaneous melanoma tumors. After alternating magnetic field (AMF) exposure, the targeted delivery of MNPs by the NPCs resulted in a mild decrease in tumor size (Chapter-2). Monocytes/macrophages (Mo/Ma) are known to infiltrate tumor sites, and also have phagocytic activity which can increase their uptake of MNPs. To test Mo/Ma-mediated MHT we transplanted Mo/Ma loaded with MNPs into a mouse model of pancreatic peritoneal carcinomatosis. We observed that MNP-loaded Mo/Ma infiltrated pancreatic tumors and, after AMF treatment, significantly prolonged the lives of mice bearing disseminated intraperitoneal pancreatic tumors (Chapter-3). 2. **Targeted cancer treatment could be achieved by engineering tumor homing cell surfaces with tumor proteases cleavable, cancer cell specific recombinant therapeutic proteins.** To test this, Urokinase and Calpain (tumor specific proteases) cleavable; prostate cancer cell (CaP) specific (CaP1 targeting peptide); apoptosis inducible (Caspase3 V266ED3)- rCasp3V266ED3 chimeric protein was designed *in silico*. Hypothesized membrane anchored chimeric protein (rCasp3V266ED3, rMcherry red) plasmids were constructed. Membrane anchoring and activity of designed proteins were analyzed in RAW264.7 Mo/Ma and HEK293 cells *in vitro*. Further, Urokinase (uPA) mediated cleavage and release of rCasp3V266ED3 from engineered cells was tested (Chapter-4). Animal models for cancer therapy are invaluable for preclinical testing of potential cancer treatments. Final chapter of present report shows evidence for **immune-deficient line of pigs as a model for human cancers** (Chapter-5)

CELL MEDIATED THERAPEUTICS FOR CANCER TREATMENT: TUMOR HOMING CELLS AS THERAPEUTIC DELIVERY VEHICLES

by

SIVASAI BALIVADA

M.S., Kansas State University, 2009

A DISSERTATION

submitted in partial fulfillment of the requirements for the degree

DOCTOR OF PHILOSOPHY

Department of Anatomy & Physiology
College of Veterinary Medicine

KANSAS STATE UNIVERSITY
Manhattan, Kansas

2013

Approved by:

Major Professor
Deryl L Troyer

Copyright

Abstract

Many cell types were known to have migratory properties towards tumors and different research groups have shown reliable results regarding cells as delivery vehicles of therapeutics for targeted cancer treatment. Present report discusses proof of concept for 1. Cell mediated delivery of Magnetic nanoparticles (MNPs) and targeted Magnetic hyperthermia (MHT) as a cancer treatment by using *in vivo* mouse cancer models, 2. Cells surface engineering with chimeric proteins for targeted cancer treatment by using *in vitro* models. 1. **Tumor homing cells can carry MNPs specifically to the tumor site and tumor burden will decrease after alternating magnetic field (AMF) exposure.** To test this hypothesis, first we loaded Fe/Fe_3O_4 bi-magnetic NPs into neural progenitor cells (NPCs), which were previously shown to migrate towards melanoma tumors. We observed that NPCs loaded with MNPs travel to subcutaneous melanoma tumors. After alternating magnetic field (AMF) exposure, the targeted delivery of MNPs by the NPCs resulted in a mild decrease in tumor size (Chapter-2). Monocytes/macrophages (Mo/Ma) are known to infiltrate tumor sites, and also have phagocytic activity which can increase their uptake of MNPs. To test Mo/Ma-mediated MHT we transplanted Mo/Ma loaded with MNPs into a mouse model of pancreatic peritoneal carcinomatosis. We observed that MNP-loaded Mo/Ma infiltrated pancreatic tumors and, after AMF treatment, significantly prolonged the lives of mice bearing disseminated intraperitoneal pancreatic tumors (Chapter-3). 2. **Targeted cancer treatment could be achieved by engineering tumor homing cell surfaces with tumor proteases cleavable, cancer cell specific recombinant therapeutic proteins.** To test this, Urokinase and Calpain (tumor specific proteases) cleavable; prostate cancer cell (CaP) specific (CaP1 targeting peptide); apoptosis inducible (Caspase3 V266ED3)- rCasp3V266ED3 chimeric protein was designed *in silico*. Hypothesized membrane anchored chimeric protein (rCasp3V266ED3, rMcherry red) plasmids were constructed. Membrane anchoring and activity of designed proteins were analyzed in RAW264.7 Mo/Ma and HEK293 cells *in vitro*. Further, Urokinase (uPA) mediated cleavage and release of rCasp3V266ED3 from engineered cells was tested (Chapter-4). Animal models for cancer therapy are invaluable for preclinical testing of potential cancer treatments. Final chapter of present report shows evidence for **immune-deficient line of pigs as a model for human cancers** (Chapter-5).

Table of Contents

List of Figures

List of Tables

Acknowledgements

I would like to acknowledge my major professor, Dr. Deryl L.Troyer, for giving me the opportunity to work in his lab. I would like to thank Dr. Stefan Bossmann, Dr. Viktor Chikan, Dr.Masaaki Tamura and Dr.Duane Davis for devoting their time as my committee members. I would like to thank my lab members Marla Pyle, Dr.Rajashekar Rachakatla, Dr. Gwi-Moon Seo, Dr.Matthew T.Basel, Dr.Tej shrestha, Dr.Mausam Kalita, Dr.Hamad Alsheitaiwi for their help in my research work. I would also like to thank members of Dr. Bossmann's, Dr.Chikan's and Dr.Tamura's labs for their help in my projects.

Chapter 1 - Introduction & Literature review

Introduction

Cancer is one of the leading causes of deaths in worldwide [1]. Compared with other diseases and pathological conditions biology of cancer disease is complex [2, 3]. Although many research groups are working to understand the biology of cancer, the information we know about the disease is not complete [2]. In starting, cancer cells were known as normal cells that lost their control over cell dividing ability and form disorganized tissues called tumors [4]. These cells acquire ability to migrate to other parts of the body and can form metastatic tumors eventually lead to problems in the physiology of whole animal [4]. But with extensive research with human and mouse cancer models, the number of biological characteristics identified with cancer cells and their malignant tumors were increased and still increasing [4]. As Weinberg et al., models every few years about cancer disease with his "Hallmarks of cancer" title, the number of characteristics that were identified with cancer cells are as follows- sustained proliferative signaling, evading growth suppressors, resisted to cell death , enabling replicative immortality, inducing angiogenesis, activating invasion and metastasis [2, 4]. Cancer cells acquire these properties by genomic instability causing mutations in important genes [2, 4]. Apart from these genetic mutations cancer cells cause recruitment of normal cells that contribute to malignant tumor with favorable microenvironment formation [2, 4, 5]. With present understanding, cancer tissue was defined as more of disorganized tissue system that have cancer cells as parenchymal cells with different kinds of supporting cells, immune cells and stem/progenitor cells [5]. Again above mentioned properties acquisition and expression is different between different types of cancers [2].

Urgency of treating cancer patients led to the discovery of treatments such as surgery, chemotherapy and radiation therapy in 19^{th} and 20^{th} century and they are still the predominant procedures used in clinics [6, 7] . These treatments were rationalized based on the primary observation of unstoppable dividing ability of cancer cells and abnormal tumor growth [7]. Clinicians were using these treatments with or without adjuvant therapies based on type of cancer and its stage at the time of diagnosis [7]. Although these treatments/treatment combinations giving remission from the disease for some period of time, relapse of the disease and the side effects caused from these treatments making them as not an ideal option for cancer

treatment [7]. Lack of treatments that can target specifically to cancer cells or malignant tumors, made these treatments still as dominant ones in cancer therapy [7] .

Comparatively increased understanding of cancer cells and malignant tumor characteristics led to discovery of chemicals and proteins that have cancer cell specificity [7]. For example identification of Philadelphia chromosome mutation and Gleevec (tyrosine kinase inhibitor), Her2 receptor over expressing tumors and Trastuzumab (antibody against Her2 receptor -Herceptin) [7]. Identification of mutated genes and their proteins dis-functionality in different types of cancers helped in designing therapeutics that can interact with these abnormal proteins to achieve cancer cell specific treatments [2]. These targeted treatments worked only for few types of malignant tumors, because of the differences in number of mutated genes and variability in the genes that were mutated in different types of cancer cells [2, 3]. Treatments with these higher rationale chemicals or proteins helped at some level in cancer therapy, but still they didn't solve all the problems and lots of these treatments have significant side effects. Problems associated with small molecular drugs and protein therapeutics are like pharmacodynamics (PD) & pharmacokinetics (PK) of injected therapeutics and level of targeting towards malignant tumors & cancer cells [8]. Although, Nanoparticle based therapeutics were proposed to solve above mentioned problems still the amount of targeting that can be achieved with nanoparticles may not be enough and PD,PK associated problems will still be there [8].

Tumor stroma contains supporting cells, stromal cells, immune cells that helps cancer cells in complete formation of cancer tissue [2, 5]. During malignant tumor formation these supporting cells migrate to that place and help cancer cells by directly assisting their growth or constructing environment that helps in tumor tissue formation [2, 5]. Cancer cells with stromal cells secrete cytokines that helps in migration of different cells into tumor environment [5]. By using these cells as delivery vehicles problems associated with available therapies can be solved. Migrating ability of cells towards cancer tissue increases the targeting efficiency of therapeutics towards tumors, which is the main problem in available cancer therapeutics. Cell mediated therapeutics my not have PD, PK related issues because of their directed migration towards tumor tissues[8]. Several research groups have been used this hypothesis and tested different cell mediated delivery of therapeutics in pre-clinical mouse cancer models [9, 10]. Based on this background information hypothesis were proposed and tested in this present dissertation. In

chapter-2& 3 tumor homing cells mediated targeted Magnetic hyperthermia system was tested and in Chapter-4 tumor homing cells mediated chimeric protein therapeutic system was tested.

Literature Review

Cell mediated delivery of therapeutics

Multiple cell types were known to contribute in important ways to the formation of tumors and its microenvironment [2, 5]. Cancer associated fibroblasts, Angiogenic vascular cells and infiltrating immune cells are the three major cell types that were identified in tumor stroma [2]. During tumorigenesis cytokines released from cancer cells and its resident stromal cell types involve in recruitment of these tumor stromal cells [2, 5]. These recruited tumor stromal cells can variably contribute to, or in some cases oppose, acquisition of identified hallmarks of cancer [5]. Neonatal or adult tissue derived Mesenchymal stem cells (MSCs) [11], Neural stem cells (NSCs) [12], Macrophages [13] are the cell types that were used extensively in pre-clinical testing for cell mediated therapeutic delivery hypothesis till date. Apart from these cells there were few reports on MDSCs (myeloid derived suppressor cells) [14] and endothelial cells [15] as delivery vehicles. Signaling molecules that were known to cause recruitment of tumor stromal cells involve in tumor tropic ability of above mentioned cell types [5, 11, 12]. Although a definitive mechanism for these cells homing (recruitment, rolling, arrest, transmigration) into tumor microenvironment yet to be fully elucidated, studies have shown that cytokines like vascular endothelial growth factor (VEGF), CC chemokine ligand, CCL5/RANTES, angiopoietin 2 released from tumors into circulation guide the migration of receptor positive cells [5, 11, 12]. Therapeutic systems that were tested till date by using tumor homing cells as delivery vehicles are as follows; Antitumor cytokines, Gene directed prodrug therapy systems, Antibodies, Oncolytic viruses, Nanoparticles, Drugs, Radiation therapy and Photodynamic therapy

Antitumor cytokines

Antitumor cytokines are signaling molecules comprised of proteins, peptides, glycoproteins that are produced by immune cells that can cause antitumor (immune) response [16]. Cytokines that were known to have antitumor properties that were tested in pre-clinical and clinical trials are- Interleukins (IL-2,3,4,6,7,10,12,13,15,18), Colony stimulating factors (M-CSF, GM-CSF) , Interferons (α, γ) , Tumor necrosis factors (TNF-α), TGF-β, TRAIL,

lymphotactin, FLT3 ligand[16]. Systemic delivery of these antitumor cytokines was thought to be viable cancer treatment, but yielded different side effects [16]. Tumor homing cells could be engineered to secrete these cytokines and targeted delivery could be achieved that can decrease systemic delivery mediated side effects and can potentiate those cytokines antitumor effect. Many research groups tested this hypothesis by engineering tumor homing cells with secreted antitumor cytokines like IFN-β [17-20], IFN-γ [9, 19-21] , IL-12 [20, 22-24] , TRAIL [20, 25-33], IL-18 [20, 34] , CX3CL-1 [35, 36] on different mouse/rat cancer models and showed convincing results. Targeted combination therapies like engineering cells to express two or more cytokines / cytokines and other therapeutics were also reported in literature [18, 28]. Most of studies that were mentioned above used either Mesenchymal stem cells (MSCs) or neural stem cells (NSCs) as delivery vehicles.

Gene directed enzyme/prodrug therapy (GDEPT)

Gene-directed enzyme/prodrug therapy (GDEPT) has been used with varying levels of success to achieve targeted cancer therapy [37, 38]. This strategy uses a vector targeted gene for an enzyme that will convert a relatively inactive prodrug to its active drug counterpart [37, 38]. Two steps are needed for this to happen. First, the gene that can make the enzyme must be targeted to or produced by the tumors and the prodrug then needs to be delivered to the tumor for activation [39]. Enzyme/prodrug systems that were tested in clinical trials are- Herpes simplex virus thymidine kinase / Ganciclovir (HSVtk / GV), Cytosine deaminase / 5-Fluoro cytosine (CD/5FC), Nitroreductase / CB1954, Cytochrome P450 / Cyclophosphamide, Carboxy peptidase G2 / CMDA, Horseradish peroxidase / Indole 3-acetic acid, Carboxyl esterase / ironotecan (CE/CPT-11) [39]. Although, improvements in the gene targeting methods helped in this system as a targeted cancer treatment, still there are problems that need to be clarified [39]. Tumor homing cells could be engineered to secrete these enzymes and can convert the prodrug into drugs specifically in tumor environment. Research groups have tested HSVtk / GV, CE/CPT-11, CD/5FC systems by using cells like MSCs, NSCs and macrophages on mouse cancer models [40-45]. Targeted combination therapies like engineering cells to express antitumor cytokine / prodrug converting enzyme were also reported in literature [46, 47].

Therapeutic Antibodies

Monoclonal antibodies (mAbs) based cancer therapy achieved considerable success in recent years [48]. Pharmacokinetics (PK), size and immunogenicity of designed antibodies are associated problems in antibody therapy of cancer [48]. By engineering tumor homing cells to secrete these antibodies, above mentioned problems could be escaped. As a proof of this concept, engineered neural stem cells expressing Trastuzumab showed significant outcome in HER2 expressing breast cancer models than systemic administration of Trastuzumab [49].

Oncolytic virotherapy

Oncolytic virotherapy is a novel approach in which viruses are genetically modified to selectively replicate in tumor cells [50]. These viruses can distinguish tumors from normal tissues and induce tumor cell specific oncolysis [50]. A number of oncolytic viruses (OVs) showed antitumor activity in pre-clinical and clinical trials in past two decades [51]. But, host antiviral immune response and inefficient distribution OVs were preventing the advancement in oncolytic virotherapy [52]. Cell mediated delivery of these OVs can solve the immune response and distribution related problems. MSCs [52], NSCs [52], MDSCs [14], Macrophages [13] were successfully used as delivery vehicles for OVs in pre-clinical mouse models.

These four therapeutic systems were extensively tested till date as cell mediated therapeutics. Apart from these systems several other groups used cells as delivery vehicles for nanoparticles (gold nanoparticles/targeted photothermal ablation[53], liposomes/drug delivery[54]), radiation therapy (sodium iodide symporter/ ^{131}I) [55] and photodynamic therapy [56]. There are several other studies that used dendritic cells, T-cells, B-cells and other immune cells for immune based cancer therapy (Adoptive cellular therapy)[57].

Magnetic hyperthermia as a cancer treatment

Hyperthermia

Temperature is one of the essential factors that controls cell survival. Changes in temperature can cause structural modifications in cells and higher temperatures were known to be toxic. Hyperthermia (HT) is a therapeutic approach to treat cancer by exposing tumors to lethal temperatures resulting in changing the physiology of cancer cells finally leading to apoptosis or necrosis [58, 59]. Side effects caused by hyperthermia are less compared to other

cancer treatments, because of tumor tissues and cancer cells susceptibility to thermal toxicity [60]. HT has been shown to improve the prognosis of different cancers when used in combination with other therapies [61-69]. In several ways HT treatment can be administered such as hot water treatment, microwave, radiofrequency, ultra sound, and alternating magnetic field (AMF) based Magnetic hyperthermia and each of these treatment has its own limitations[59]. In addition to this, the type of heat administration may vary: it will be either local, regional (at a specific place), or whole body hyperthermia [58, 70].

Heat-induced changes in cancer cells leads to either apoptosis or necrosis in cancer cells [71]. If cells are exposed to 40-43˚C -apoptosis results, while temperatures greater than 45˚C cause necrosis and again it depends on the exposure time [58]. Lipid bilayer and membrane bound ATPases are the least thermally stable components and are most responsible for heat induced tissue necrosis [71]. Increases in temperature will also cause effects such as organelle changes, changes in protein conformation, heat shock protein (HSP) synthesis, and DNA and RNA degradation [71]. Cell death pathways involved in HT include mitochondria-mediated apoptosis, ER-mediated apoptotic pathways, and necrosis [58, 71]. Exposure to heat increases blood flow to the tumors, which improves tissue oxygenation and increases radio sensitivity [72]. In the same way, drug concentration will be less in insufficiently perfused tumors; by increasing the blood flow, HT increases the drug concentration in tumors [58]. Chemotherapy combined with HT has showed improved results in clinical trials [63, 66, 68]. To a certain point, hyperthermia causes cells to overexpress heat shock proteins (HSPs), thus helping cells to recover from the temperature-induced damage by repairing proteins, synthesizing enzymes that prevent protein aggregation, and degrading severely damaged proteins [73]. But above a threshold temperature increase, inhibition of HSP synthesis occurs [74]. HSPs released from necrotic cancer cells will have attached tumor specific antigens, and shown to aid in the innate and adaptive immune response against tumors [75, 76]

Magnetic hyperthermia (MHT)

Magnetic nanoparticles (MNPs) based Magnetic hyperthermia treatment (MHT) became a major temperature-based treatment modality because of the number of advantages compared to other hyperthermia treatments [59]. When MNPs are exposed to alternating magnetic field (AMF) they convert the magnetic energy into thermal energy and increases the temperatures in their surroundings [77-79] Heat generation depends on the frequency, amplitude, and time

exposed to AMF and on Curie temperature, Specific Absorption Rates (SAR), shape, size, dispersity (mono or poly), and type of MNPs [59, 80]. When exposed to AMF, MNPs cause heat generation either by hystersis loss or Neel-Brownian relaxation and it depends on the size of MNPs [81]. If the particles are large (multi-domain particles), they will generate heat by hysteresis loss, while small size particles (single domain particles) generate heat by Neel – Brownian relaxations [81]. In multi-domain particles hysteresis loss (due to the movement of domain walls) contributes to heating, in single domain particles Neel relaxation (random flipping of spin) and Brownian motion (rotation of entire particles) generates heat [81, 82]. The transition between the two mechanisms occurs between 5-12 nm for various materials, but it also varies with frequency [83].

Among MNPs, super paramagnetic nanoparticles have more heat generating capacity (more SARs) [59, 80, 84]. Super paramagnetic Iron oxide MNPs are commonly used for MHT because of their biodegradability, low toxicity, and higher SAR values [59, 85]. Apart from MHT, MNPs have different uses in biomedicine like drug delivery, gene delivery, stem cell tracking, MRI, biosensing, cell isolation, cellular proteomics [59, 86].Several research groups have conducted preclinical studies in animal tumor models by directly injecting MNPs into tumors and observed tumor attenuation [59, 80, 87, 88]. This technique works in case of tumors which are hard to operate and accessible to inject MNPs, but the main problem in cancer patients is metastatic deep disseminated tumors that are smaller in size. In majority of clinical cases, clinicians will not have access to these tumors to inject MNPs directly into them for MHT treatment and sometimes these metastatic tumors are not even identifiable with available diagnostic techniques. Systemic intravenous administration of MNPs followed by AMF exposure showed tumor attenuation or increased survival in mouse models [89, 90], but these articles reported accumulation of MNPs in other healthy tissues which can cause severe side effects.

Chapter 2 - Attenuation of Mouse Melanoma by A/C Magnetic Field after Delivery of Bi-Magnetic Nanoparticles by Neural Progenitor Cells

Raja Shekar Rachakatla[a**], **Sivasai Balivada**[a**], Gwi-Moon Seo[a], Carl B Myers[d], Hongwang Wang[b], Thilani N. Samarakoon[b], Raj Dani[b], Marla Pyle[a], Franklin O. Kroh[c], Brandon Walker[c], Xiaoxuan Leaym[c], Olga B. Koper[c], Viktor Chikan[b], Stefan H. Bossmann[b], Masaaki Tamura[a], Deryl L. Troyer[a]

** Both of these authors contributed equally to this work.

a Department of Anatomy and Physiology, Kansas State University, Manhattan, KS 66506, USA

b Department of Chemistry, , Kansas State University, Manhattan, KS 66506, USA

c NanoScale Corporation, 1310 Research Park Drive, Manhattan, KS 66502, USA

d Department of Diagnostic Pathobiology, Kansas State University, Manhattan, KS 66506

Abstract

Localized magnetic hyperthermia as a treatment modality for cancer has generated renewed interest, particularly if it can be targeted to the tumor site. In this present study, tumor-tropic neural progenitor cells (NPCs) ability to utilize as cell delivery vehicles for achieving preferential accumulation of core/shell iron/iron oxide magnetic nanoparticles (MNPs) within a mouse model of melanoma was examined. Aminosiloxane−porphyrin functionalized MNPs loading efficiency, cellular level toxicity was examined on NPCs and transplanted NPCs loaded with this cargo into mice with melanoma. NPCs were efficiently loaded with core/shell Fe/Fe_3O_4 MNPs with minimal cytotoxicity; the MNPs accumulated as aggregates in the cytosol. The NPCs loaded with MNPs could travel to subcutaneous melanomas, and after A/C (alternating current) magnetic field (AMF) exposure, the targeted delivery of MNPs by the cells resulted in a measurable regression of the tumor volume. Temporary tumor attenuation was observed for a short time (24 h) after the last of three AMF exposures.

Introduction

Hyperthermia has been a cancer therapy method for decades. Tumors have shown increased susceptibility to thermal toxicity versus healthy tissue due to their increased rate of cell cycling, increased hypoxia, poor fluid exchange and increased acidity [70, 91]. Whole body hyperthermia is an easy way to take advantage of this differential toxicity to treat cancer. Unfortunately, 'extreme' whole body hyperthermia (>41.5°C), which elevates core temperatures to the level where direct thermal toxicity is observed, can cause severe side effects, which may limit its usefulness [92-96]. Fever-level whole body hyperthermia (~39-41°C) can mitigate many of these side effects and has potential to be an effective cancer treatment, but this lower heat level is thought, primarily, to stimulate the immune system and the benefits of direct thermal toxicity are reduced [97, 98]. Generating localized 'extreme' hyperthermia at the cancer site could alleviate many of the side effects associated with whole body hyperthermia while still taking advantage of the thermal susceptibility of tumors.

One particularly promising method for generating localized hyperthermia is using magnetic nanoparticles (MNPs) to absorb energy from alternating magnetic fields (AMF) and converting this energy into heat. This method is promising because the body is extremely permeable to AMF, which itself produces no known effects in the body [99, 100]. For magnetic hyperthermia, super paramagnetic iron oxide nanoparticles are usually used for absorbing the magnetic field[79]. In most of the pre-clinical and clinical studies, MNPs were directly injected into the tumors and exposed to AMF to achieve hyperthermic temperatures in tumors [87, 88, 101].

MHT of disseminated or deep tumors is currently complicated because it is difficult to target MNPs to the tumors. To date, most reports of localized magnetic hyperthermia have described the direct tumor injection of milligram amounts of magnetic materials [87, 88, 90]. Many attempts have been made to increase localization of various kinds of nanoparticles, including magnetic nanoparticles for imaging or therapy, to tumors. For example, particles have been tagged with antibodies recognizing tumor-specific epitopes [102, 103] or peptides binding to receptors on tumor cells or neo-vasculature [104, 105]. In some cases, limited success has been realized after antibodies or other ligands have been attached to MNPs [106]. However, further improvements in tumor targeting are needed. Both direct killing effects and sensitization to other treatment modalities with MHT treatment are dependent on distribution of MNPs in

tumors and duration of temperature elevation during AMF exposure [107, 108]. Bi-magnetic particles (10−40 nm) are able to generate substantial heat within a magnetic field of low strength and frequency. The bi- magnetic nanoparticles (MNPs) used in this present study have a strong ferromagnetic iron core, which produces high temperatures with short AMF exposure [78],a magnetic iron oxide shell for MRI [109], an aminosiloxane-anchored oligoethylene glycol stealth coating, and chemically attached porphyrins (TCPP, tetra-4-carboxyphenyl porphyrin) (Figure 2-1A).

Tumor-homing cells have been used as delivery vehicles for targeted gene therapy for preclinical models of cancer [9, 12, 47, 110-116]. In addition to being used to deliver genes, bone marrow stem cells have been loaded with iron oxide nanoparticles and used to target murine lung cancer for MRI [117]. Neural progenitor cells (NPCs) or Neural stem cell (NSCs) are known to have tumor-tropic properties, and many groups have successfully used NPCs as therapeutic delivery vehicles to tumors [10, 12, 118-121].

By considering these rationales we hypothesized that tumor targeted MHT can be achieved by delivering MNPs through NPCs on mouse melanoma tumors. To test this hypothesis, first Aminosiloxane-coated Fe/Fe_3O_4 core/shell bi magnetic nanoparticles (MNPs) toxicity, loading efficiency was analyzed on C17.2 neural progenitor cells. Temperature increase in MNPs loaded NPCs after AMF exposure was demonstrated by using *in vitro* models. Intravenously injected MNPs loaded NPCs homed to subcutaneous B16-F10 melanoma tumors after 4 days of transplantation. Mild melanoma tumor volume decrease was observed after three 10mins AMF exposures on these mice (not statistically significant). Apoptosis assay on AMF treated tumors revealed increased apoptosis positive cells (qualitative observation). Suggesting that tumor homing cells can be used as delivery vehicles for tumor targeted MHT treatment.

Materials and Methods

TCPP-Linked Stealth-Coated Fe/Fe3O4/ASOX Nanoparticles

Aminosiloxane-coated Fe/Fe_3O_4 core/shell nanoparticles (MNPs) were synthesized by NanoScale Corporation (Manhattan, KS). Dopamine stealth coating and TCPP targeting units attachment were performed by Stephen Bossmann's lab. Nanoparticles synthesis and their characteristics were explained in detail in Rachakatla et al., 2010 [122] (MNPs schematic picture was presented in Figure 2-1A).

Tissue Culture of C17.2 Neural Progenitor Cells and B16-F10 Melanoma Cells

B16-F10 melanoma cells were purchased from ATCC (Manassas, VA) and maintained in Dulbecco's modified Eagle medium (DMEM; Invitrogen, Carlsbad, CA) supplemented with 10% fetal bovine serum (FBS; Sigma-Aldrich, St. Louis, MO) and 1% penicillin/streptomycin (Invitrogen) at 37 °C in a humidified atmosphere containing 5% carbon dioxide.
C17.2 neural progenitor cells (NPCs) and firefly luciferase expressing C17.2 neural progenitor cells (NPC-Flucs) were a gift from V Ourednik (Iowa State University). Originally developed in Evan Snyder's lab [123], these cells were maintained in DMEM supplemented with 10% FBS (Sigma-Aldrich), 5% horse serum (Invitrogen), 1% glutamine (Invitrogen), and 1% penicillin/streptomycin (Invitrogen).

Cytotoxicity of MNPs on Neural Progenitor Cells and B16-F10 Cells

Potential cytotoxic effects of MNPs were studied by incubating C17.2 NPCs and B16-F10 melanoma cells in different concentrations of MNPs (as determined by iron content). NPCs and B16-F10 cells were plated at 50,000 cells/cm^2 and incubated overnight with their respective media containing MNPs at concentrations of 5, 10, 15, 20, or 25 μg/mL iron. After incubation, medium was removed and cells were washed twice with DMEM. Cells were lifted *via* trypsinization, and mixed with collected medium and washed DMEM. Live and dead cell numbers were counted *via* hemocytometer with Trypan blue staining. This method allows counting of viable (colorless) and nonviable (blue stained) cells since only the dead cells allow the blue stain into the cell.

Prussian Blue Staining on NPCs

The loading efficiency of MNPs into NPCs was assessed using Perl's Prussian blue stain kit (Polysciences, Inc., Warrington, PA). After overnight incubation in NPC medium containing 25 μg/mL iron in MNPs, NPCs were washed twice with DMEM and PBS and fixed with 4% glutaraldehyde for 10 min. Fixed NPCs were incubated in a solution containing equal amounts of 4% potassium ferrocyanide and 4% HCl for 20 min. After 20 min incubation, NPCs were washed twice with 1× PBS and counterstained with nuclear fast red solution for 5 min. Images were captured using a Zeiss Axiovert 40 CFL microscope (New York) and a Jenoptik ProgRes C3 camera (Jena, Germany).

Loading Strategy of MNPs and Determination of Iron Amounts

The loading efficiency of NPCs with various iron concentrations of MNPs was determined spectrophotometrically using a Ferrozine based iron estimation method [124]. For this method, cells were incubated overnight with NPC medium containing different concentrations of MNPs and then washed twice with DMEM and 1× PBS. Cells in medium without MNPs were used as controls. All NPCs (control cells and cells loaded with various iron concentration of MNPs) were trypsinized, counted, and centrifuged, and total cells were resuspended in 2 mL of distilled water. Cells were then lysed by adding 0.5 mL of 1.2 M HCl and 0.2 mL of 2 M ascorbic acid and incubating at 65−70 °C for 2 h. After 2 h, 0.2 mL of reagent containing 6.5 mM Ferrozine (HACH, Loveland, CO), 13.1 mM neocuproine (Sigma-Aldrich, St. Louis, MO), 2 M ascorbic acid (Alfa Aesar, Ward Hill, MA), and 5 M ammonium acetate (Sigma-Aldrich, St. Louis, MO) was added and incubated for 30 min at room temperature. After 30 min, samples were centrifuged at 1000 rpm for 5 min, and supernatant optical density was measured by a UV−vis spectrophotometer (Shimadzu, Columbia, MD) at 562 nm. A standard curve was prepared using 0, 0.1, 0.2, 0.5, 1, 2, and 5 μg/mL ferrous ammonium sulfate samples. Water with all other reagents was used as a blank. From the standard curve, iron concentration in cell samples was determined. Iron concentration per single cell was estimated by dividing the iron amount in each cell sample by the total number of cells in that sample assuming all the cells were loaded with equal amount of MNPs.

AMF-Induced Temperature Changes In Vitro

To verify the temperature increase by NPCs loaded with MNPs in a simulated matrix environment, NPCs were loaded overnight with MNPs equivalent to 15 μg/mL Fe. After incubation, cells were washed twice with DMEM and twice with 1× PBS to remove free MNPs. Cells were lifted with 0.1% trypsin-EDTA, and 1×10^6 cells were pelleted by centrifugation in 2 mL centrifuge tubes; 1.5 mL of 4% agarose solution was added on top of the cell pellet to make a solid matrix. Agarose centrifuge tubes containing pelleted NPCs without MNPs were used as negative controls and were made as described above. The experiment was conducted in triplicate. Before each tube was exposed to AMF, two optical probes (Neoptix, Quebec, Canada) were inserted into the tube: one at the pellet, and the second one at the middle of the agarose

solid. Tubes were exposed to AMF for 10 min, and the temperature difference over time was measured by the probes.

Evaluation of Selective Engraftment of NPCs and Magnetic Hyperthermia

Female, 6−8 week old, C57BL/6 mice were purchased from Charles River Laboratories (Wilmington, MA). Mice were held for 1 week after arrival to allow them to acclimate. Mice were maintained according to approved IACUC guidelines in the Comparative Medicine Group facility of Kansas State University. All animal experiments were conducted according to these IACUC guidelines. On day 0, 3.5×10^5 B16-F10 melanoma cells were injected subcutaneously into 45 C57BL/6 mice, day-4 after tumor cells injection tumor diameters were measured and mice were stratified into four groups (unbalanced design). On day 5, 1×10^6 NPCs loaded with MNPs at 20 μg/mL iron concentration were injected intravenously to two groups (NPC(Fluc)-MNP, group III and NPC(Fluc)-MNP+AMF, group IV); simultaneously NPC(Fluc)s were injected to group II and 1x PBS was injected into group I (Figure 2-5). On the ninth, 10th, and 11th days after tumor inoculation, group IV mice with NPC-loaded MNPs were exposed to AMF for 10 min daily using an alternating magnetic field apparatus (Superior Induction Company, Pasadena, CA). The frequency is fixed (366 kHz, sine wave pattern); field amplitude is 5 kA/m. Tumor diameters were measured using a caliper on days 8, 10,12,13,14 and 15; tumor volumes were calculated using the formula $0.5a \times b^2$, where a is the larger diameter and b the smaller diameter of the tumor (the above formula assumes tumor is in ellipsoidal shape). All of the mice were then euthanized on day 15, tissues were collected and tumor weights were measured.

Histological Analysis

All mice were sacrificed 15 days after tumor inoculation by CO_2 inhalation and cervical dislocation. Tumor, lung, liver, and spleen were snap-frozen in liquid nitrogen for histological analysis. Tissues were sectioned on a cryostat (Leitz Kryostat 1720, Germany) at 8−10 μm and used for histological studies. Prussian blue staining was performed on these sections using Perl's Prussian blue stain kit to identify NPCs loaded with MNPs. Apoptotic cell detection in the tissue sections was determined using the DeadEnd fluorometric terminal deoxynucleotidyl transferase dUTP nick end labeling (TUNEL) system (Promega Corporation, Madison, WI), as per the manufacturer's protocol.

Protein Preparation for Two-Dimensional Electrophoresis (2-DE)

To identify protein expression differences between tumors from mice receiving AMF after IV saline injection or after IV NPC-MNP injection, 3.5×10^5 B16-F10 melanoma cells were injected subcutaneously into two mice. On day 5, 1×10^6 NPCs loaded with MNPs at 20 μg/mL iron concentration were injected intravenously into one mouse; simultaneously, saline was injected into the other mouse. On days 9, 10, and 11, tumors were exposed to AMF. On day 11, mice were euthanized and tumors were collected immediately after AMF exposure.
Total protein was prepared from the tumors for use in two-dimensional gel electrophoresis (2-DE) analysis. The following protein isolation protocol was used [125]. Briefly, melanoma tissues were homogenized using a Pellet Pestle Mortar (KONTES, Vineland, NJ) in the presence of 0.5 mL of lysis buffer (8 M urea, 2 M thiourea, 4% 3-cholamidopropyldimethylammonio-1-propanesulfonate (CHAPS), 100 mM dithiothreitol (DTT), 25 mM Tris-Cl, and 0.2% ampholyte (pH 3−10) (Amersham Pharmacia Biotech, Piscataway, NJ). The supernatant was collected and then precipitated using 2 volumes of ice-cold acetone. The final protein pellet was dissolved in 100 μL of the sample buffer (8 M urea, 2 M thiourea, 4% CHAPS, 100 mM DTT, 25 mM Tris-Cl, and 0.2% ampholyte (pH 3−10)). Protein concentrations were determined using a reducing agent-compatible and detergent-compatible protein assay kit (Bio-Rad, Hercules, CA).

2-DE Analysis

Fifty micrograms of total protein was resolved at 20 °C in the first dimension by isoelectric focusing (IEF) in an IEF cell system (Bio-Rad, Hercules, CA) using 7 cm long, pH 3−10, precast immobilized pH gradient strips (Bio-Rad). The IEF parameters were 250 V for 15 min, followed by 4000 V for 5 h. At the end of the IEF, the strips were equilibrated sequentially for 10 min each in 1 mL of equilibration buffer I (375 mM Tris-HCl [pH 8.8], 6 M urea, 2% sodium dodecyl sulfate (SDS), 2% DTT) and buffer II (375 mM Tris-HCl [pH 8.8], 6 M urea, 2% SDS, 2.72 mg of iodoacetamide/mL, 0.001% bromophenol blue). Subsequently, second-dimension SDS-polyacrylamide gel electrophoresis analysis was performed on the strips in a Mini-PROTEAN Tetra system by using 12% polyacrylamide gels (Bio-Rad) for 40 min at 200 V at room temperature in a 50 mM Tris-glycine buffer. The 2-DE resolved gels were stained by using a Biosafe Coomassie G-250 kit (Bio-Rad). Coomassie stained gels were digitalized by using an HP Scanjet 7400c scanner (Hewlett-Packard, Houston, TX).

Matrix-Assisted Laser Desorption Ionization (MALDI)-TOF MS Analysis of Melanoma Tissues Treated with AMF and AMF with NSC-MNP Proteins

After resolution by 2-DE, proteins from melanomas from mice treated with AMF and MNP-NPC+AMF were picked individually from Coomassie blue stained gels using PROTEINEER spII with sp-Control 3.0 software (Bruker Daltonics, Bremen, Germany) according to the manufacturer's protocol. Coomassie blue stained proteins were digested as described by Shevchenko *et al* [125]. An aliquot of in-gel-digested solution was mixed with an equal volume of a saturated solution of 1 μL of 2,5-dihydroxybenzoic acid (DHB) in 50% aqueous acetonitrile, and 1 μL of mixture was spotted onto a target plate. Protein analysis was performed with a Bruker UltraFlex II MALDI-TOF using MTP AnchorChip with 384 matrix spots. MALDI-TOF spectra were externally calibrated using a combination of nine standard peptides: bradykinin 1-7 (757.39 Da), angiotensin II (1046.54 Da), angiotensin I (1296.68 Da), neurotensin (1672.91 Da), renin substrate (1758.93 Da), ACTH clip 1-17 (2093.08 Da), ACTH clip 18-39 (2465.19 Da), ACTH clip 1-24 (2932.58 Da), and ACTH clip 7-38 (3657.92 Da), spotted onto positions adjacent to the samples. Protein identification was carried out by automatic comparison of experimentally generated monoisotopic values of peptides using MASCOT with a tolerance of 0.5−0.3 Da and 0−1 missed cleavage, and oxidation of methionine was allowed.

Statistical Analysis

Statistical analyses were performed using WinSTAT (A-Prompt Corporation, Lehigh Valley, PA). Cytotoxicity of MNPs data were analyzed by using one way analysis of variance (ANOVA) with least significant difference (LSD) multiple comparisons. Iron concentration per single NPC cell (Loading efficiency of MNPs) was estimated by using iron standards as linear model and estimated iron concentration per single NPC cells again modeled by using linear model. AMF induced temperature changes and overall differences in tumor volumes between all *in vivo* groups were analyzed by using Repeated measures ANOVA. Tumor weights were analyzed by using one way ANOVA. A p value less than 0.05 was considered as significant for one way ANOVA and repeated measures ANOVA and significance for LSD post hoc multiple comparisons was set at $p < 0.05$. All of the tumor volume data are represented as mean ± standard error (SE) on graphs.

Results

Loading Studies of MNPs on NPCs

MNPs efficiently loaded into NPCs. After Prussian blue staining, MNPs were detected in NPCs as blue staining material (Figure 2-1B). Transmission electron microscope (TEM) images of NPCs showed loaded MNPs as aggregates in the cell cytoplasm (Figure 2-1C). Close examination of additional TEM images revealed that in some images the aggregates were surrounded by fragmented unit membrane, indicating they were possibly in an endosomal compartment (Figure 2-1D). In most images, they did not appear to be so enclosed. On the basis of these results, there is possibility that the MNPs are taken up *via* the LDL receptor and traffic in the endosomal−lysosomal system but cause endosomolysis with subsequent release of MNPs into the cytosol (need further confirmation). The loading efficiency of MNPs into NPCs increased with increasing concentration of MNPs in medium. The highest concentration of 1.6±0.2 pg of iron per cell was identified in cells incubated with medium containing 25 μg/mL iron (Figure 2-2).

Cytotoxicity of MNPs on Neural Progenitor Cells and B16-F10 Cells

MNP toxicity was tested based on iron concentration in MNPs. Media containing various iron concentrations of MNPs were added to NPCs and B16-F10 cells and incubated overnight. The toxic effect of these MNPs increased with increasing iron concentration. Cell viability assessment for varying concentrations of MNPs on NPCs and B16-F10 cancer cells is shown in Figure 2-3A and B respectively. NPCs tolerated the MNPs well through 20 μg/mL iron concentration (Figure 2-3A), so this MNPs concentration was used for subsequent experiments. However, the B16-F10 cell number was decreased upon exposure to only 10 μg/mL iron concentration (Figure 2-3B). Difference in cytotoxicity of these MNPs on NPCs and B16F10s could be because of differences in growth rates of the used cell lines.

AMF-Induced Temperature Changes In Vitro

Temperature increase over time was compared between NPC controls and MNP-loaded NPCs (NPCs-MNPs) (Figure 2-4). There was a ~2.6 °C increase between control and MNP-loaded cells (not significant) at cell pellet position after 10 min of AMF exposure. There is no identifiable difference in temperature in the middle of agarose between NPCs and NPCs –MNPs after 10 min of AMF exposure suggesting heat generated at pellet position is not distributing through agarose.

NPC-MNP and A/C Magnetic Field Effect on Melanoma

Substantial numbers of MNP-loaded NPCs were identified in tumor sections at the borders of tumors after 4 days after IV administration (Figure 2-7D). To test the hypothesis that administration of NPCs loaded with MNPs followed by AMF application would reduce the tumor burden, NPC (Fluc)-MNPs were injected intravenously into melanoma-bearing mice. Tumor volume comparisons are graphed in Figure 2-6A. Although tumor volume differences between groups were not significant overall (Repeated measures ANOVA), NPC (Fluc)+MNP+AMF group tumor volume has mild regression trend after day-10 compared with other groups (Figure 2-6A). After 15 days, all of the mice were euthanized and tumor weights were measured. There is no significant difference between tumor weights of different groups (Figure 2-6B). There are no prussian blue positive cells in tumor tissues from mice subjected to AMF exposure, evaluated at the end of the experiment (Figure 2-7C). This absence may indicate that the NPCs perished and released their cargo, which was subsequently removed from the site by phagocytic cells.

To find potential mechanisms of this mild tumor volume attenuation, tumor tissues were collected 24 h after the last AMF treatment on some of the mice. There was an increase in the apoptotic index in the NPC-MNP IV transplanted group after three rounds of AMF, indicating that the targeted magnetic hyperthermia had a measurable effect on cell viability 24 h after the last treatment (Figure 2-7E). This corresponds to the time at which subcutaneous tumor volumes in the group receiving NPCs loaded with MNPs and subsequent AMF were less than tumor volumes in any of the other groups (Figure 2-6A- not significant). Hence, apoptosis appears to be a mechanism involved in reduced tumor volumes.

Proteomic Analysis

To further investigate the mechanisms tumors were excised from mice receiving either NPC-MNP followed by AMF or PBS followed by AMF. Total protein was extracted from these tumors, and the extracted proteins were separated using 2-D gel electrophoresis. Gel spots representing 12 proteins expressed differentially in the 2 mouse groups were pinpointed using the MASCOT identification search software for identifying peptide mass fingerprinting (PMF). These protein spots are noted in Figure 2-8. We attempted to identify each of the proteins comprising the 12 differentially expressed spots using MALDI-TOF mass spectrometry. Identified proteins are listed in Table 2-1. As can be seen, phosphoglycerate kinase 1 (PGK1) and neurotensin receptor 1 protein were much more highly expressed in tumors from the mice receiving intravenous NPC-MNP followed by AMF treatment than in the PBS+AMF controls. The group receiving NPCs+ AMF alone was not included in this comparison because Prussian blue staining failed to identify any intact NPCs in NPC-MNP treated tumor tissue at the end of the experiment, indicating that the NPCs had been killed at some point by the A/C magnetic field exposure. Thus, it is unlikely that any differences in protein levels are due to the presence of the delivery cells. Also, it is unlikely that the NPCs, which are a minor population, could secrete enough protein to register as a difference to be picked as spots on the second dimension gels even had they survived. Of the seven protein spots found in the treated group but not the saline group (see Table 2-1), one candidate protein identified that could potentially exert an antitumor effect is PGK1, which is anti-angiogenic when overexpressed in some tumors [126]. However, overexpression of PGK1 in prostate cancer has been shown to facilitate tumor growth [127]. On the other hand, there were five protein spots present in the saline control group that were not present in the treated group. One of these was TNF receptor-associated factor 5 (TRAF5), which is known to activate NF-κB [128]. Another, biliverdin reductase B, also increases NF-κB expression [129]. NF-κB is a central player in the transition to a more invasive state in many tumors [130]. Biliverdin reductase B was identified as a specific protein marker in microdissected hepatocellular carcinoma [131], elevated in methotrexate-resistant colon cancer cells [132], and is induced in renal carcinoma [133]. Hence, it possible that down-regulation of these genes could have been a factor in reduction of tumor size. While preliminary, these findings provide the background for further investigation to reveal potential mechanisms of tumor attenuation by AMF after targeted delivery of MNPs by tumor-tropic stem cells.

Discussion

This is the first report in literature showing that tumor-tropic cells loaded with MNPs *ex vivo* and administered intravenously can result in mild regression of preclinical tumors after A/C magnetic field exposure. In a previous report, we showed that even microgram amounts of these bi magnetic MNPs given intra-tumorally or intravenously could reduce subcutaneous melanomas [90]. However, Prussian blue staining for iron was much more pronounced in the lungs and liver than in the work reported here. Thus, an advantage of the cell-based delivery of the MNPs seems to be that it avoids agglomeration of MNPs in the reticulo-endothelial (mononuclear phagocytic) system.

Although the probable accumulation of MNPs reported here is low compared to most reported tumor accumulations *in vivo*, the iron core of the MNPs used in this work may allow smaller amounts of the MNPs to respond to an A/C magnetic field *in vivo* than would be expected for iron oxide MNPs. Based on *in vitro* loading efficiency studies (Figure 2-2) the amount of iron (represents MNPs amount) present in single MNPs loaded cell is 1pg (with 20μg/mL iron MNPs incubation), so the amount transplanted with 1×10^6 NPCs is ~1μg of iron MNPs. Temperature increase observed with 1×10^6 MNP loaded NPCs is ~2.6 °C (Figure 2-4), which is more of mild hyperthermia temperature than increases observed in other MHT pre-clinical studies. Again for *in vitro* model used here to identify the AMF induced temperature, all the MNPs loaded NPCs were taken as pellet form, which is different from the NPCs distribution observed in tumors (Figure 2-7D). Therefore, “hot spots” featuring a high temperature may exist during A/C magnetic heating, which can lead to local damage of the cells at multiple locations, even when the total temperature of the tumor tissue is not significantly enhanced (need further studies to confirm this hypothesis).

It is possible that mild tumor attenuation effect observed in present study could be by other factors in addition to A/C magnetic field exposure after MNP delivery to tumor by NPCs. Cytokines released by the NPC-MNP after mild hyperthermia may helped in this mild attenuation; a recent report indicates that conditioned medium from heat-treated mesenchymal stem cells significantly inhibited proliferation of cancer cells *in vitro* [134, 135]. Another factor that could enhance the antitumor effect of mild to moderate regional hyperthermia *in vivo* is stimulation of the innate immune response. Recently, for example, it has been shown that elevating local tumor temperature to only 41−43 °C is sufficient to activate natural killer (NK)

cells [136].NK cells are part of the innate immune system and are potent tumor-lytic agents when activated [137]. Kubes *et al.* showed that high numbers of activated monocytes with increased cytotoxic effector function were recruited into B16-F10 melanoma-bearing mice after mild local microwave hyperthermia [138].

MHT treatment potentiality depends on the distribution of MNPs in tumors, amount of MNPs present in tumors during AMF exposure, exposure time to AMF[107]. By, loading high amounts of MNPs in delivery cells and by repeated injections of MNPs loaded cells; increased accumulation of MNPs can be achieved in tumors. Increasing exposure time to AMF also can increase the targeted MHT treatment ability. In present study, injected NPCs were observed only at the borders of tumor (Figure 2-7D) which can limit the overall tumor heating. Tumor homing cells that can distribute all over the tumor can potentiate the effect observed in this present study. By considering the points explained in above discussion – Amount of MNPs in delivery cells, Number of cells for treatment, AMF exposure time next hypothesis was proposed and tested in Chapter 2 - .

Conclusions

In conclusion, These studies show here that (1) NPCs efficiently load with core/shell Fe/Fe_3O_4 bi-magnetic nanoparticles (MNPs); (2) the MNPs accumulate with time as aggregates in the cytosol; (3) the MNPs cause minimal toxicity in those cells; (4) NPCs loaded with MNPs travel to subcutaneous melanomas; (5) after A/C magnetic field exposure, the targeted delivery of MNPs by the cells results in a mild regression of the tumor volumes; and (6) this treatment results in apoptosis of cancer cells and alters the tumor proteome.

Figure 2-1 Loading studies of MNPs on NPCs

A. Schematic picture of TCPP-targeting units containing Fe/Fe3O4/Aminosilaxane/stealth nanoparticles, B. Bright-field image of NPCs loaded with MNPs showing positive Prussian blue staining for the presence of iron and counterstained with nuclear fast red (magnification 20x), C. TEM image of NPC loaded with MNPs (arrows) (magnification 30000x), D.TEM picture showing MNPs (black arrow) aggregate surrounded by membrane fragments (white arrow) (magnification 70000x).

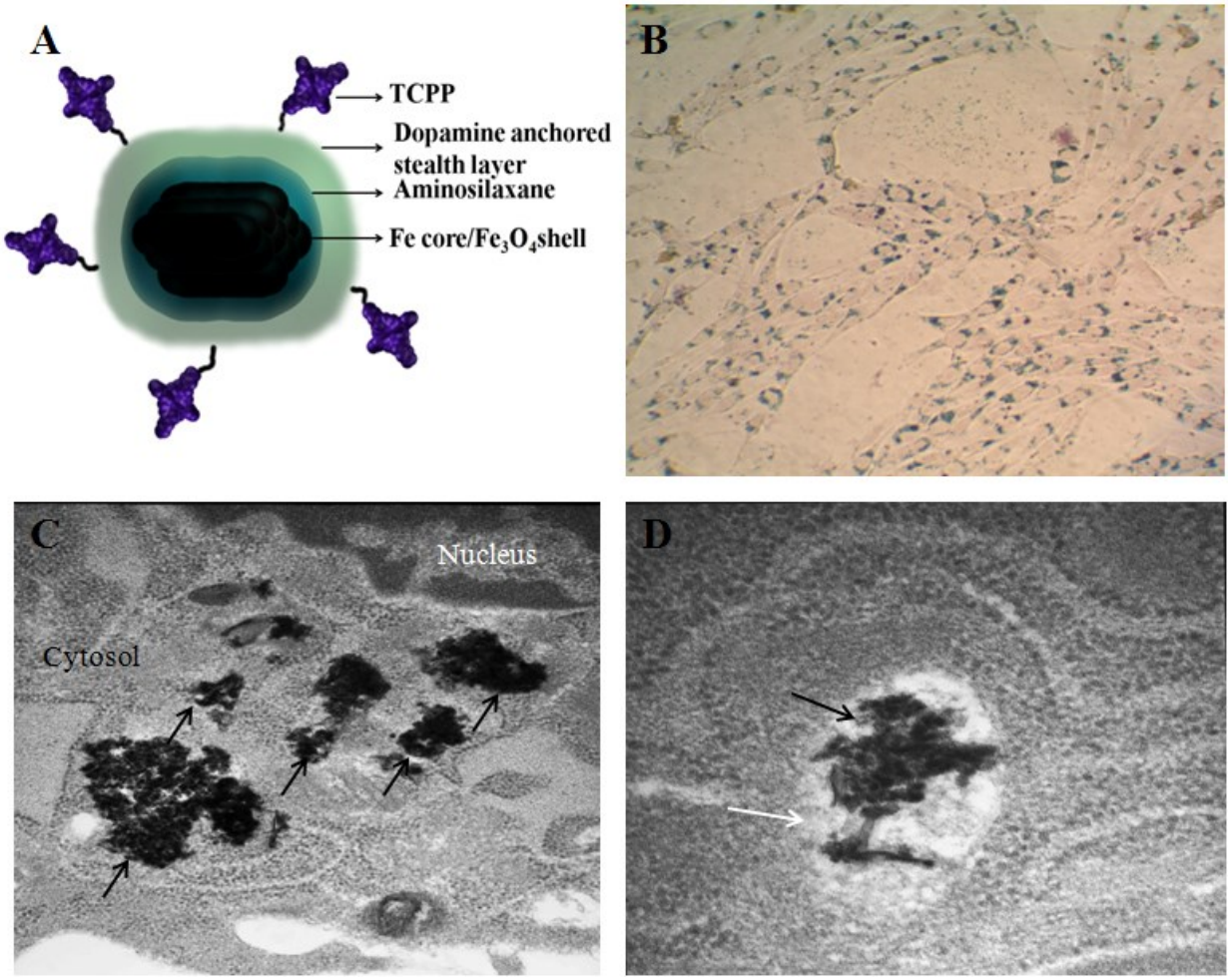

Figure 2-2 Loading efficiency of MNPs on NPCs

Iron concentration per NPC cell incubated with various concentrations of MNPs containing medium (Pearson correlation coefficient- 0.9, one-sided significance- <0.05).

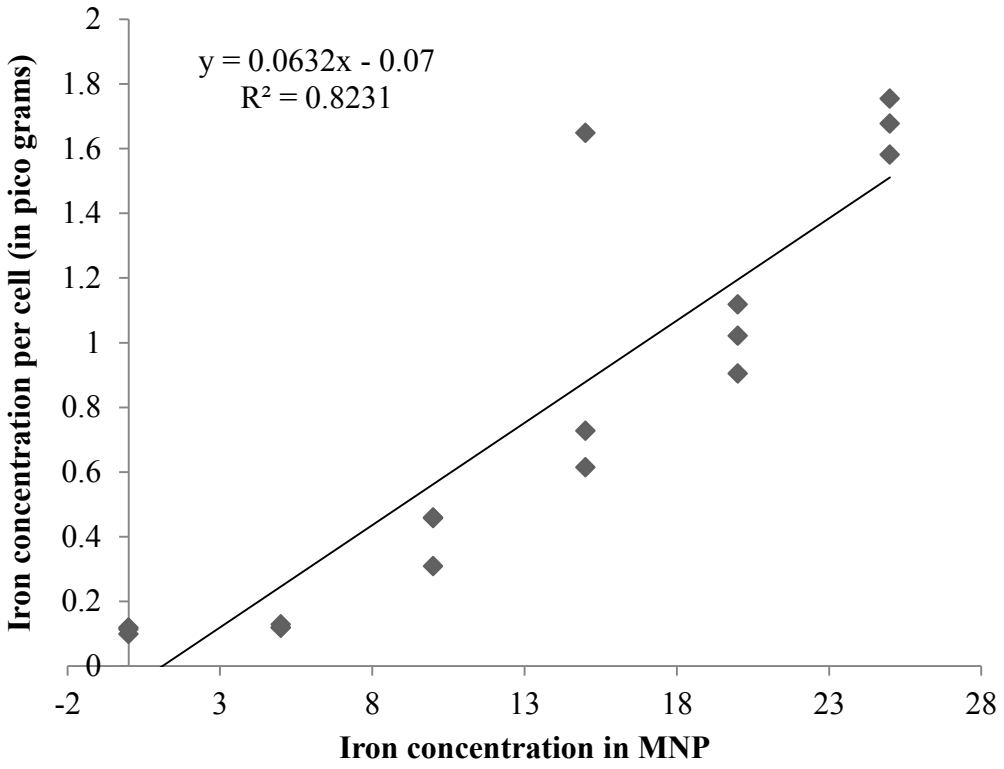

Figure 2-3 Cytotoxicity of MNPs on Neural progenitor cells (NPCs) and B16F10 melanoma cells

A. *In vitr*o cell viability of NPCs cultured in medium containing increasing concentrations of MNPs (One way ANOVA- <0.1, LSD at 0.05 significance level 25µg/mL vs all other groups except 20µg/mL), B. In vitro cell viability of B16-F10s cultured in medium containing increasing concentrations of MNPs (One way ANOVA- <0.05, LSD at 0.05 significance level control vs all other groups except 5µg/mL; 5µg/mL vs 15, 20, 25 µg/mL; 10µg/ mL vs 20, 25 µg/mL).

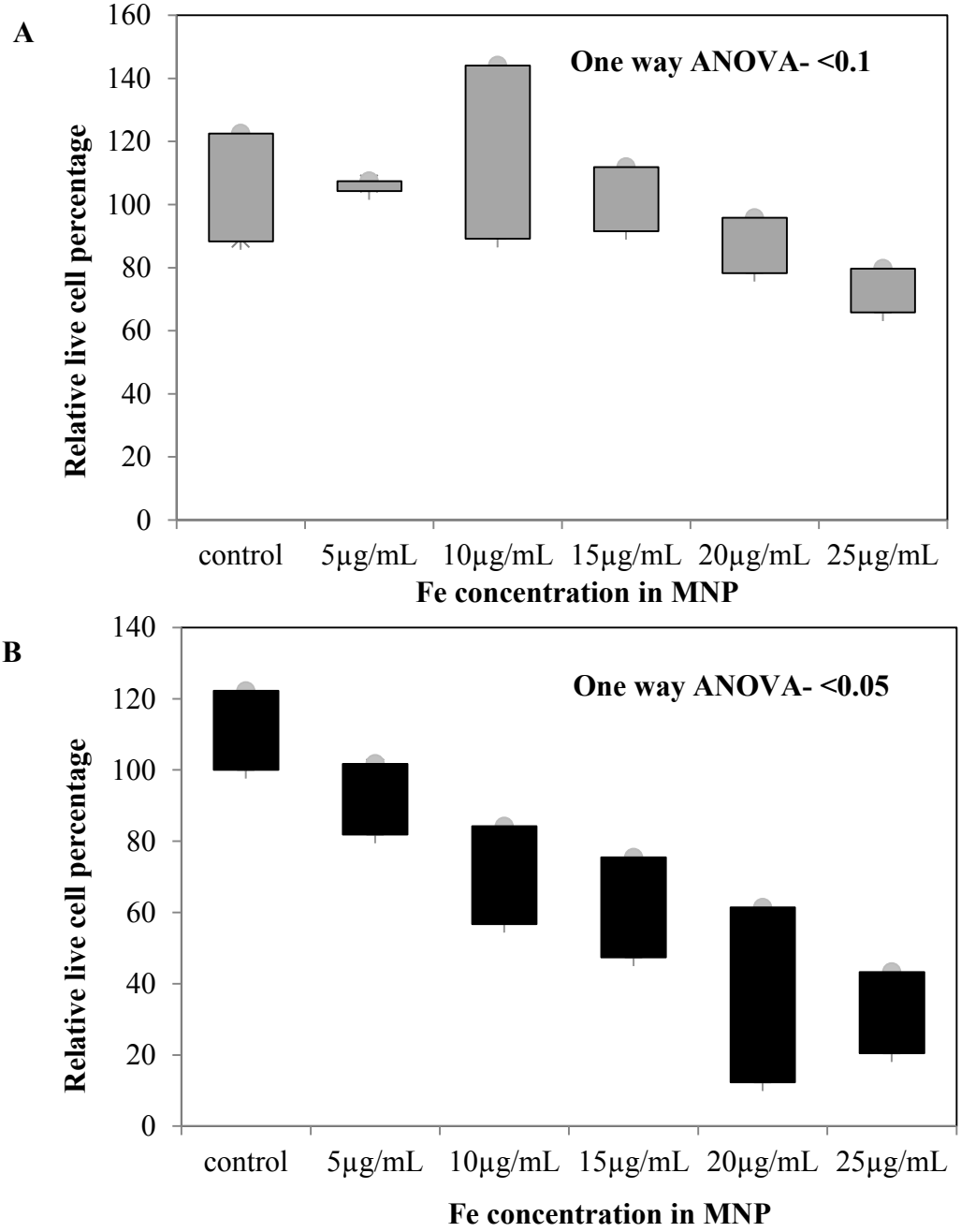

Figure 2-4 Alternating magnetic field (AMF) induced temperature changes in vitro
Temperature measurements after AMF of NPCs loaded with MNPs and NPC controls at the pellet and in the agarose solid. (Repeated measures ANOVA- not significant).

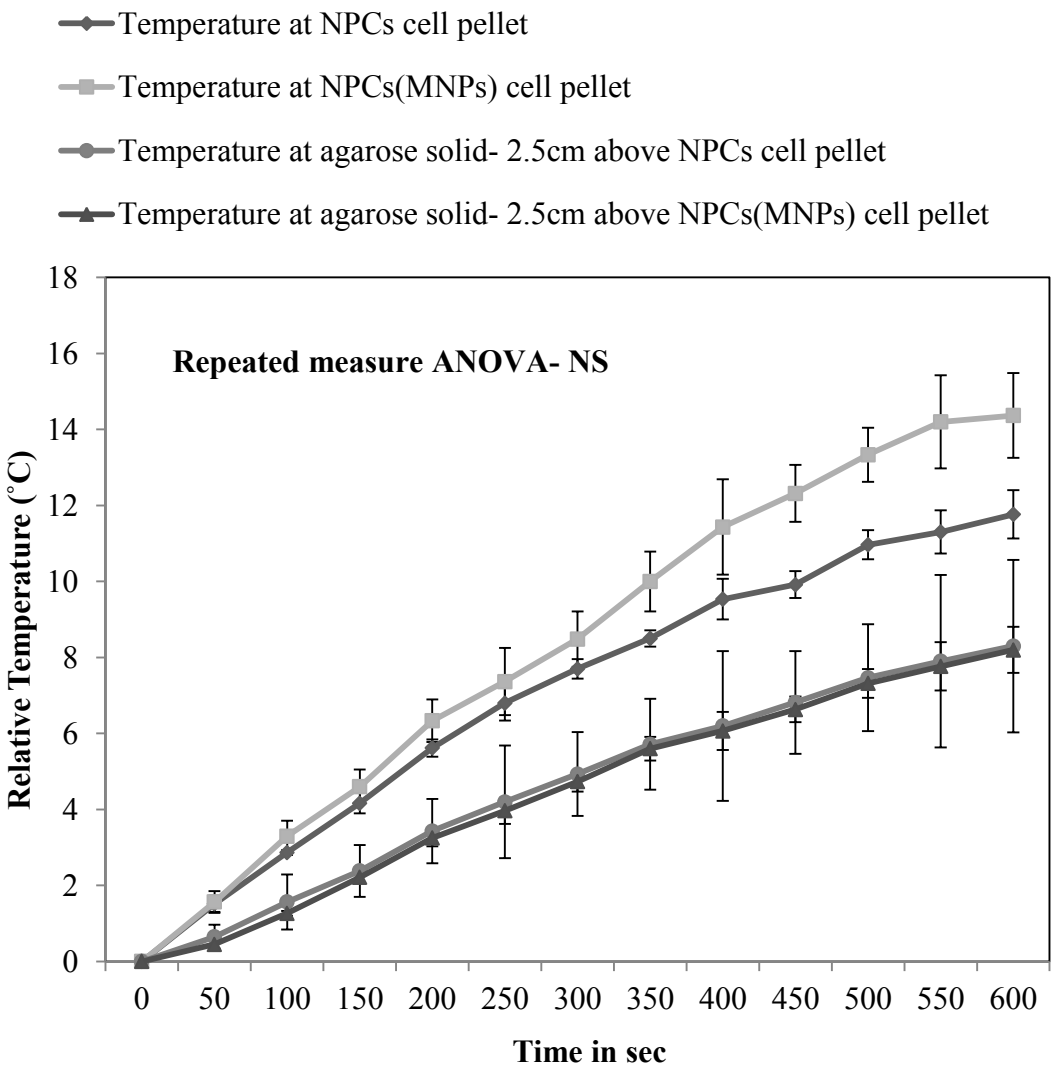

Figure 2-5 Experimental design for Magnetic nanoparticles (MNPs) loaded Neural progenitor cells (NPCs) mediated Magnetic hyperthermia treatment (MHT)

A. Days schedules of NPC-MNP and A/C Magnetic field effect on Melanoma experiment, B. Groups and number of mice in each group.

A

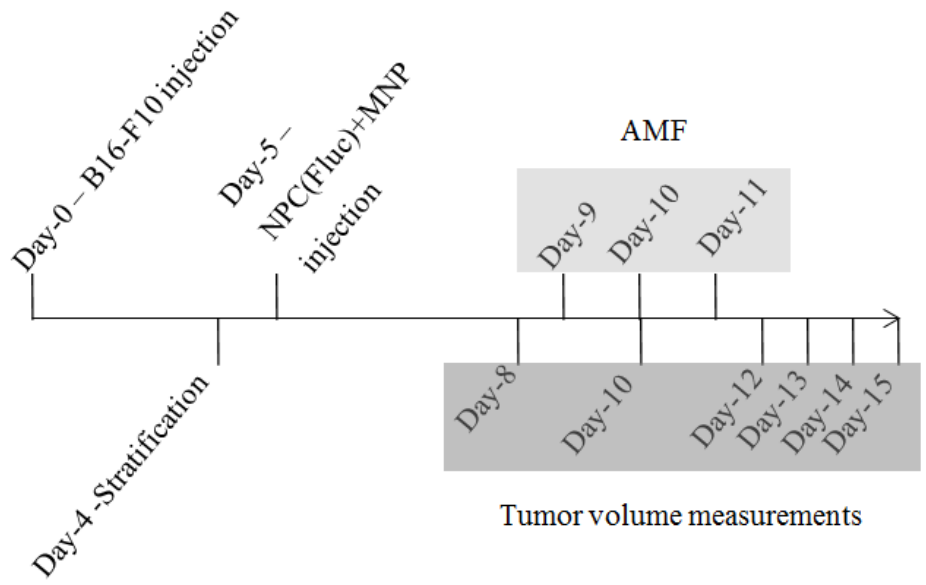

B

Number	Group	Sample size
I	PBS	11
II	NPC(Fluc)	10
III	NPC(Fluc)+MNP	11
IV	NPC(Fluc)+MNP+AMF	13

Figure 2-6 Neural progenitor cells (NPCs) loaded with MNPs and A/C Magnetic field effect on melanoma

A Calculated tumor volume comparison between different groups from day-8 to day-15, data were analyzed by using repeated measures ANOVA (not significant) B. Tumor weights comparison between different groups on day-15, data were analyzed by using one way ANOVA (not significant).

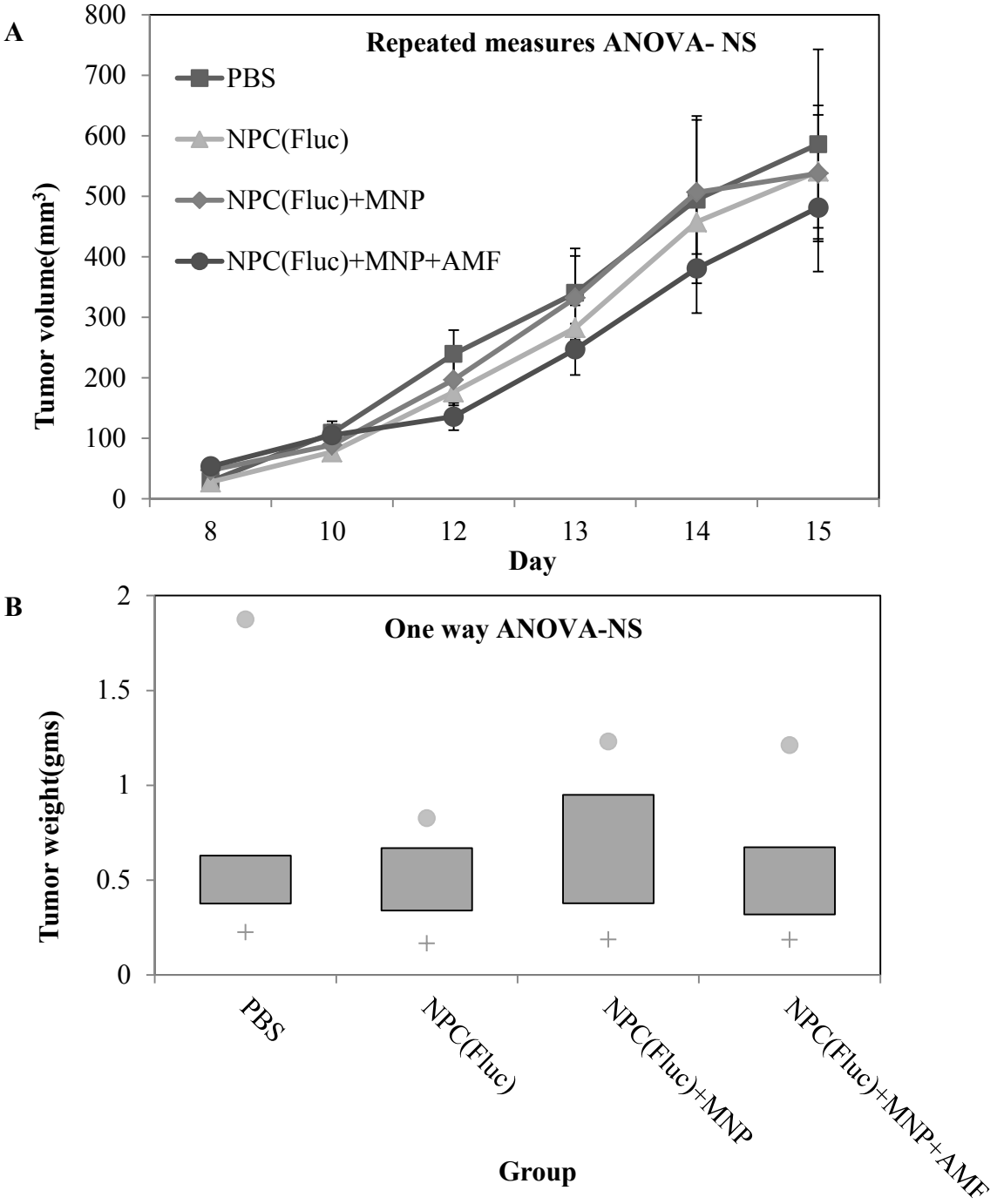

Figure 2-7 Histological analysis of mouse tissues

(A-D) Prussian blue stained tissue sections, counterstained with nuclear fast red of melanoma tumor bearing mice which received NPC-MNP followed by AMF treatment: liver(A), lung(B), tumor(C); note the absence of Prussian blue stained NPCs in tumor sections. Prussian blue stained NPCs loaded with MNPs in tumor section of mouse which received NPC-MNP but no AMF treatment (D). (E,F) TUNEL assay: green apoptotic cells in tumor- bearing mouse with NPC-MNP+AMF (E) compared to few apoptotic cells in tumor-bearing mice with saline only treatment (F).

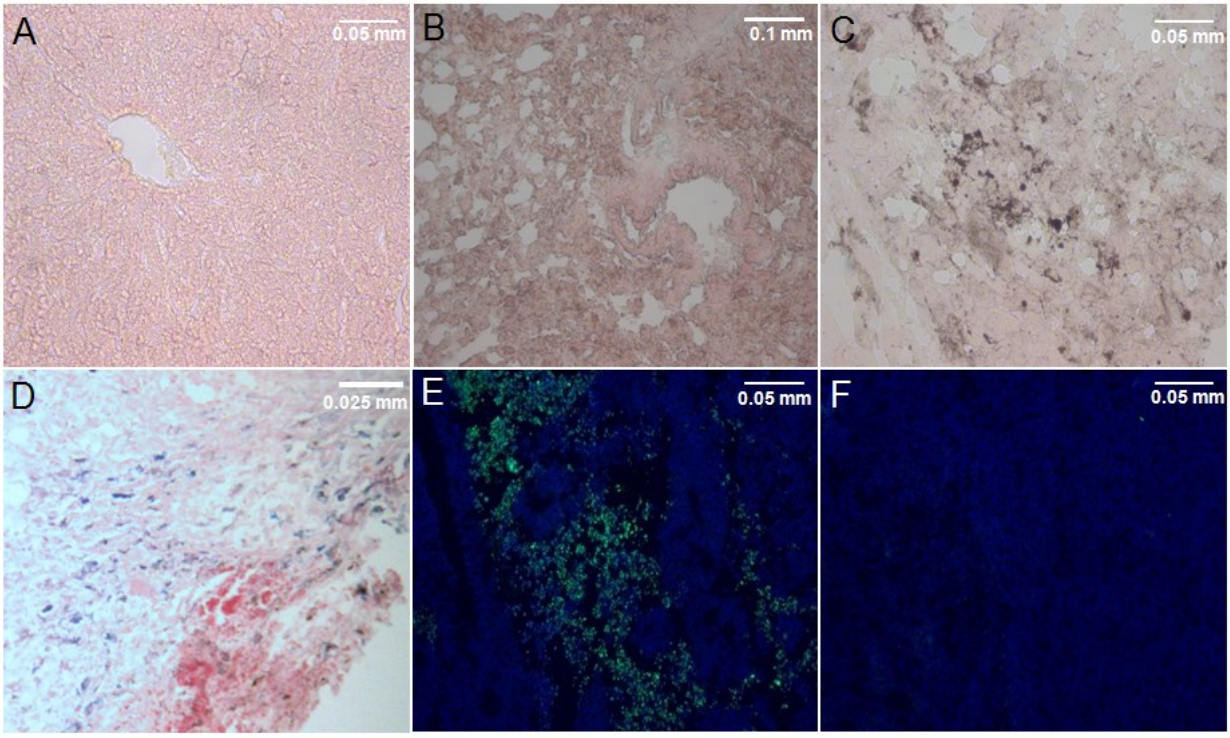

Figure 2-8 Two-dimensional gels of melanoma tissues from mice treated with PBS + AMF or NPCs-MNP + AMF

Tumor samples from mice received PBS+AMF (A) and NPCs-MNP+AMF (B) were harvested and processed for the first dimension, electrophoretically separated on 12% acrylamide gels and stained with Biosafe coomassie G-250 stain. Numbers with arrowhead lines refer to protein spots identified by MALDI-TOF analysis.

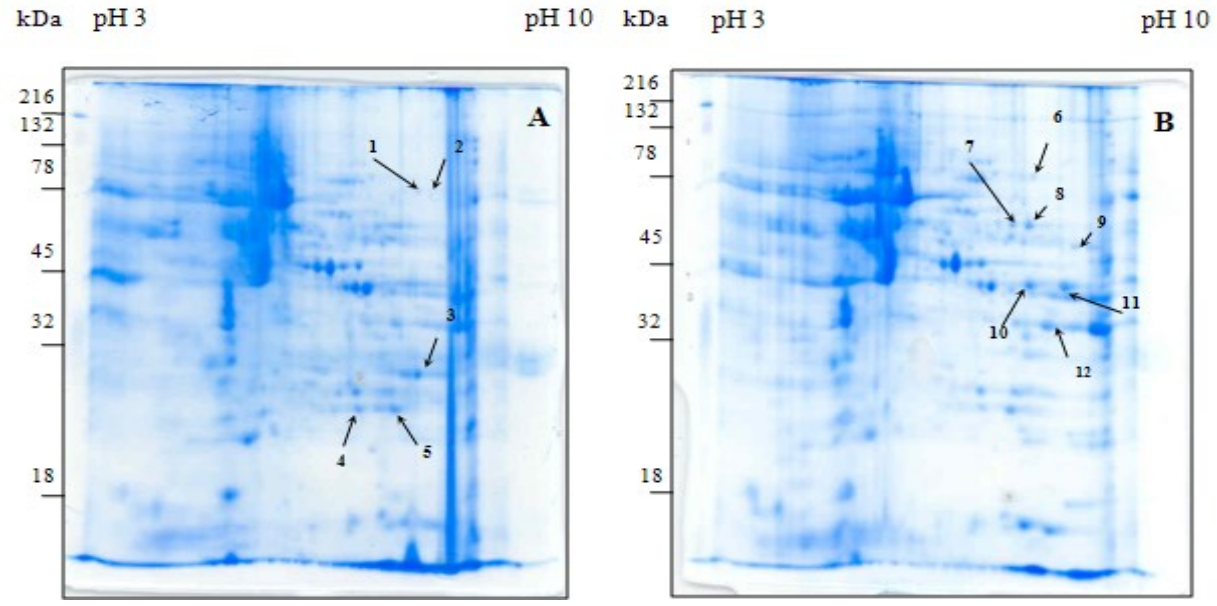

Table 2-1 Proteins of Melanoma tumor treated with PBS+AMF and NPCs-MNP+AMF, analyzed by MALDI-TOF

Spot number	Protein identification	GenBank Numbers	Theoretical MW (Da)	pI	Sequence coverage (%)
Saline + AMF					
1	TNF receptor-associated factor 5	gi|6755867	65679	7.71	14
2	Aste1 protein	gi|68534685	69927	8.31	12
3	Beta-globin	gi|156257677	15823	7.14	78
4	Biliverdin reductase B	gi|21450325	22299	6.49	53
5	Unnamed protein product	gi|74222020	27054	6.90	39
NPC-MNP + AMF					
6	Zmym1 protein	gi|116283425	103513	8.88	10
7	Neurotensin receptor 1	gi|9055296	47708	9.39	19
8	Unnamed protein product	gi|74211198	54416	10.00	13
9	Unnamed protein product	gi|74211198	51420	9.09	16
10	Phosphoglycerate kinase 1	gi|70778976	44928	8.02	43
11	Phosphoglycerate kinase 1	gi|70778976	44928	8.02	53
12	Similar to Glyceraldehyde-3-phosphate dehydrogenase	gi|149252413	34190	8.45	27

Chapter 3 - Cell-delivered magnetic nanoparticles caused hyperthermia-mediated increased survival in a murine pancreatic cancer model

Matthew T. Basel[1*], **Sivasai Balivada[1]**, Hongwang Wang[2], Tej B. Shrestha[1], Gwi Moon Seo[1], Marla Pyle[1], Gayani Abayaweera[2], Raj Dani[2], Olga B. Koper[2,3], Masaaki Tamura[1], Viktor Chikan[2], Stefan H. Bossmann[2*], and Deryl L. Troyer[1*]

[1]Department of Anatomy and Physiology, College of Veterinary Medicine,

[2]Department of Chemistry, Kansas State University;

[3]Nanoscale Corporation, Manhattan, KS

* Matthew T. Basel gave permission to use his paper as one of the chapters in this dissertation, Since Sivasai Balivada contributed equally to this work

Abstract

Using magnetic nanoparticles to absorb alternating magnetic field energy as a method of generating localized hyperthermia has been shown to be a potential cancer treatment. This report demonstrates a system that uses tumor homing cells to actively carry iron/iron oxide nanoparticles into tumor tissue for alternating magnetic field treatment. Paramagnetic iron/ iron oxide nanoparticles were loaded into RAW264.7 cells (mouse monocyte/ macrophage-like cells), which have been shown to be tumor homing cells. A murine model of disseminated peritoneal pancreatic cancer was then generated by intraperitoneal injection of Pan02 cells. After tumor development, monocyte/macrophage-like cells loaded with iron/ iron oxide nanoparticles were injected intraperitoneally and allowed to migrate into the tumor. Three days after injection, mice were exposed to an alternating magnetic field for 20 minutes to cause the cell-delivered nanoparticles to generate heat. This treatment regimen was repeated three times. A survival study demonstrated that this system can significantly increase survival in a murine pancreatic cancer model, with an average post-tumor insertion life expectancy increase of 31%. This system has the potential to become a useful method for specifically and actively delivering nanoparticles for local hyperthermia treatment of cancer.

Introduction

Pancreatic cancer is known to be one of the most lethal forms of cancer, with five year survival rates of less than 5% [139]. Discovering new methods for successfully treating pancreatic cancer is a virtual necessity for combating this disease. Through Chapter-1 Neural progenitor cells directed hyperthermia has been successfully demonstrated to cause mild attenuation of mouse melanomas (Figure 2-6) [122]. As mentioned previously in Chapter-1, Magnetic hyperthermia treatment (MHT) treatment potentiality depends on the distribution of Magnetic nanoparticles (MNPs) in tumors, amount of MNPs present in the tumors during alternating magnetic field (AMF) exposure, exposure time to AMF[107]. By, loading high amounts of MNPs in delivery cells and by repeated injections of MNPs loaded cells; increased accumulation of MNPs can be achieved in tumors. Increasing exposure time to AMF also can increase the targeted MHT treatment ability. Tumor homing cells that can distribute all over the tumor can potentiate MHT treatment effect. By considering the points explained above– Amount of MNPs in delivery cells, number of cells per treatment and number of treatments, exposure time to AMF present hypothesis was designed.

Monocytes and macrophages are known to infiltrate tumor sites and thus could act as cytotherapeutic drug delivery vehicles [140, 141]. Several recent studies have demonstrated the feasibility of delivering therapy to tumors using monocytes or macrophages, including targeting liposomes containing fluorescent markers to gastric tumors [54], targeting adenovirus to prostate tumors [13], and targeting gold nanoshells to gliomas [142]. Macrophages were known as professional phagocytic cells [143] and can engulf high amounts of MNPs compared with non-phagocytic cells [144, 145].

Here we demonstrate a system that uses monocyte-like tumor homing cells to deliver MNPs directly into the tumor tissue. We have demonstrated that RAW264.7 cells (monocyte/macrophage-like cells, Mo/Ma, ATCC TIB-71) specifically infiltrate pancreatic tumors when injected intraperitoneally (i.p.) without infiltrating other organs. These cells were loaded with MNPs in order to deliver the MNPs specifically to the tumor for localized hyperthermia. To test this system, a murine model of disseminated peritoneal carcinomatosis of the pancreas was generated by injecting Pan02 cells i.p. into C57BL/6 mice [146]. MNPs loaded Mo/Ma were then injected and allowed to infiltrate the tumor tissue. Three days after Mo/Ma injection, mice were treated with AMF. This treatment system significantly increased the

survival time of mice bearing i.p. pancreatic tumors, with an average lifespan increase post tumor injection of 31%.

Materials and Methods

Reagents and Cells

C57BL/6 mice (11 weeks old) were purchased from Charles River (Wilmington, MA). RAW264.7 cells were purchased from ATCC (Manassas, VA, authenticated by ATCC using cell morphology, karyotype analysis, and cytochrome C oxidase analysis, and cultured for less than six months). Pan02 cells were obtained from the DCTD Tumor Repository (NCI) (Frederick, MD, authenticated by NCI using cell morphology, and cultured for less than six months). Fetal bovine serum (FBS), neocuproine, ascorbic acid, ammonium acetate, concentrated hydrochloric acid (HCl) were purchased from Sigma-Aldrich (St. Louis, MO). RPMI, Geneticin (G418), hygromycin and penicillin-streptomycin were purchased from Invitrogen (Carlsbad, CA). Thiazolyl blue and sodium dodecyl sulfate were purchased from Fisher Scientific (Pittsburgh, PA). Iron/iron oxide (Fe/Fe_3O_4) nanoparticles were obtained from NanoScale Corporation (Manhattan, KS). Ferrozine was purchased from Hach (Loveland, CO).

Cell Culture of RAW264.7monocyte/macrophages and PanO2 pancreatic adenocarcinoma cells

RAW264.7 cells were cultured in RPMI medium containing 10% FBS, with 100 μg/mL G418 and 100 μg/ml hygromycin in a 37°C humidified incubator with 5% CO_2. Pan02 cells were cultured in RPMI with 10% FBS and 1X penicillin-streptomycin in a 37 °C humidified incubator with 5% CO_2.

Synthesis of Nanoparticles

Complete synthesis and characterization of Iron/iron oxide (Fe/Fe_3O_4) stealth coated bi magnetic nanoparticles (MNPs) used in this study were explained in detail in Matt et al., 2012 [147]

Loading Mo/Ma with Nanoparticles and Determination of Iron Loading Concentration

To determine the optimal concentration for nanoparticle loading, Mo/Ma were plated in 24 well plates and allowed to come to 70% confluency. Medium was removed from the cells and fresh medium was added containing from 0 to 200 μg/mL iron from the nanoparticles. Sixteen hours later the medium was removed, the cells were washed with PBS, and fresh medium was added. Loading confirmation and concentration were obtained by lifting the cells and running a ferrozine assay for iron content. The percent of cells loaded was measured using flow cytometry. Cytotoxicity was measured using the MTT assay.

For injections, Mo/Ma were cultured to 70% confluency in T75 flasks. Sixteen hours before using the cells, cells for groups 3 and 5 (see below) were given nanoparticles consisting of 373μg (37.3 μg/mL) of iron added to the media in 100 μL of PBS and mixed well. At the same time, cells for groups 1, 2, and 4 were given 100 μL of PBS. The next morning, the medium was removed, the cells were washed with PBS, and fresh medium was added. The cells were lifted by scraping and counted in a hemocytometer. The correct cell density was attained by spinning the cells in 15 mL conical tubes at 1000 RPM for 5 minutes and resuspending in the correct volume of PBS to give 2,000,000 cells in 100 μL.

Loading Strategy of MNPs and Determination of Iron Amounts

To determine the iron content of the nanoparticle solutions and the nanoparticle loaded cells, a ferrozine assay for iron was carried out. Ferrozine reagent was prepared by dissolving 9.7g ammonium acetate and 8.8g of ascorbic acid in 10 mL of water. 80mg of ferrozine and 80mg of neocuprine were added to the solution and water was added to bring the total volume to 25 mL. The sample to be measured (either cell suspension or nanoparticle solution) was diluted to appropriate concentrations in deionized water. For cell suspension samples, the cells were counted on a hemocytometer using trypan blue before dilution. 2 mL of the diluted sample was then placed in a test tube and 0.5 mL of 1.2 M HCl and 0.2 mL of 2M ascorbic acid was added. The sample was then vortexed and incubated at 70°C for 1 hour. 0.2 mL of the ferrozine reagent was then added to the test tube and the sample was incubated at room temperature for 30 min. A standard curve was also prepared with 0, 0.1, 0.2, 0.5, 1, 2, and 5 μg/mL iron and treated in the same way. After the second incubation, the absorbance at 562 nm of the standard curve and the

samples was measured. The absorbance at 562nm *versus* iron concentration was plotted for the standard curve and the sample concentration was determined.

Determination of MNPs loaded cells by using Flowcytometry

To find the percent of MNP loaded Mo/Ma, cells were treated with nanoparticles consisting of 5,10,15,20,or 25 μg/mL Fe. The cells were incubated overnight and were washed twice with 1x PBS and analyzed by flow cytometry (Guava Easycyte Plus System, Millipore Corporation, MA). Side scatter was measured and was used as a marker for nanoparticles; cells with increased side scatter compared to control cells were counted as MNP loaded cells. Experiment was conducted in triplicate and 10,000 cells were analyzed for each replicate. Data were analyzed by using Cytosoft software (Guava Easycyte Plus System, Millipore Corporation, MA).

MTT Assay

Thiazolyl blue was dissolved in PBS at 5 mg/mL to give the reagent solution. MTT buffer solution was prepared as 10% (w/v) sodium dodecylsulfate and 0.1 M HCl in water. To assay cell viability the reagent solution was added 1:10 to the cell medium and the cells were placed back into the incubator. After four hours, the MTT buffer solution was added 1:1 to the medium and the plates were placed back into the incubator overnight. After incubating, the absorbance at 550 nm and 690 nm was recorded. The quantity $ABS_{550} - ABS_{690}$ was calculated and the control value was scaled to 100% cell viability.

Evaluation Tumor Homing ability of Raw 264.7 cells towards PanO2 tumors

To test the homing ability of Mo/Ma cells on Pan02 tumors, $7x10^5$ Pan02 cells were injected i.p. to two mice on day 0. On day 4, $1x10^6$ PKH26 red fluorescent dye labeled Mo/Ma cells were injected i.p. (manufacturer's instructions were followed for PKH26 labeling). Mice were euthanized on day 7 and 10, and tissues (mesentery/tumor, kidney, liver, spleen, lung) collected and fixed in buffered neutral formalin. Twenty-four hours after fixation, tissues were incubated in sucrose gradient and snap frozen. 5-8 micron sections were made and stained with Hoechst for nuclear counter-staining; serial sections were stained with hematoxylin and eosin (H&E).

To verify that Mo/Ma cells were in Pan02 tumors, $7x10^5$ Pan02-fluc cells (which express firefly luciferase intracellularly) were injected i.p. to five mice on day 0. On day 13, $1x10^6$ Hoescht labeled Mo/Ma cells were loaded with MNP and were injected i.p. Mice were euthanized on day 17 and tissues were snap frozen. 5-8 micron sections were made and stained with rabbit α-firefly luciferase antibody and DyLite649 conjugated sheep α-rabbit Igg antibody.

Magnetic Heating Apparatus to generate AMF

The AMF was generated by a converted 10 kW commercial inductive heater. In these experiments, only 1.5 kW power was used to produce 145 kHz sinusoidal alternating magnetic field in a copper coil. The magnetic field intensity has been calculated to be approximately 0.05 Tesla. The 4 turn 1" diameter coil is coated with silver and water cooled to eliminate residual heating effects from the resistive loss. The diameter of the coil was chosen to facilitate the complete inclusion of mice studies in the experiments including a perforated plastic tube.

Intratumoral Nanoparticle Heat Generation

Six C57BL/6 mice (11 weeks old) were injected with 700,000 Pan02 cells in 100 μL PBS subcutaneously. To create a model for intratumoral heat generation by the loaded Mo/Ma, 21 days later, when tumors were palpable, 1,000,000 Mo/Ma loaded with nanoparticles were injected in 10 μL PBS intratumorally at multiple places to three of the mice. The other three mice received 1,000,000 unloaded Mo/Ma in 10 μL PBS intratumorally. After injections, the mice were euthanized and the tumors were removed. The temperature of the tumors was recorded using an infrared camera. The tumors were then exposed to AMF for 15 min and the temperature of the tumors was again measured using the infrared camera. The difference in temperature before and after AMF was calculated and the loaded and unloaded monocyte groups were compared.

In Vivo Experiment

C57BL/6 mice (11 weeks old) were injected with 700,000 Pan02 cells in 100 μL PBS intraperitoneally (i.p.) on day 0 to generate a murine model of disseminated pancreatic cancer. These mice were then randomly divided into five groups as follows: (1) tumor control; (2) Mo/Ma control; (3) nanoparticle control; (4) AMF control; and (5) AMF treatment.

On day 5, 2,000,000 Mo/Ma loaded with the nanoparticles were injected in 100 μL PBS i.p. to groups 3 (nanoparticle control) and 5 (AMF treatment). Groups 2 (Mo/Ma control) and 4 (AMF control) also received 2,000,000 Mo/Ma which were not loaded. Group 1 (tumor control) received 100 μL PBS i.p. This procedure was repeated on days 9 and 13.

On day 8, mice from groups 4 (AMF control) and 5 (AMF treatment) were anesthetized with isofluorane and exposed to an AMF for 20 minutes. This procedure was repeated on days 12 and 16.

After three rounds of treatments, the mice were closely observed and allowed to continue until they displayed signs of clinical symptoms of cancer, at which point they were euthanized using CO_2, and the tumors were collected and weighed (Figure 3-5A).

Duration to Clinical Symptoms

The measured outcome for this study was mouse survival. To minimize potential pain and distress of the mice, however, a system was developed that allowed the euthanasia of the mice shortly before they died. The mice were scored numerically 1 - 5 based on the body condition of the mice (primarily the spine and dorsal pelvic bone prominence) with a score of 3 indicative of a healthy mouse. This initial score was then modified by the presence of extreme lethargy, dehydration, ataxia, head tilt, severe hunching, limb dragging, severe raised hair, Harderian gland secretions, ascites, labored breathing, or bloody tail. If pronounced, these symptoms led to a subtraction of 1 point from the BCS score while mild cases led to the addition of a ‘minus symbol‘ to the score (e.g. 3-). The mice were scored by this system every 12 hours and any mouse that scored a 2 or less was euthanized and the day/time was recorded. The euthanasia day/time data were then treated like survival data and modeled using Kaplan-Meier statistics to determine the statistical significance of the data.

Results

Toxicity and Loading of Nanoparticles

The nanoparticles did not show any toxicity at concentrations less than 100 μg/mL Fe, although some slight toxicity was shown at 100 and 200 μg/mL Fe (Figure 3-1A). Mo/Ma took up the nanoparticles in a manner proportional to the iron concentration (Figure 3-1B). The percentage of cells containing nanoparticles (defined as cells that exhibit increased side scatter

after loading) also increased in a manner proportional to the iron concentration (Figure 3-1C). Based on these results, to prevent undesired toxicity while maximizing the amount of iron loaded, nanoparticles were loaded at 37.5 μg/mL Fe for the *in vivo* experiment. To determine the exact amount of iron loaded in the cells for the *in vivo* experiment, when Mo/Ma were lifted for the *in vivo* experiment, excess cells were collected and iron content was measured using the ferrozine assay. The iron content of Mo/Ma injected was 2.12 +/- 0.37 pg Fe/cell or 4.25 +/- 0.74 μg Fe/2,000,000 cells.

Tumor Homing Studies

To determine if monocyte-like cells would home to Pan02 tumors, two mice bearing i.p. Pan02 tumors were injected i.p. with PKH26 labeled Mo/Ma. Three days after injection, the first mouse was euthanized. Tissue imaging showed that the monocyte-like cells effectively homed to the tumor, but did not infiltrate other organs, including the pancreas, spleen, liver, and kidney. At six days, the second mouse was sacrificed and tissue imaging showed again that the monocyte-like cells penetrated tumor tissue but not healthy tissue (Figure 3-2).

To further verify that the monocyte-like cells were, in fact, in tumor tissue, five mice bearing i.p. Pan02 tumors expressing firefly luciferase were injected i.p. with Hoescht labeled Mo/Ma which were loaded with MNP. Four days after injection, the mice were euthanized. Antibody staining for firefly luciferase demonstrated that the Mo/Ma were in tumor tissue (Figure 3-3). H&E staining of serial sections demonstrate that the tissue that the Mo/a home to is highly disorganized, indicative of tumor tissue (Figure 3-3B).

Nanoparticle Heating of Tumors

To verify that the cell-delivered nanoparticles could cause significant heating of the tumor, a subcutaneous Pan02 model was generated. (The subcutaneous model was used to give more accessible tumors for measurement purposes). The temperature change caused by AMF induced hyperthermia using the nanoparticle loaded Mo/Ma was 4.0+/-0.7°C after 15 min of AMF exposure, or moderate hyperthermia. As a comparison, the temperature change using the unloaded Mo/Ma was 1.0+/-0.5°C (Figure 3-4, p value = 0.0056).

Mouse Survival

To determine the effectiveness of the treatment, Pan02 tumors were given i.p. to C57BL/6 mice and the mice were treated as described in the methods section. The euthanasia data were collected and modeled using Kaplan-Meier survival statistics. The data are reported as days subsequent to tumor injection (day 0) (Figure 3-5B). The Kaplan-Meier test showed that the survival curves were significantly different ($p<0.005$). All of the mice from the tumor control group were euthanized due to clinical symptoms (here after referred to as 'succumbed') by day 23. Similarly all of the Mo/Ma control mice succumbed by day 25, all of the nanoparticle control mice succumbed by day 26 and all of the AMF control mice succumbed by day 25. Modeling with Kaplan-Meier statistics showed no significant difference between any of these groups. The AMF treatment mice survived substantially longer, with mice lasting until 33.5 days. The survival of the AMF treatment group was shown to be significant against all control groups ($p<0.005$ for all comparisons). The average increase in survival *versus* tumor control for the nanoparticle treatment group was 7 days, a 31% increase in life expectancy post tumor insertion.

Discussion

Here we have shown that tumor-homing cells can specifically deliver MNP for AMF therapy, and this treatment can significantly prolong the lives of mice bearing deep and disseminated intraperitoneal pancreatic tumors. MNP were loaded into Mo/Ma cells which we demonstrated to be tumor homing cells. The Mo/Ma cells were injected i.p. into tumor bearing mice and trafficked specifically to the tumor. Three days later, the mice were exposed to AMF, which caused the nanoparticles to generate heat, leading to localized hyperthermia.
We found that the mouse monocytes homed effectively to the pancreatic tumors after i.p. administration. This is not surprising because monocytes and/or macrophages are often found as tumor-associated cells. Rat monocytes were shown to efficiently invade rat glioma spheroids *in vitro*, and peritoneal macrophages specifically migrated to rat gliomas after intravenous or intracarotid administration [140, 141]. Interestingly, in this case, the mouse monocytes physically migrated only to the tumors within the peritoneal cavity, while normal tissues did not contain monocytes.

Classically, hyperthermia kills tumor tissue by heating proteins and other macromolecules to the point of denaturing faster than the cell can renature them. Since the

system demonstrated here was substantially effective with only 4 μg of iron injected into the mouse per treatment cycle, other mechanisms of action may be present. The nanoparticle control group demonstrates that the nanoparticles themselves do not have any treatment value; similarly, the AMF control group demonstrates that AMF treatment does not have any stand-alone value. The Mo/Ma control group demonstrates that the Mo/Ma neither increase nor decrease tumor growth. Thus, AMF activation of the MNP is primarily responsible for the effect. Low grade hyperthermia has been shown to recruit various immune cells including dendritic cells, natural killer (NK) cells, neutrophils, and cytotoxic T cells [148-156]. Although future studies need to be done, this or another similar mechanism may have greatly increased the effectiveness of the treatment and could explain why such a low dose of MNP can effect such a large survival advantage. We are currently investigating potential mechanisms involved in mediating the survival extension, and those results will be described in a subsequent report.

Conclusion

In this report, we have described the development of a localized hyperthermia treatment using tumor-tropic cells, monocyte/macrophage-like cells, to deliver MNP for AMF activation . The system we describe here holds potential for further development as a specific delivery method for MNP-generated localized hyperthermia for targeted therapy of pancreatic and other types of cancer.

Figure 3-1 MNPs toxicity and loading studies on RAW 264.7 Mo/Ma cells

Mo/Ma were cultured overnight in increasing concentrations of nanoparticles. The next morning cells were washed and assayed. **A**. Toxicity of Nanoparticles: Cells were assayed for viability using MTT. **B**. Loading of Nanoparticles: Cells were assayed for iron content using the ferrozine assay. **C**. Percent of Cells Loaded: Cells were assayed for increased side scatter using flow cytometry. Error bars are standard deviation.

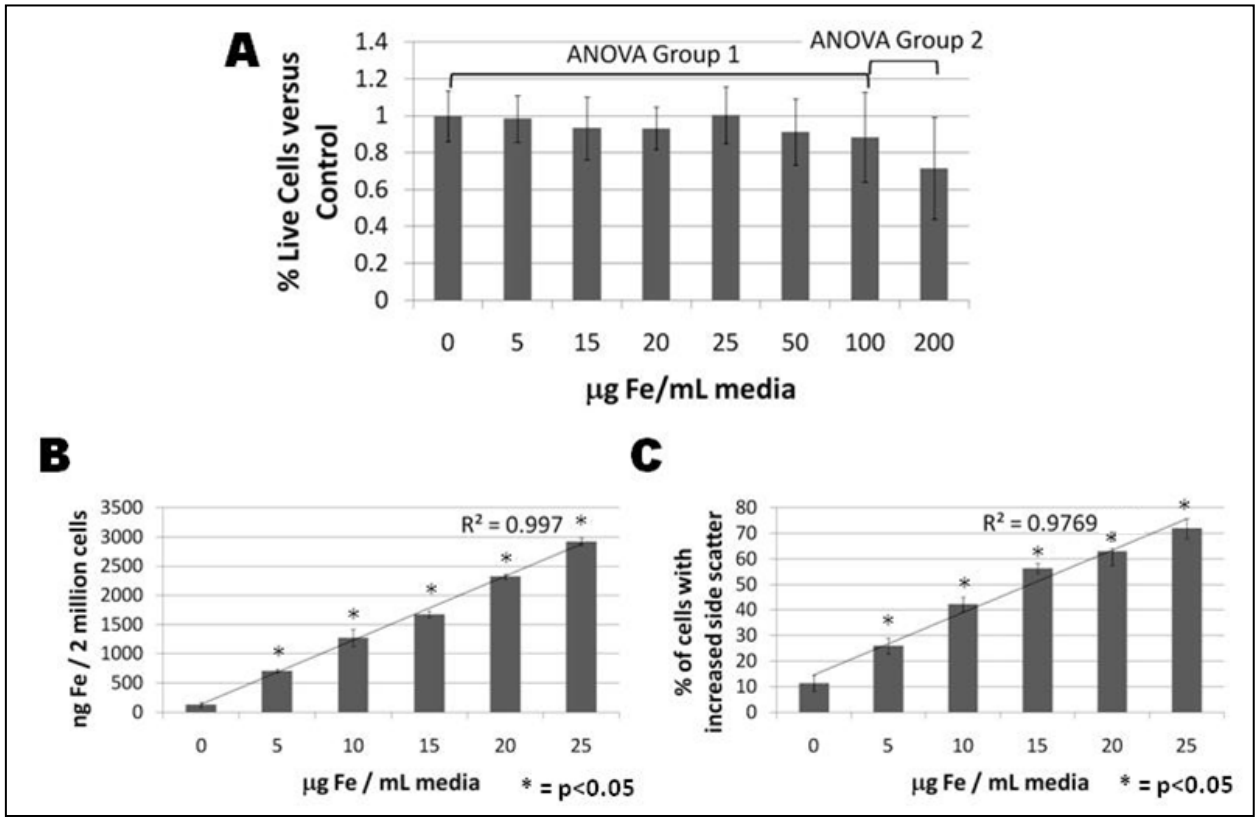

Figure 3-2 RAW 264.7 Mo/Ma homing studies on PanO2 pancreatic tumors

PKH26 labeled monocytes were injected i.p. into mice bearing i.p. Pan02 tumors. A-F. Mice were euthanized three days after monocyte injection and organs were harvested and imaged for PKH26 (monocytes). Representative images are shown. A. Tumor 10x; B. Tumor 40x; C. Pancreas; D. Kidney; E. Liver; F. Lung. G-L. Mice were euthanized six days after monocyte injection and organs were harvested and imaged for PKH26 (monocytes). Representative images are shown. G. Tumor (note healthy pancreas at the top left); H. Tumor; I. Pancreas; J. Kidney; K. Liver; L. Lung. Blue is DAPI (nuclear counterstain), Red is PKH26 (monocytes). All scale bars are 100 □m, objective is 20x unless otherwise specified.

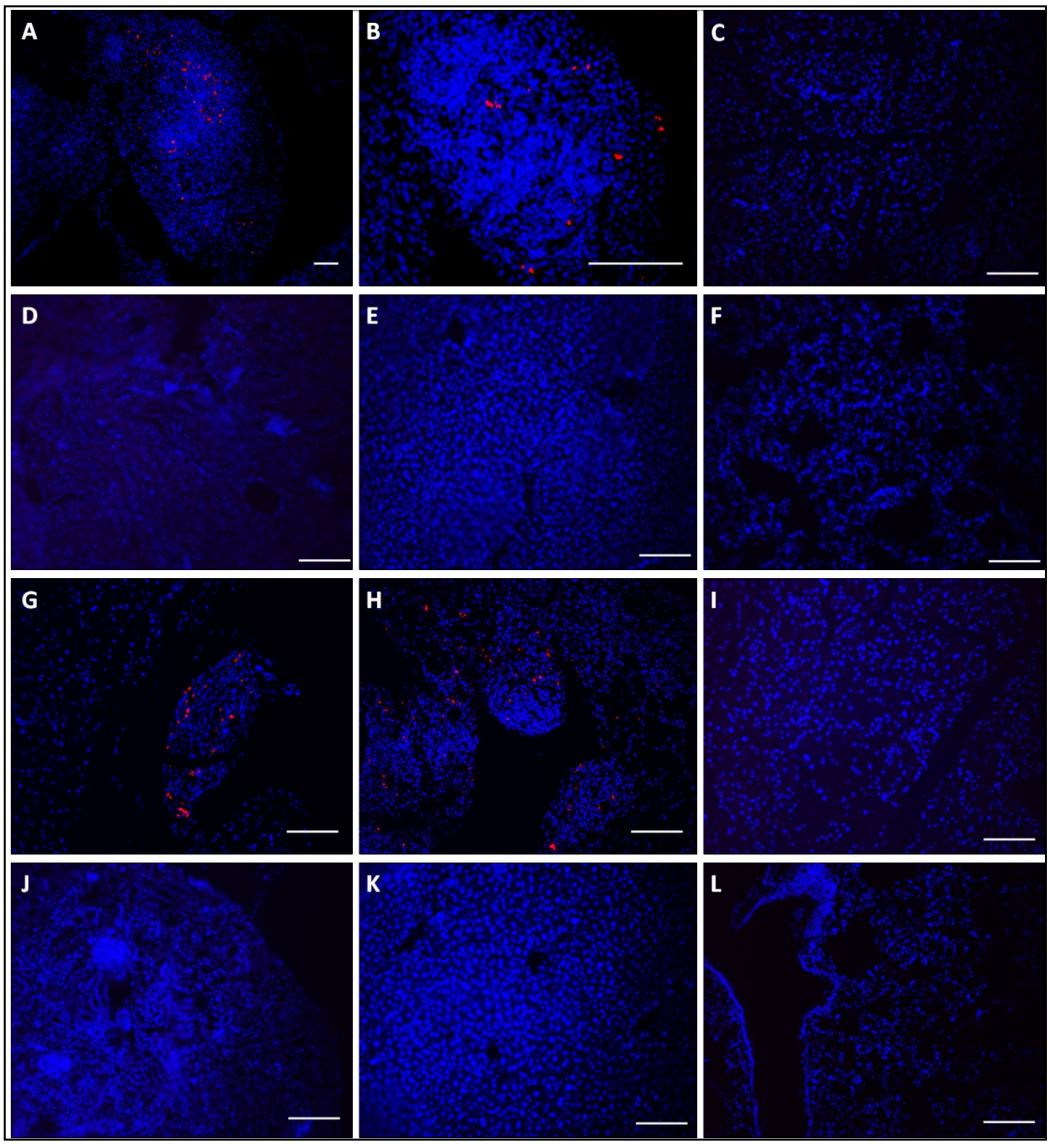

Figure 3-3 Mo/Ma infiltration into Pan02 tumors.

A, B. Mo/Ma loaded with PKH26 were injected into mice bearing i.p. Pan02 tumors. Six days later mice were euthanized and tumors were harvested. **A**. Dapi counterstained section shows Mo/Ma labeled with PKH26 in tumor. Blue = Dapi, Red = PKH26 (Mo/Ma). **B**. H&E staining of serial sections shows irregular morphology demonstrating that the targeted area is a tumor. Scale bars = 100 μm. **C**. Mo/Ma loaded with Dapi were injected into mice bearing Pan02(fluc) tumors. Five days later mice were euthanized and tumors were harvested. Sections were stained with rabbit anti-firefly luciferase and DyLite649-goat anti rabbit. Immunohistochemistry verifies that the Mo/Ma infiltrate pancreatic tumors. Blue = Dapi (Mo/Ma), Red = DyLite 649 (Pan02 cells). Scale bar = 100 μm.

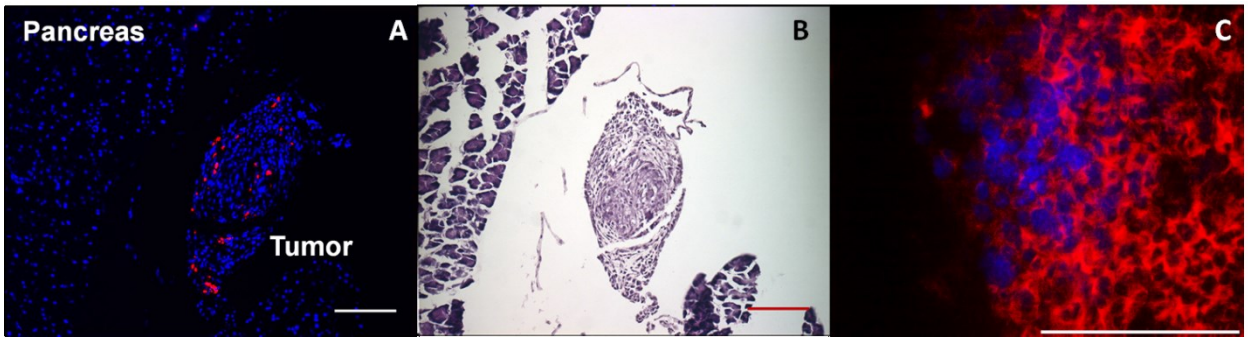

Figure 3-4 Heat generation by nanoparticle loaded Mo/Ma

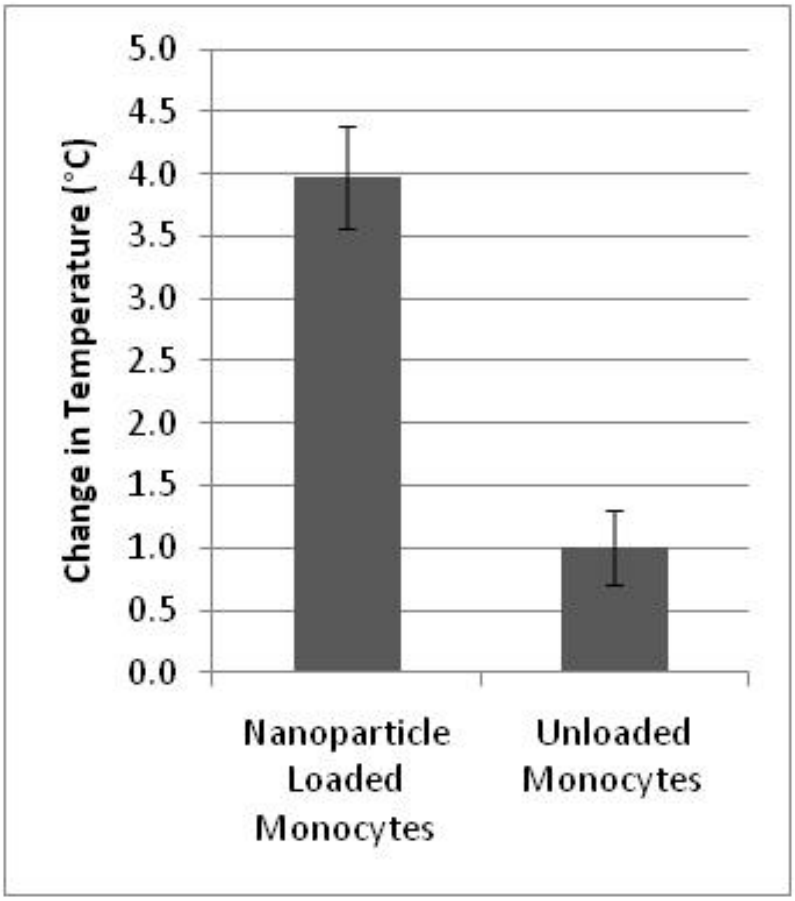

Figure 3-5 Survival study after Mo/Ma (MNP) mediated AMF treatments

A. *In vivo* experiment design, B. Duration to Clinical Symptoms ('Survival'). Mice were treated and monitored as described. Mice were euthanized when they displayed clinical signs of cancer and the day/time was recorded (n=5 or 6 for each group). $p<0.005$ for AMF treatment versus all other groups.

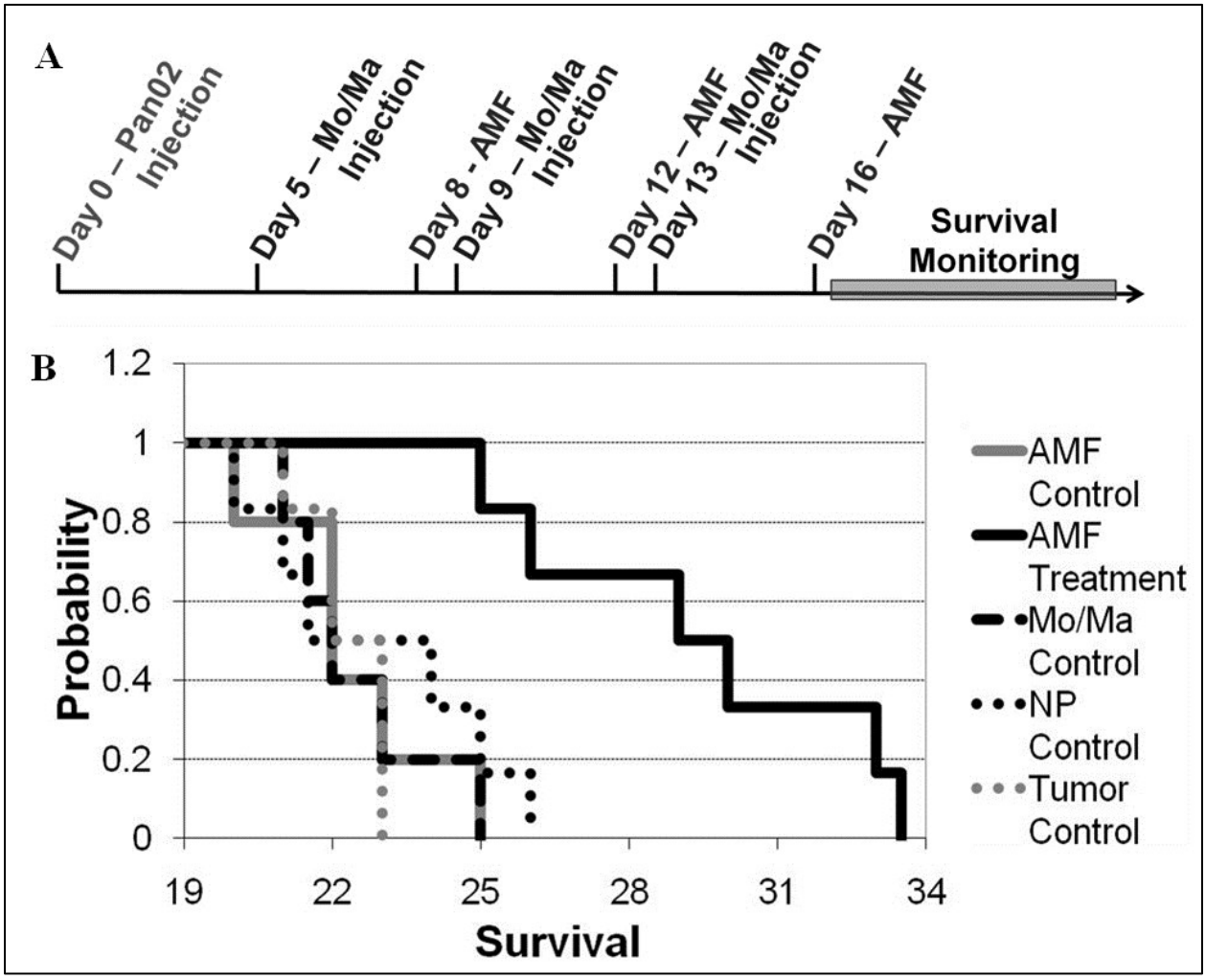

Chapter 4 - Cell surface engineering: Designing and engineering tumor homing cells expressing GPI anchored uro-kinase (uPA) and calpain protease cleavable prostate cancer cell specific recombinant caspase3 V266ED3 therapeutic protein

Sivasai Balivada[1], Marla M. Pyle[1], Tej B. Shrestha[1], Matthew T. Basel[1], Hamad Alsheitaiwi[1], Stefan H. Bossmann[2] and Deryl L. Troyer[1]

[1]Department of Anatomy and Physiology, Kansas State University, Manhattan, KS

[2]Department of Chemistry, Kansas State University, Manhattan, KS

Abstract

Engineered tumor homing cell mediated targeted delivery of therapeutic proteins has been shown to be a potential cancer treatment in pre-clinical studies. This treatment approach depends on homing ability and distribution of engineered cells in tumor microenvironment. By designing therapeutic chimeric proteins that have tumor microenvironment specific activity, increased tumor targeting could be achieved. This report demonstrates design and *in vitro* testing of a chimeric therapeutic protein that has properties such as apoptosis inducing (Caspase3 V266ED3), prostate cancer cell (CaP) specificity (CaP1 targeting peptide), tumor protease specificity (Urokinase and calpain cleavable)- rCasp3V266ED3. By engineering tumor homing cells expressing this protein on their membrane (cell surface engineering) different levels of treatment specificity that depends on complex characteristics of cancer cells/ tumor microenvironment may be attained. In this report, the hypothesized membrane anchored chimeric protein (rCasp3V266ED3, rMcherry red) plasmids were constructed, membrane anchoring and activity of designed proteins were confirmed in RAW264.7 Mo/Ma and HEK293 cells *in vitro* and potential problems that are associated in testing this system were identified.

Introduction

Prostate cancer is the second leading cancer causing death of men in the USA [157]. Available chemotherapeutics for late stage metastatic prostate cancer only have modest improvements in survival of patients [158, 159]. Cell based therapeutics for cancer treatment becoming a viable treatment approach, because of the targeting ability that can be achieved through cells [8]. Many different cells are known to have migratory properties towards tumors through complex tumor specific cytokines sensing and response systems [5, 9, 12]. By engineering these tumor trophic cells to secrete anti-cancer therapeutics, different research groups have shown reliable pre-clinical results supporting the cell based therapeutic approach [22-25, 27, 47, 111, 114, 121]. Specificity of an anti-cancer protein secreting, cell mediated therapeutic approach depends on the homing ability of the cells towards tumors and distribution of cells and secreted anti-tumor protein in the tumor environment [8]. Rapidly developing engineering approaches to manipulate cells are helping in design more sophisticated cell based therapeutics [8, 160]. By controlling the expression of anti-tumor therapeutics in delivery cells with cancer microenvironment specific promoters, more targeting can be achieved [13] . At the same time by designing chimeric therapeutic proteins that have tumor microenvironment dependent activity, increased tumor targeting can potentially be attained.

Caspase3 V266ED3 is a mutant Caspase 3 protein that has apoptosis inducing properties and could be used as therapeutic protein [161, 162]. In the present study, chimeric therapeutic protein (rCasp3V266ED3) containing properties such as apoptosis inducing (Caspase3 V266ED3), prostate cancer cell (CaP) specificity (CaP1 targeting peptide), tumor proteases specificity (Urokinase and calpain clevable) was designed [163, 164]. By engineering tumor homing cells expressing this protein on their membrane (cell surface engineering) different levels of treatment specificity that dependent on complex characteristics of cancer cells/ tumor microenvironment can potentially be attained. The designed therapeutic protein sequence with assigned specificities is shown in Figure 4-1. Targeting levels that may be possible with this hypothesized system are as follows; 1. Migration of engineered tumor homing cells towards tumors, 2. Urokinase/Urokinase plasminogen activator (uPA) mediated cleavage and release of chimeric protein that is present on tumor homing cells into tumor microenvironment, 3. CaP1 prostate cancer cell specific targeting peptide mediated uptake of chimeric protein into prostate cancer cells and 4. Calpain mediated release of Caspase3 V266ED3 protein inside prostate

cancer cells and apoptosis. In this report, two hypothesized membrane anchored chimeric protein (rCasp3V266ED3, rMcherry red) plasmids were constructed, membrane anchoring and the activity of designed proteins were analyzed in RAW264.7 Mo/Ma and HEK293 cells. Further, Urokinase (tumor specific protease) mediated cleavage and release of chimeric protein was tested.

Materials and Methods

Reagents and cells

Raw264.7 and HEK293 cells were purchased from ATCC (Manassas, VA). Dulbecco's Modified Eagle's Medium (DMEM), Roswell Park Memorial Institute medium 1640 medium (RPMI 1640), penicillin (10,000 units/mL)/streptomycin (10,000 µg/mL) were purchased from Life Technologies (Grand Island, NY). Fetal bovine serum (FBS), Glutamax, Sodium pyruvate, Trypsin- ethylenediaminetetraacetic acid (EDTA), Phospholipase C- Phosphoinositidyl specific enzyme (PI-PLC), were purchased from Sigma-Aldrich (St. Louis, MO). Turbofect transfection reagent was purchased from Thermo scientific. Rediplate 96 Enz check caspase-3 assay kit, pVac1-MCS plasmid, Alexa fluor 568 goat anti-rabbit secondary antibody and Alexa fluor 488 goat anti-mouse secondary antibody were purchased from Invitrogen (Eugene,OR). Rabbit monoclonal antibody to Caspase-3 was purchased from Abcam. Rabbit anti mcherry Ab was purchased from Biovision. HRP conjugated goat anti-rabbit was purchased from Millipore. Beta actin antibody was purchased from Fritzgerald (Acton,MA). Recombinant human Urokinase plasminogen activator (rhUPA) was purchased from R&D systems (Minneapolis, MN). Native membrane protein extraction kit was purchased from Calbiochem. Fluorescence measurements for DEVD assay and mcherry red were conducted by using an IVIS lumina-II imaging system (Perkin-Elmer).

Cell culture

RAW264.7 cells were cultured in phenol red free RPMI medium containing 10% FBS, with 1% penicillin/ streptomycin in a 37°C humidified incubator with 5% CO_2. HEK293 cells were cultured in phenol red free DMEM medium containing 10% FBS, 1x sodium pyruvate, 1x Glutamax with 1% penicillin/ streptomycin in a 37°C humidified incubator with 5% CO_2. PC3

prostate adeno carcinoma cells were cultured in F12-K medium containing 10%FBS with 1% penicillin/ streptomycin in a 37°C humidified incubator with 5% CO_2.

Recombinant gene design (in silico) and designed plasmids preparation

Recombinant Caspase-3V266ED3 (rCasp3V266ED3) gene was designed in CLC work bench software. The constitutively active human Caspase 3 V266ED3 gene sequence was used as the main back bone in gene design [161, 162]. Literature referenced urokinase plasminogen activator (uPA) cleavage site (SGRSA) [165] and calpain (PLFAER) [166] cleavage site amino acid sequences were reverse translated into DNA sequences *in silico*. Calpain cleavage site DNA sequence was attached to N-terminal side of Caspase 3 V266ED3 sequence and uPA cleavage site DNA sequence was attached to C-terminal side of Caspase 3 V266ED3 sequence. Prostate cancer specific targeting peptide-1 (Cap1) (SGESVQVKSTKIG) DNA sequence was attached before calpain cleavage site DNA sequence.Cap1 prostate cancer specific peptide was identified in Dr. Eskew lab in KUMC by using peptide phage display against human prostate cancer cell line PC3 (not yet published). Bam H1, EcoR1 restriction sites were attached at 5' and 3' respectively for sub-cloning into pVac1- MCS vector. Complete rCasp3V266ED3 gene sequence with its estimated protein sequence was shown in Figure 4-1. Recombinant mcherry red (rMcherry red) gene was designed in the same way as explained above, but instead of Caspase 3 V266ED3 gene sequence Pubmed referenced mcherry red sequence was used. Designed rCasp3V266ED3 and rMcherry red sequences containing PUC19 vectors were purchased from Genescript and sub cloned into pVac1-MCS vector by restriction digestion and ligation.

Constructed pVac1- rCasp3V266ED3 (Figure 4-2A) and pVac1-rMcherry red plasmids were confirmed by using EcoR1 and BamH1 restriction double digestion and digested products size verification (Figure 4-2B). IL-2 signal sequence and the glycosylphosphatidyl inositol (GPI) anchoring domain of human PLAP of pVac1-MCS plasmid helps in expressed rCasp3V266ED3 protein secretion and cell membrane anchoring. Constructed pVac1- rCasp3V266ED3 plasmid map and predicted rCasp3V266ED3 protein tertiary structure was shown in Figure 4-2A and C.

rCasp3V266ED3 protein expression studies on Raw 264.7 Mo/Ma cells

Testing rCasp3V266ED3 protein expression mediated toxicity

To check designed rCasp3V266ED3 expression mediated toxicity, Raw 264.7 Mo/Ma cells were transfected with pVac1- rCasp3V266ED3 plasmid by using Turbofect transfection reagent following manufacturer's protocol. 24 and 48 hours after transfecion, cell viability was analyzed by using trypan blue counting. Un-transfected (No transfection), Turbofect added and pVac1-rMcherry red transfected cells were used as controls for relative comparison of live cell numbers.

Membrane anchored rCasp3V266ED3 protein expression confirmation

To confirm designed rCasp3V266ED3expression and membrane anchoring Raw 264.7 Mo/Ma cells were transfected with pVac1-rCasp3V266ED3 plasmid. 24-48 hrs after transfection cells were incubated with 1:50 Rabbit monoclonal antibody against human Caspase3 (Abcam) (Assuming Caspase3 antibody can attach to rCasp3V266ED3 protein) for 1hour after 4%paraformaldehyde fixation and blocking. After primary antibody incubation, transfected cells were incubated with Alexa fluor 568 goat anti-rabbit secondary antibody (Molecular probes-1µg/mL) for 1hour. Nuclei were counterstained with 2µg/mL Hoechst 33342. Un-transfeted and secondary antibody treated cells were used as controls for relative comparison. The antibody used here has no cross reactivity with mouse caspase3 and cells were not pemeabilized before primary antibody incubation (membrane immunostaining).

Direct co-culture of rCasp3V266ED3 expressing Mo/Ma cells with PC3 cells

PC3 cells were known to secrete uPA into their culture medium [167]. Based on the proposed hypothesis direct co-culture of PC3 cells with rCasp3V266ED3 expressing Mo/Ma cells should lead to release of rCasp3V266ED3 protein from Mo/Ma cells and should show toxicity on PC3 cells. To test this, Raw 264.7 Mo/Ma cells were transfected with pVac1-rCasp3V266ED3 plasmid and co-cultured with PC3 cells in 1:1 ratio cell number. PC3 cells co-cultured with un-transfected Mo/Ma and pVac1-rMcherryred transfected Mo/Ma cells were used as controls for cell viability comparison. Cell viability was analyzed by using MTT assay after 48 and 72 hrs of co-culture

rhUPA treatment on rCasp3V266ED3 protein expressing Raw 264.7 Mo/Ma cells and DEVD assay

Based on design of the protein, urokinase treatement should cleave the membrane attached rCasp3V266ED3 protein and release it from the cells. To check this hypothesis Raw 264.7 Mo/Ma cells were transfected with pVac1-rCasp3V266ED3 plasmid. 24-48 hrs after transfection cells were washed with 1xPBS and assay buffer containing 10mM Trisc-Cl pH7.4/0.25M sucrose/10mM glucose for three times. Around 200,000 cells were suspended in 50µL of assay buffer containing 1.5units of recombinant human urokinase plasminogen activator (rhUPA) and incubated for 1.5hrs at 37˚C in incubator. After incubation, cells were spun at 12000g and supernatant were collected. Collected supernatants DEVD activity was measured by using Rediplate 96 Enz check caspase-3 assay kit by following manufacturer's protocol. pVac1-rCasp3V266ED3 transfected but rhUPA untreated and Un-transfected rhUPA treated or untreated Mo/Ma cells were used as controls for this experiment.

Total cell protein rCasp3V266ED3 protein activity confirmation

Caspase-3 V266ED3 protein is known to have DEVD peptide cleavage ability [161]. To check DEVD peptide cleavage activity Raw 264.7 Mo/Mo cells were transfected with pVac1-rCasp3V266ED3 plasmid. 24-48 hrs after transfection and total cellular proteins from 6 $x10^6$ transfected cells were separated and DEVD activity was measured by using Rediplate 96 Enz check caspase-3 assay kit following manufacturer's protocol. Ac-DEVD-CHO was used as a blocker control for the assay. Un-transfected cell protein test of DEVD activity was used as controls for relative comparison. At the same time to check the kit working capacity, doxorubicin treated PC3 cells proteins were used as positive control.

rCasp3V266ED3 protein expression studies on HEK293 cells

Testing rCasp3V266ED3 protein expression mediated toxicity

To check designed rCasp3V266ED3 expression mediated toxicity, HEK293 cells were transfected with pVac1- rCasp3V266ED3 plasmid by using Turbofect transfection reagent following manufacturer's protocol. 24 -48 hours after transfecion, cell viability was analyzed by using trypan blue counting. Un-transfected (control), pVac1-MCS (empty vector) and pVac1-rMcherry red transfected cells were used as controls for relative comparison of live cell numbers.

rCasp3V266ED3 protein activity confirmation

To check DEVD peptide cleavage activity, HEK293 cells were transfected with pVac1-rCasp3V266ED3 plasmid. 24-48 hrs after transfection total cellular proteins from 2 x10^6 transfected cells were separated and protein concentration estimated. DEVD activity was measured by using Rediplate 96 Enz check caspase-3 assay kit following manufacturer's protocol, For each sample ~130µg of protein was used. Ac-DEVD-CHO was used as a blocker control for the assay and pVac1-MCS (empty vector) transfected HEK293 cell proteins DEVD activity was used as control for relative comparison. Protein samples were immunoblotted with Caspase 3 antibody after DEVD assay. The same blots were re-blotted with β-actin antibody for relative protein amount comparison.

Membrane anchored rCasp3V266ED3 protein expression and activity confirmation

To confirm designed rCasp3V266ED3 membrane expression and activity, HEK293 cells were transfected with pVac1-rCasp3V266ED3 plasmid. 24 -48 hours after transfection membrane proteins were separated by using Calbiochem proteo extract native membrane protein extraction kit following manufacturer's protocol. Separated proteins were concentrated by using Millipore amicon filters and protein concentration was estimated. ~50µg membrane protein DEVD activity was measured by using Rediplate 96 Enz check caspase-3 assay following manufacturer's protocol. Un-transfected (control), pVac1-MCS (empty vector) transfected HEK293 cells membrane proteins were used as controls for relative comparison. Protein samples were immunoblotted with Caspase 3 antibody after DEVD assay.

rhUPA or PLC treatment on rMcherry red protein expressing HEK293 cells

Based on design of the rMcherry red protein, urokinase treatement or Phospholipase (PLC) treatment should cleave the membrane attached rMcherry red protein and release it from the cells. To check this hypothesis HEK293 cells were transfected with pVac1-rMcherry red plasmid. 24-48 hrs after transfection cells were washed with 1xPBS and assay buffer (10mM Trisc-cl pH7.4/0.25M sucrose/10mM glucose) for three times. 200,000 cells were resuspended in 50µL of above mentioned buffer and 1unit of rhUPA or 1 unit of PLC was added to cells and incubated for 1.5hrs at 37˚C in incubator. After incubation, cells were spun at 12000g and supernatant were collected. Collected supernatant fluorescence was measured. pVac1-rMcherry red transfected rhUPA untreated and Un-transfected rhUPA treated/untreated HEK293 cells were

used as controls for relative supernatant fluorescence comparison. Same above experiment was repeated with 400,000 and 800,000 transfected cells.

rCasp3V266ED3 protein expression studies on PC3 cells

PC3 cells were known to secrete uPA into their culture medium[167]. Based on the proposed hypothesis, membrane expressed rCasp3V266ED3 should be cleaved from the membrane and should show toxicity on PC3 cells after pVac1-Casp3V266ED3 transfection. To test this concept, PC3 prostate carcinoma cells were transfected with pVac1-rCasp3V266ED3 and 24-48hrs after transfection cell viability was analyzed by using trypan blue counting. pVac1-rMcherryred transfected PC3 cells were used as control for comparative analysis.

Statistical analysis

Statistical analyses were performed using WinSTAT (A-Prompt Corporation, Lehigh Valley, PA). Experiments that were designed based on one factor were analyzed by using one way ANOVA with LSD post hoc analysis. Experiments that were designed based on two factors were analyzed by two way ANOVA (with interaction effect) and LSD post hoc analysis. All the bars in graphs were represented by mean ± standard error. p-Value <0.05 was considered as significant for all the analyses.

Results &Discussion

rCasp3V266ED3 protein expression studies on Raw 264.7 Mo/Ma cells

Testing rCasp3V266ED3 protein expression mediated toxicity

To determine whether rCasp3V266ED3 protein expression has any toxic effect, pVac1-rCasp3V266ED3 transfected Mo/Ma cell viability was analyzed by using trypan blue counting after 24 and 48 hrs of transfection. There is no significant difference between pVac1-rMcherry red transfected Mo/Ma and pVac1-rCasp3V266ED3 transfected Mo/Ma live cell percentage (Figure 4-3A). Although there was significant difference between un- transfected cells (No transfection) and pVac1-rCasp3V266ED3 transfected Mo/Ma live cell percentage, similar toxic effect was observed with pVac1-rMcherry red transfected Mo/Ma cells. So, the observed toxic effect could be because of plasmid DNA and tubofect polymer complex or plasmid DNA itself.

rCasp3V266ED3 protein membrane expression in pVac1- rCasp3V266ED3 transfected Mo/Ma cells were confirmed with immunocytochemistry (Figure 4-3A(b)). The antibody used here only reacts with human caspase 3 but it doesn't react with mouse caspase 3.As from the picture (Figure 4-3A(b)) very few cells were expressing rCasp3V266ED3 protein on their membrane, indicating that the transfection efficiency was very low. At the same time rMcherry red membrane expression was confirmed in pVac1- rMcherry red transfected Mo/Ma cells (Figure 4-3A(a)) by using anti mcherry red antibody. Some cells expressing rMcherry red protein (Figure 4-3A(a)- white arrows) didn't show positive for mcherry red immunocytochemistry, indicating there is difference in membrane trafficking of designed chimeric rMcherry red protein in transfected cells.

Direct co-culture of rCasp3V266ED3 expressing Mo/Ma cells with PC3 cells

PC3 cells are known to secrete uPA into their culture medium [167]Based on the proposed hypothesis, direct co-culture of PC3 cells with rCasp3V266ED3 expressing Mo/Ma cells should lead to release of rCasp3V266ED3 protein from Mo/Ma cells and should show toxicity on PC3 cells. To test this hypothesis, pVac1- rCasp3V266ED3 transfected Mo/Ma cells were directly co-cultured with PC3 cells (1:1 ratio) and cell viability was analyzed by MTT assay after 48hrs and 72hrs of co-culture. As shown in Figure 4-4 there is no significant difference between viability of PC3 cells co-cultured with Mo/Ma cells expressing rCasp3V266ED3 and PC3 cells co-cultured with Mo/Ma cells expressing rMcherry red protein. Same co-culture experiments were repeated with 1:2 ratio of Mo/Ma and PC3 cells and similar results were observed. rCasp3V266ED3 mediated toxicity depends on number of Mo/Ma cells expressing rCasp3V266ED3 protein on their membrane (transfection efficiency of pVac1-rCasp3V266ED3) and amount of uPA released by PC3 cells into culture medium. Although Figure 4-4 is opposing the proposed hypothesis, above mentioned reasons could be a potential technical problem to test the system.

rCasp3V266ED3 protein activity confirmation

To check whether the designed protein has activity or not pVac1- rCasp3V266ED3 transfected cell lysates DEVD activity was analyzed. When compared with un-transfected and pVac1- rMcherry red transfected Mo/Ma cell lysates, no significant difference in DEVD activity

was observed (Figure 4-5B cell proteins-NS). Rediplate 96 Enz check caspase-3 assay kit working efficiency was confirmed by using doxorubincin treated PC3 cell lysate proteins (Figure 4-5A) One of the possibilities for observing this result could be the low levels of the designed chimeric protein. .Lack of rCasp3V266ED3 protein activity could be because of additional sequences attached to N-terminal (Cap-1 and calpain cleavage site sequences) and C-terminal (uPA cleavage site) of Caspase3V266ED3 protein (Figure 4-1). But, predicted tertiary structure of rCasp3V266ED3 protein (Figure 4-2C) suggested that additional sequences were not interfering with Caspase3V266ED3 protein backbone.

rhUPA treatment on rCasp3V266ED3 protein expressing Raw 264.7 Mo/Ma cells and DEVD assay

Based on the design of chimeric rCasp3V266ED3, uPA treatment should lead to release of the protein from the membrane. To analyze uPA mediated release of the membrane attached protein, pVac1- rCasp3V266ED3 transfected cells were treated with rhUPA and supernatant DEVD activity was measured. Difference in DEVD activity observed between rhUPA untreated and treated Mo/Ma (pVac1- rCasp3V266ED3) cells supernatants was not significant (Figure 4-6). But there was significant difference between Mo/Ma and Mo/Ma (pVac1-rCasp3V266ED3) supernatants, possibly because of weak GPI anchoring of the designed protein.

The above rCasp3V266ED3 protein expression studies on Raw 264.7 Mo/Ma cells were confirming the designed chimeric protein membrane expression. Experiments conducted to analyze the rCasp3V266ED3 protein activity and rhUPA mediated cleavage of the membrane anchored protein didn't show any positive results supporting the proposed hypothesis. One of the strong possibilities for observing these results could be of low transfection efficiency of Mo/Ma cells (Figure 4-3B). HEK293 cells were known to have higher transfection efficiency[168], so to check the designed chimeric protein system further experiments were carried out with HEK293 cells.

rCasp3V266ED3 protein expression studies on HEK293 cells

Testing rCasp3V266ED3 protein expression mediated toxicity

To check whether rCasp3V266ED3 protein expression has any toxic effect, pVac1-rCasp3V266ED3 transfected HEK293 cell viability was analyzed by using trypan blue counting after 24-48 hrs of transfection. There was no significant difference between pVac1-rCasp3V266ED3 transfected HEK293 live cell percentage compared with other control groups (Figure 4-7). Turbofect transfection procedures were optimized with HEK293 cells to reduce the transfection mediated toxic effect observed with Mo/Ma cells (Figure 4-3A).

rCasp3V266ED3 protein activity confirmation

To check designed protein activity, pVac1- rCasp3V266ED3 transfected HEK293 cell lysates DEVD activity was analyzed. When compared with empty vector (pVac1-MCS) transfected HEK293 cell lysates, p-Value 0.1 significant difference in DEVD activity was observed (Figure 4-8 A cell type-0.1). Interestingly, blocker interaction was different with pVac1 rCasp3V266ED3 transfected HEK293 cell lysates compared to empty vector transfected cell lysates (Figure 4-8A interaction-0.05). Above samples were further analyzed with Caspase 3 western blot to confirm the presence of rCasp3V266ED3 protein in pVac1 rCasp3V266ED3 transfected HEK293 cell lysates. As shown in Figure 4-8B, no difference in caspase3 band thickness was observed between two groups on the blot.

Membrane anchored rCasp3V266ED3 protein activity and membrane anchoring confirmation

Although pVac1 rCasp3V266ED3 transfected HEK293 total cell lysates (Figure 4-8A) has increased activity, western blots of the analyzed samples didn't confirm the presence of rCasp3V266ED3 in tested samples. Designed protein is supposed to be anchored to the cell membrane through GPI linker. So, transfected cells membrane proteins were isolated and DEVD activity was measured. When compared to un-transfected and empty vector transfected HEK293 cells membrane protein, increased DEVD activity was observed in pVac1- rCasp3V266ED3 transfected HEK293 cells membrane proteins (Figure 4-9A). Caspase 3 immunoblot analysis further confirmed the presence of rCasp3V266ED3 protein in above samples (Figure 4-9B)

rhUPA or PI-PLC treatment on rMcherry red protein expressing HEK293 cells

rMcherry red protein was designed in same way as rCasp3V266ED3 chimeric protein with Cap1 peptide, calpain and uPA cleavage sites. Based on design of the rMcherry red protein, uPA treatment should lead to release of rMcherry red protein from the cell membrane. To check this hypothesis, pVac1- rMcherry red transfected HEK293 cells were treated with rhUPA enzyme and supernatants mcherry red fluorescence was analyzed. When compared with rhUPA untreated cell supernatants, no significant difference was observed in mcherry red fluorescence intensity (Figure 4-10A). A similar pattern of results were observed when repeated with increasing numbers of pVac1- rMcherry red transfected HEK293 cells (Figure 4-10B).

PLAP sa sequence in constructed pVac1- rMcherry red plasmid helps in GPI mediated membrane anchoring of the rMcherry red protein [169]. Phosphoinositidyl specific Phospholipase-C (PI-PLC) is a known enzyme that can cleave this GPI anchor and should release the membrane anchored rMcherry red protein [169]. PI-PLC mediated release of rMherry red protein from the cell membrane confirms the assay conditions and GPI anchoring. To test this, pVac1- rMcherry red transfected HEK293 cells were treated with PI-PLC and supernatant fluorescence was analyzed. When compared with PI-PLC untreated cell supernatants no significant difference was observed in mcherry red fluorescence intensity (Figure 4-10C). A similar pattern of results were observed when repeated with increasing numbers of pVac1- rMcherry red transfected HEK293 cells (Figure 4-10B). These results suggest that assay conditions should be modified to test uPA mediated release of membrane attached designed chimeric protein.

rCasp3V266ED3 protein expression studies on PC3 cells

PC3 cells were known to secrete uPA into their culture medium. Based on the proposed hypothesis membrane expressed rCasp3V266ED3 should be cleaved off from the membrane and should show toxicity on PC3 cells after pVac1-Casp3V266ED3 transfection. pVac1-rCasp3V66ED3 transfected PC3 cells didn't show any decrease in cell viability when compared with rMcherry red transfected cells (Figure 4-11). rCasp3V266ED3 mediated toxicity depends on number of PC3 cells expressing rCasp3V266ED3 or amount of the protein on their membrane (transfection efficiency of pVac1- rCasp3V266ED3) and amount of uPA released by

PC3 cells into culture medium. With these results, it is not possible to reject the proposed chimeric rCasp3V266ED3 system.

rCasp3V266ED3 protein expression studies on HEK293 cells confirmed the designed chimeric protein membrane expression and activity (Figure 4-9). But rhUPA treatment didn't lead to the release of chimeric protein from the membrane (Figure 4-10A,B). Experiments conducted with PI-PLC (Figure 4-10C,D) suggesting for the modifications in rhUPA assay system. One of the strong possibilities for observing these results could be low expression of designed chimeric proteins in analyzed cell systems. When the promoter was changed in the designed plasmids (rhEF1 to CMV promoter) increased expression of chimeric rMcherry protein was observed in HEK293 cells (Figure 4-12- qualitative observation). Retro or lenti viral transduction with engineered cell line establishment could help to achieve high expression of chimeric proteins on membrane and could help in testing the design protein system by surpassing expression mediated possibilities observed in above results.

Conclusion

In the present study, prostate cancer specific (cancer cell specific), urokinase (uPA) & calpain tumor proteases cleavable (tumor microenvironment specific) chimeric Caspase3V266ED3 (cell toxic protein/therapeutic protein) – "rCasp3V266ED3" was designed. Cell membrane anchored rCasp3V266ED3 transgene containing plasmid was constructed (pVac1-rCasp3V266ED3). Designed protein rCasp3V266ED3 membrane anchoring, toxicity and activity was confirmed by using RAW 264.7 Mo/Ma and HEK293 cells. uPA protease mediated release of membrane anchored chimeric protein was tested. Problems in low expression of designed protein and further improvements in testing this chimeric protein system were identified.

Figure 4-1 Designed rCasp3V266ED3 sequence

Designed rCasp3V266ED3 gene sequence with predicted open reading frame protein sequence, predicted sequence was confirmed by using BLAST. Targeting peptide (Cap1) and proteases (uPA and calpain) cleavage sequence sites were mentioned on top of designed DNA sequence.

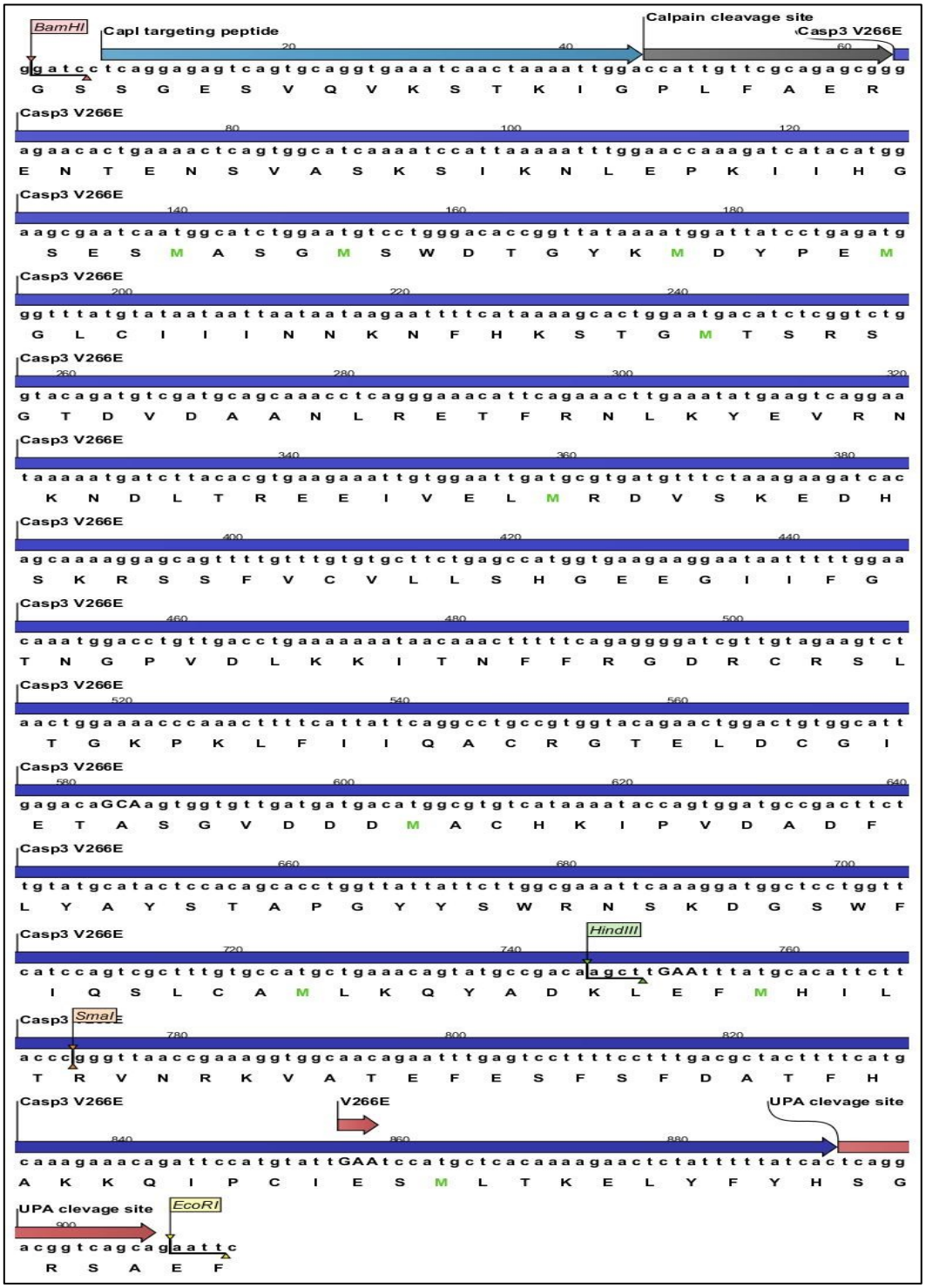

Figure 4-2 Constructed pVac1- rCasp3V266ED3 plasmid map and restriction double digestion confirmation

A. Constructed pVac1- rCasp3V266ED3 plasmid map, B. Restriction double digestion confirmation of constructed pVac1-rCasp3V266ED3 and pVac1-rMcherry red plasmids (1-1kb ladder, 2 &5 - pVac1 rMcherry red, 3&6- pVac1 rMcherry red +EcoR1-HF, 4&7- pVac1 rMcherry red +EcoR1-HF +BamH1-HF, 8 &11- pVac1 rCasp3V266ED3, 9&12- pVac1 rCasp3V266ED3+EcoR1-HF, 10&13- pVac1 rCasp3V266ED3+EcoR1-HF +BamH1-HF, 14-100bp ladder). Estimated insert sizes for pVac1 rCasp3V266ED3 and pVac1 rMcherry red are 910bps & 790bps, C. Predicted rCasp3V266ED3 protein tertiary structure indicating attached additional sequences are not interfering with Caspase3V266ED3 structure.

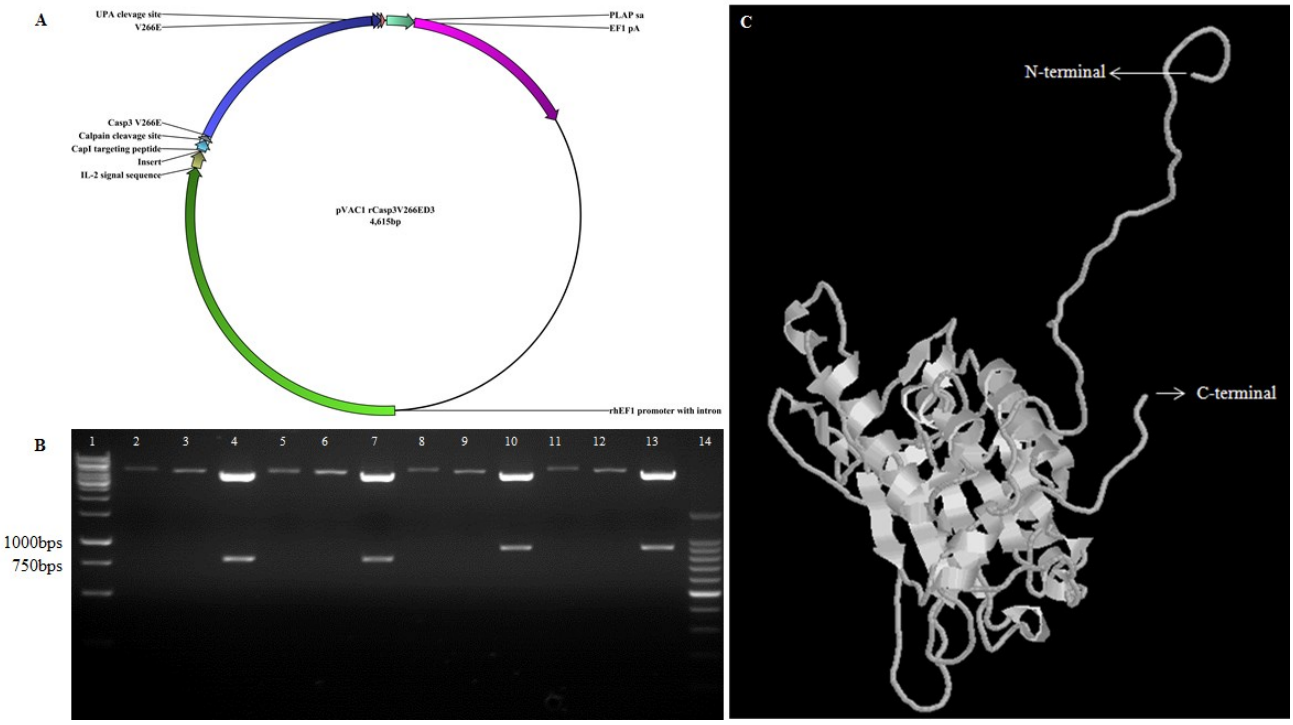

Figure 4-3 rCasp3V266ED3 expression mediated toxicity testing on RAW 264.7 Mo/Ma cells and membrane expression confirmation

A. rCasp3V266ED3 protein expression mediated toxicity on RAW264.7 Mo/Ma cells. There is no significant difference between pVac1-rMcherry red transfected Mo/Ma and pVac1-rCasp3V266ED3 transfected Mo/Ma live cell percentage, B (a).Immunocytochemistry confirmation of rMcherry red membrane expression (red bordered inlet-mcherry red fluorescence, green bordered inlet- mcherry red immuno), (b) rCasp3V266ED3 membrane expression confirmation (red bordered inlet-.Capase3 immno).

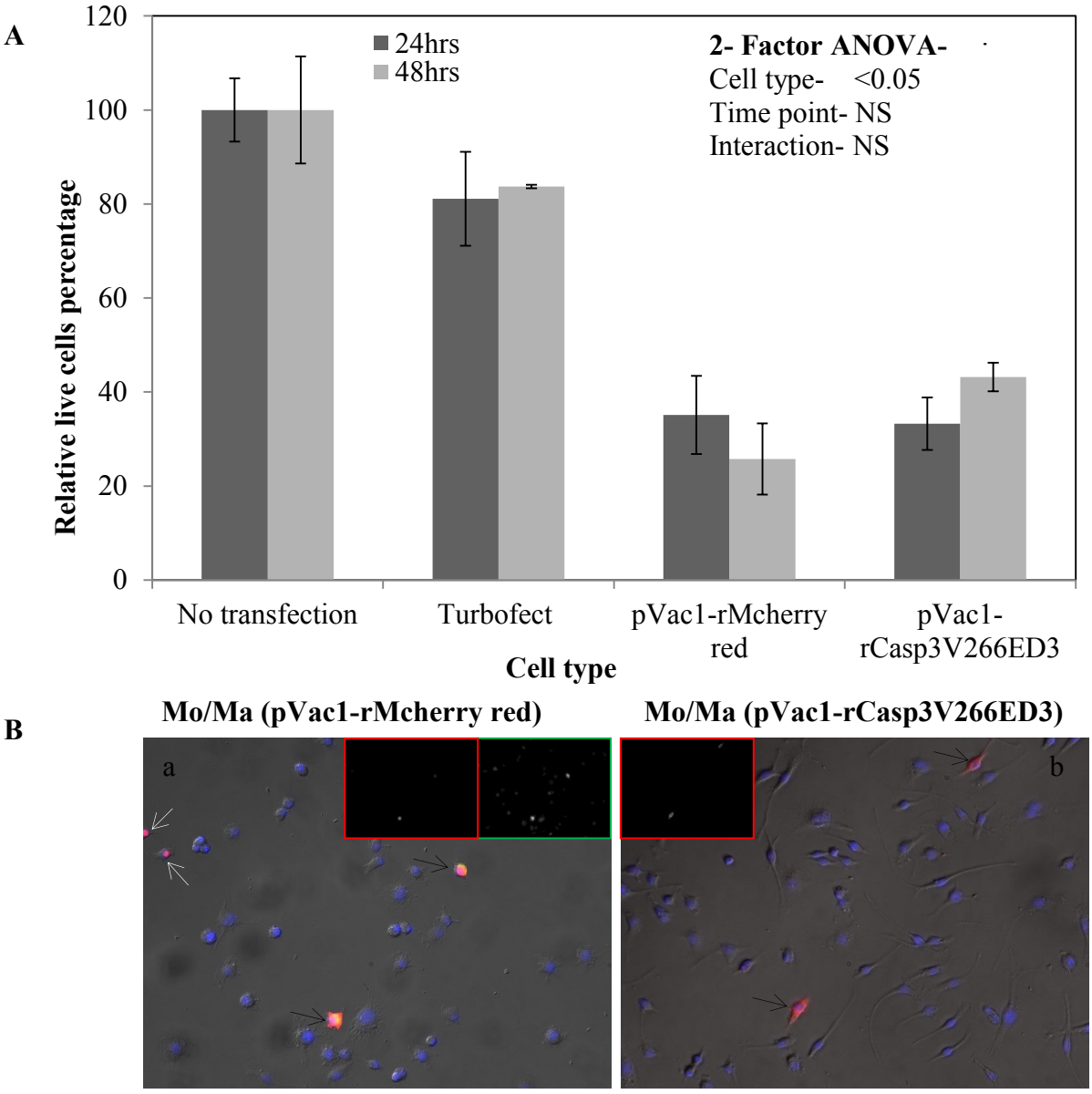

Figure 4-4 MTTcell viability analysis of PC3 cells co-cultured with rCasp3V266ED3 expressing RAW 264.7 Mo/Ma cells

Relative live cells percentage comparison between direct co-cultured PC3 cells with Mo/Ma cells after 48,72hrs. Although 2-factor ANOVA was significant, post hoc analysis didn't show any significance between PC3+Mo/Ma (pVac1-rMcherry red) and PC3+Mo/Ma(pVac1-rCasp3V266ED3).

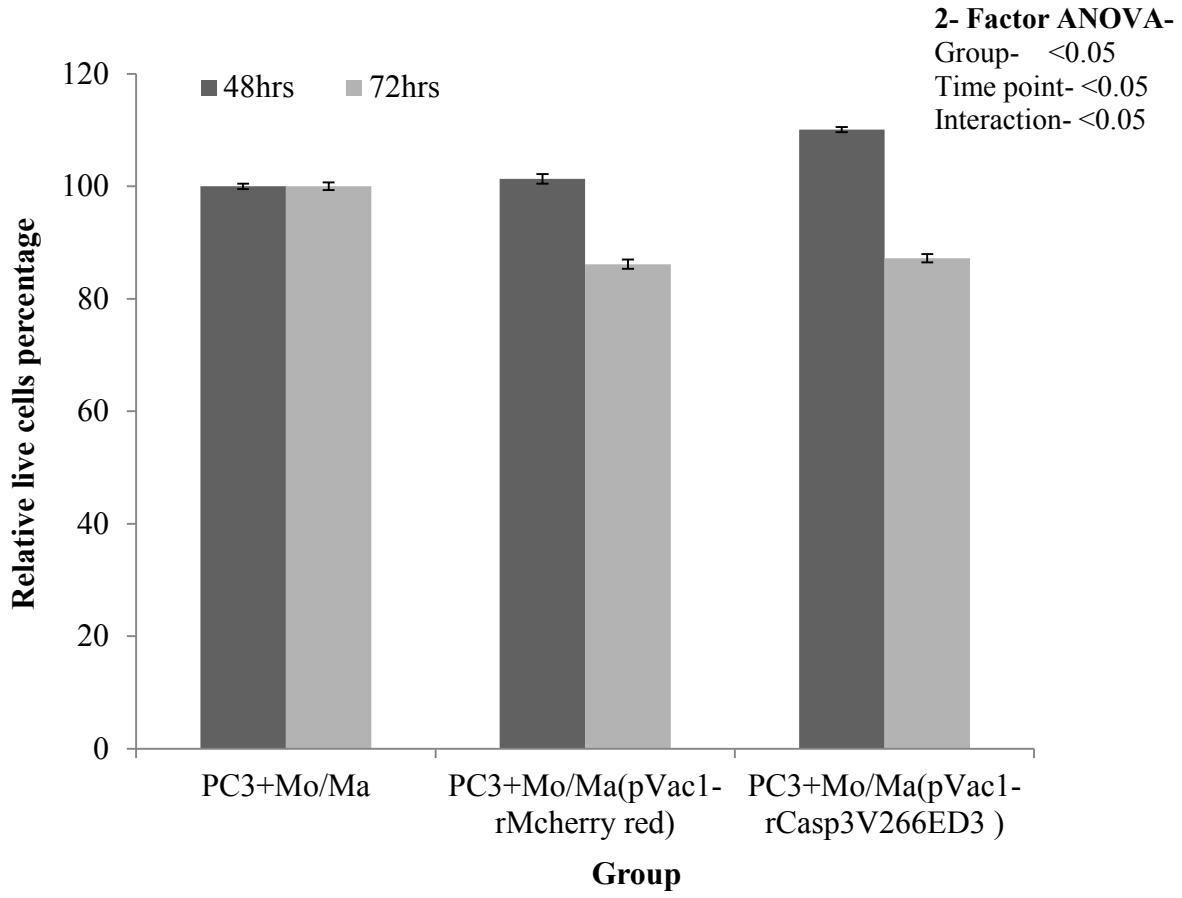

Figure 4-5 rCasp3V266ED3 expressing Mo/Ma total cell proteins DEVD assay

A. Rediplate 96 Enz check caspase-3 assay kit working efficiency confirmation, there is significant difference in DEVD activity between proteins separated from PC3 cells and proteins separated from doxorubincin treated PC3 cells confirming kit working efficiency. B.pVac1-rCasp3V266ED3 transfected Mo/Ma cells total proteins don't have significant difference in DEVD activity when compared with controls.

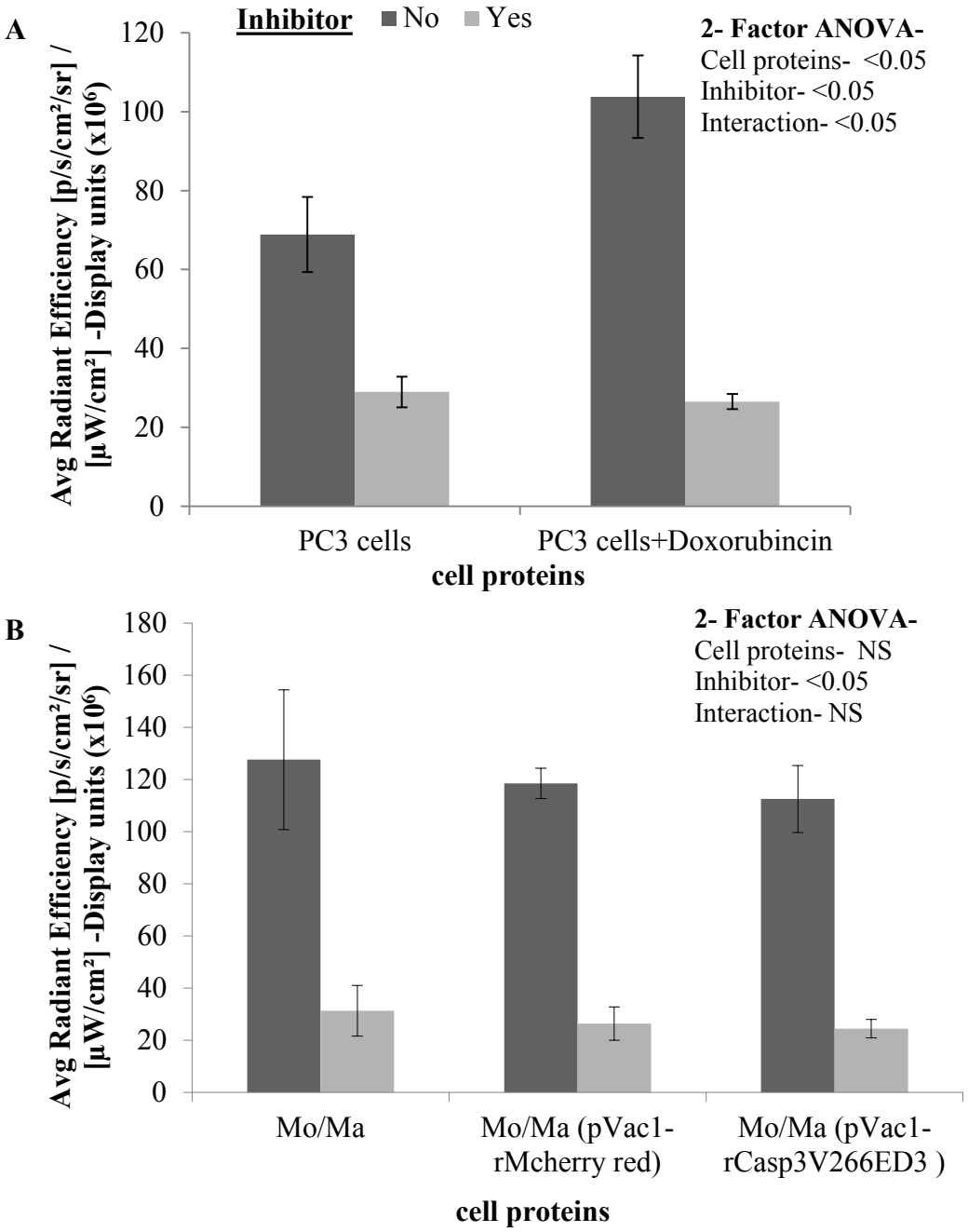

Figure 4-6 rhUPA treatment on rCasp3V266ED3 expressing Raw 264.7 Mo/Ma cells and DEVD assay

pVac1-rCasp3V266ED3 transfected Mo/Ma cells were treated with rhUPA and supernatant DEVD activity was measured and plotted. Although overall rhUPA has significant difference (rhUPA-<0.05), there is no statistically significant difference between rhUPA treated and untreated Mo/Ma (pVac1-rCasp3V266ED3), same kind of pattern was observed with rhUPA treated and untreated Mo/Ma.

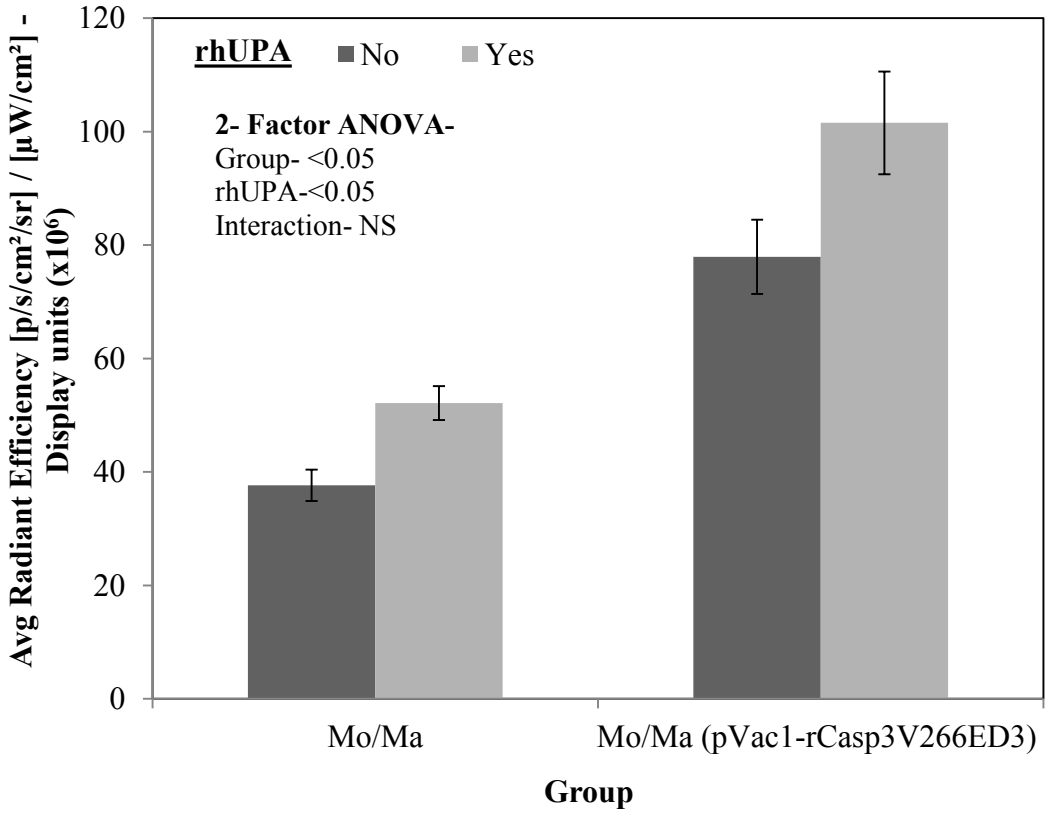

Figure 4-7 rCasp3V266ED3 expression mediated toxicity testing on HEK293 cells

There is no significant difference between pVac1-rCasp3V266ED3 transfected HEK293 live cell percentage compared with other control groups . Turbofect transfection procedures were optimized with HEK293 cells to reduce the transfection mediated toxic effect observed with Mo/Ma cells (Figure 4.3A).

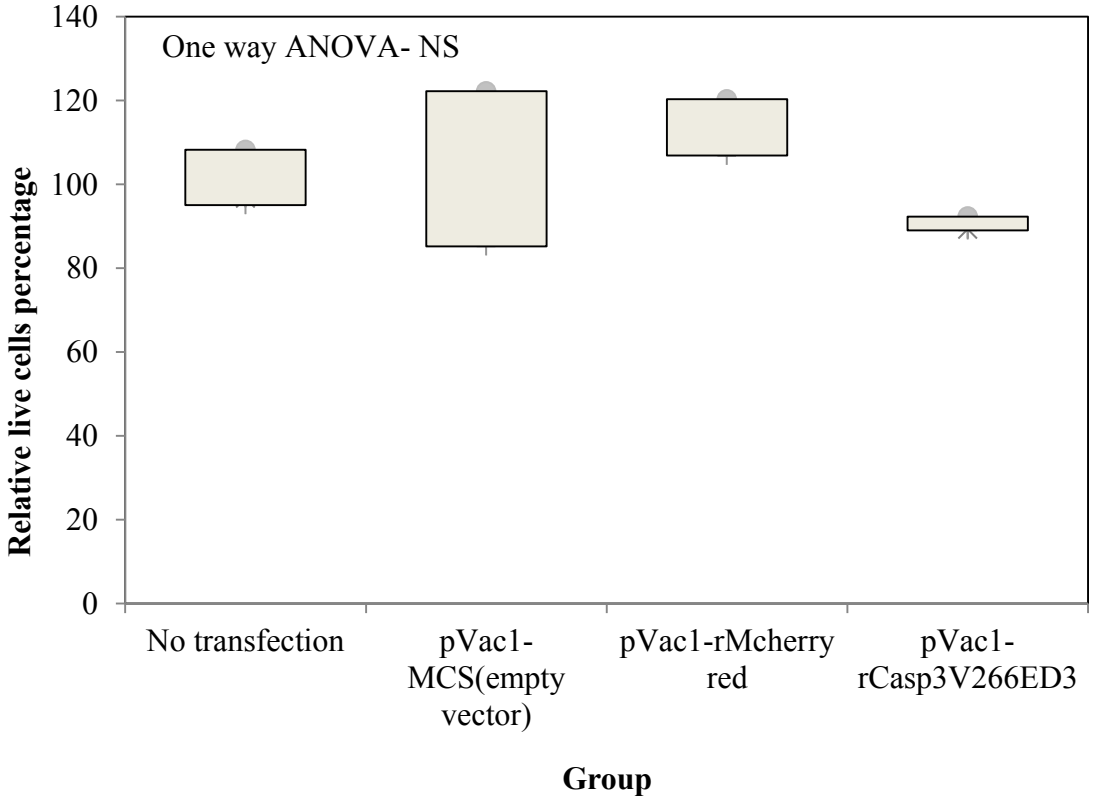

Figure 4-8 rCasp3V266ED3 protein activity confirmation

rCasp3V266ED3 expressing HEK293 total cell proteins DEVD assay A.HEK293(pVac1-rCasp3V266ED3) total cell proteins has signficant difference in DEVD activity when compared with HEK293 (pVac1-MCS) cell proteins. B. Caspase-3 westernblot on DEVD activity measured samples; 1,2,3- HEK293 (pVac1-MCS) cell protein replicates; 4,5,6- HEK293(pVac1-rCasp3V266ED3) total cell protein replicates. There is no difference in thickness of caspase-3 bands between two groups (qualitative observation).

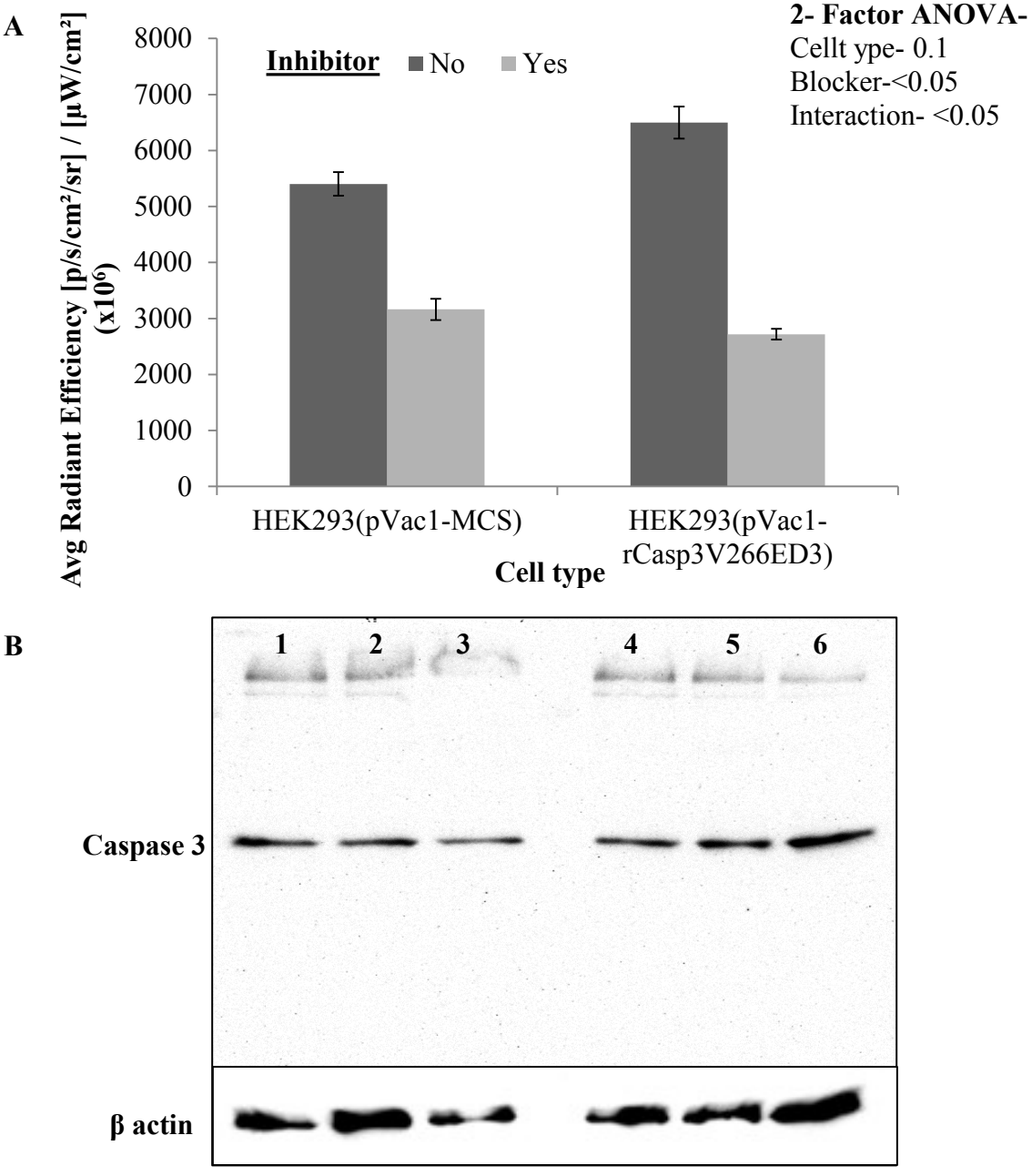

Figure 4-9 rCasp3V266ED3 membrane expression and activity confirmation on pVac1-rCasp3V266ED3 transfected HEK293 cells

A. pVac1-rCasp3V266ED3 transfected HEK293 cells membranes proteins have increased DEVD activity when compared with HEK293 or HEK293 (pVac1-MCS) membrane proteins. B. Caspase 3 westernblot on DEVD activity analyzed membrane protein samples; (1,2)- HEK293 cells membrane protein replicates, (3,4)- HEK293 (pVac1-MCS) cells membrane protein replicates, (5,6)- HEK293 (pVac1-rCasp3V266ED3) cells membrane protein replicates.

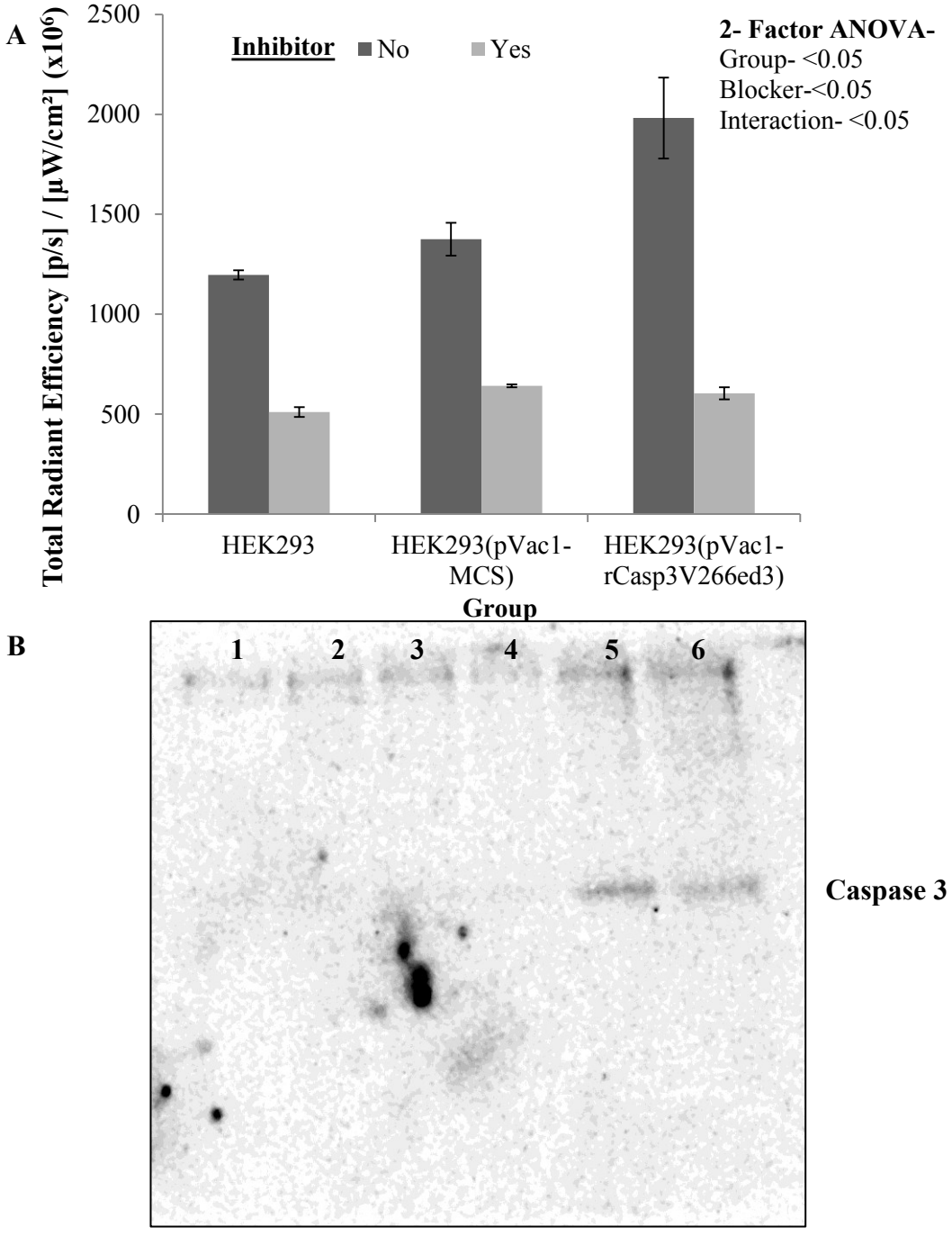

Figure 4-10 rhUPA or PI-PLC treatment on HEK293 cells transfected with pVac1-rMcherryred plasmid

A. pVac1-rMcherryred transfected HEK293 cells were treated with rhUPA and supernatant fluorescence intensity was measured and plotted. There is no difference in fluorescence intensity between rhUPA treated and untreated samples, Same pattern was observed with higher cell numbers (B). C. pVac1-rMcherryred transfected HEK293 cells were treated with PI-PLC and supernatant fluorescence intensity was measured and plotted. There is no difference in fluorescence intensity between PI-PLC treated and untreated samples, Same pattern was observed with higher cell numbers

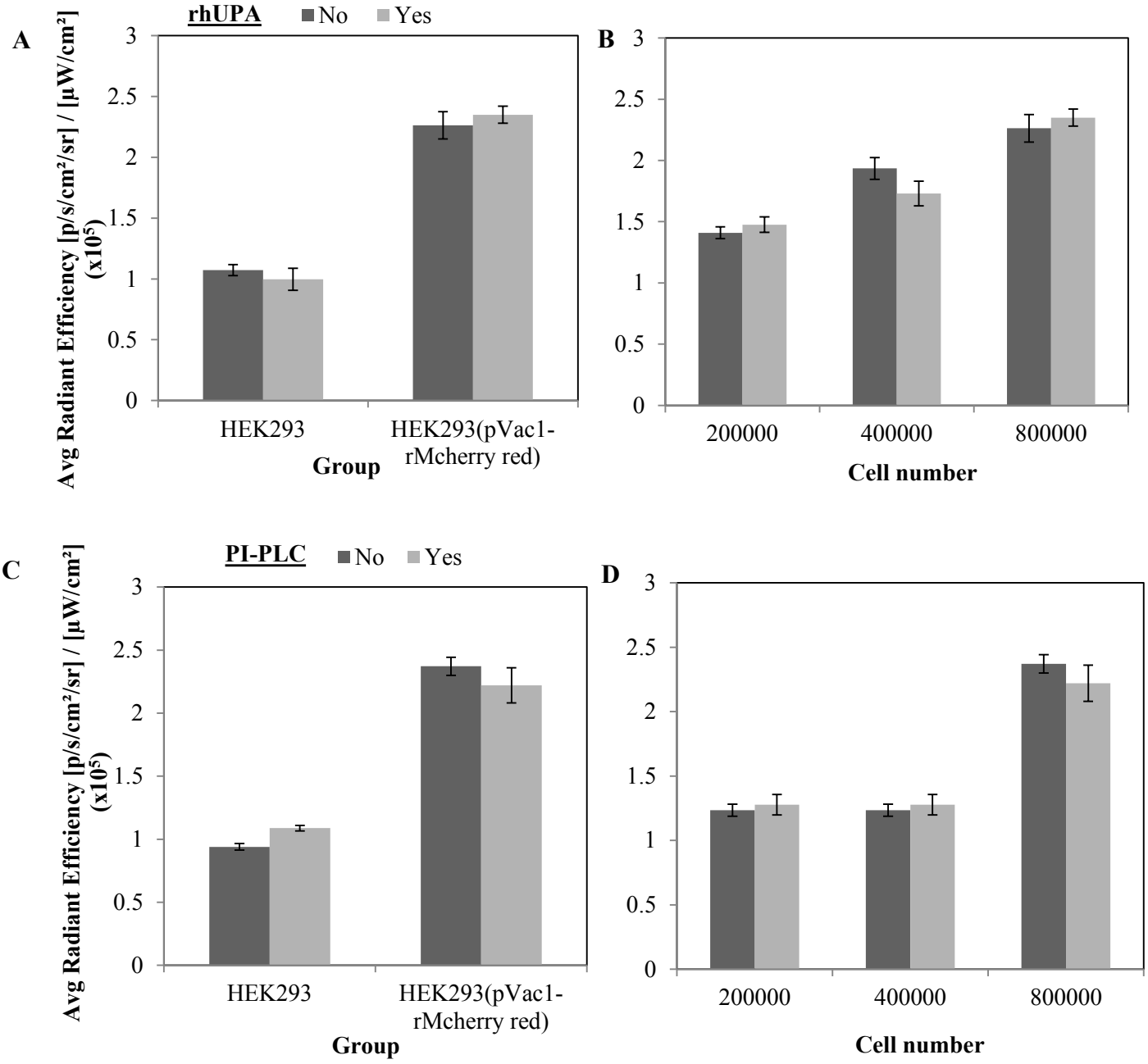

Figure 4-11 rCasp3V266ED3 expression mediated toxicity on PC3 cells

There is no significant difference in pVac1-rCasp3V266ED3 transfected PC3 cell viability when compared control (pVac1-rMcherryred transfected PC3 cells).

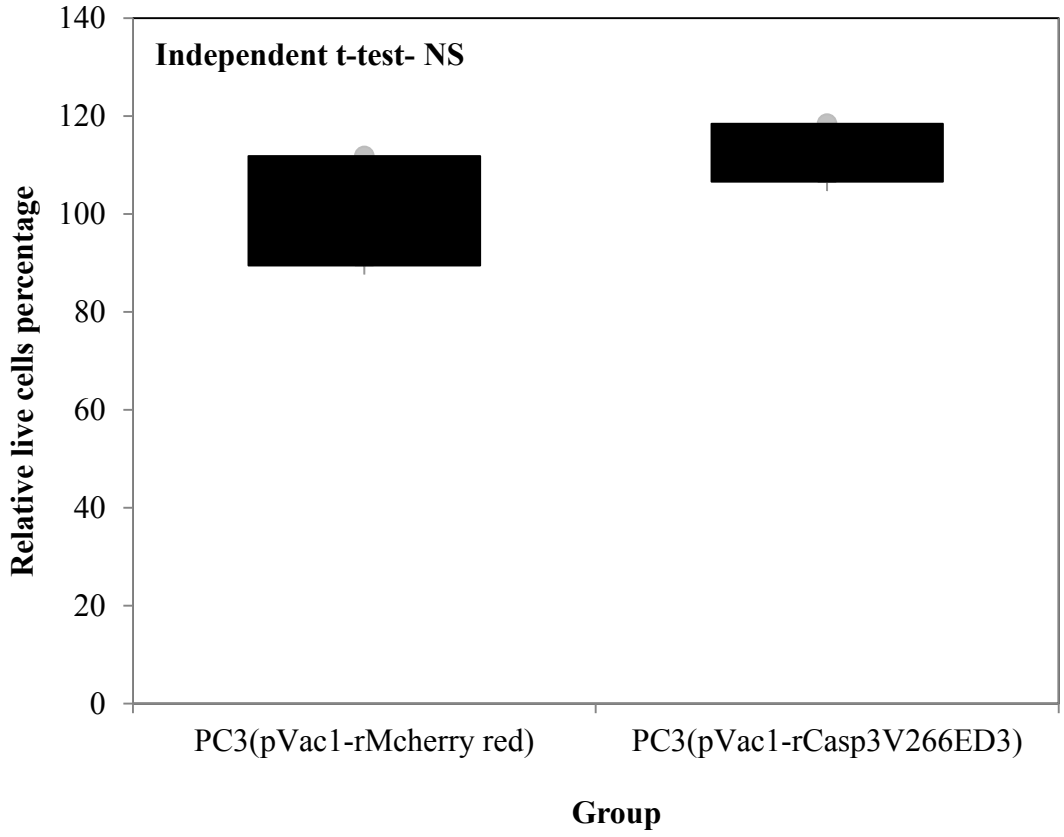

Figure 4-12 rMcherry red protein expression level difference between plasmids with different promoters

A.HEK293 cells transfected with plasmid containing rMcherry red gene under rhEF1 promoter, B. HEK293 cells transfected with plasmid containing rMcherry red gene under CMV promoter (Inlets are showing mcherry red fluorescence).

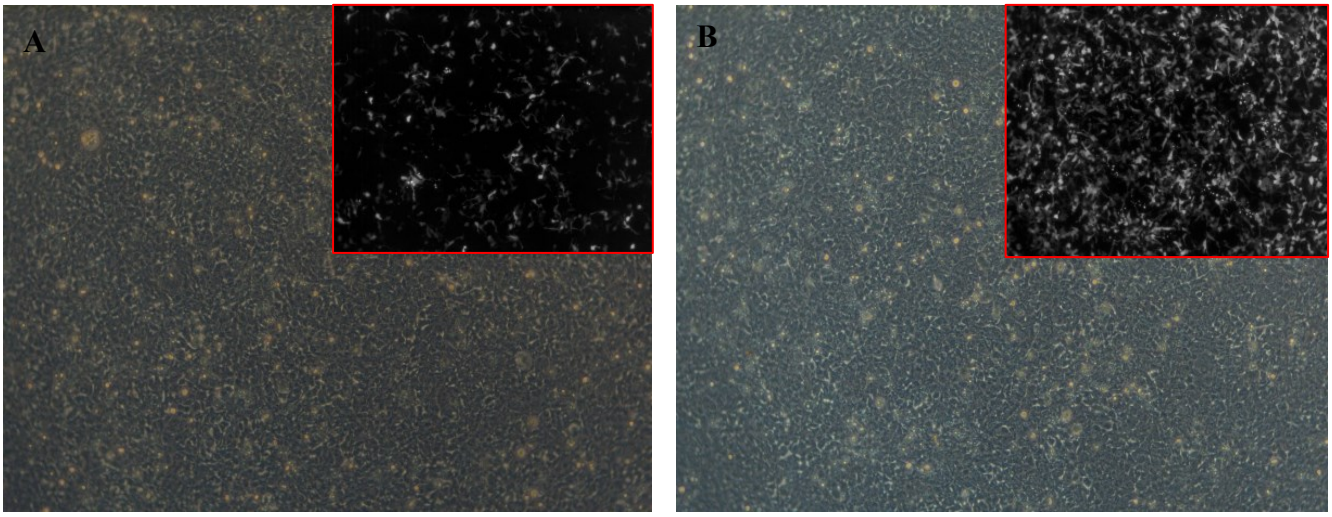

Chapter 5 - Human Xenografts Are Not Rejected in a Naturally Occurring Immunodeficient Porcine Line: A Human Tumor Model in Pigs

Matthew T. Basel[1*], **Sivasai Balivada[1*]**, Amanda P. Beck[2], Maureen A. Kerrigan[2], Marla M. Pyle[1], Carol R. Wyatt[2], Robert R. R. Rowland[2], David E. Anderson[3], Stefan H. Bossmann[4], Deryl L. Troyer[1c]

* Both of these authors contributed equally to this work

[1]Department of Anatomy and Physiology, Kansas State University, Manhattan, KS
[2]Department of Diagnostic Medicine and Pathobiology, Kansas State University, Manhattan, KS
[3]Department of Clinical Sciences, Kansas State University, Manhattan, KS
[4]Department of Chemistry, Kansas State University, Manhattan, KS

Abstract

Animal models for cancer therapy are invaluable for preclinical testing of potential cancer treatments; however, therapies tested in such models often fail to translate into clinical settings. Therefore, a better preclinical model for cancer treatment testing is needed. Here we demonstrate that an immunodeficient line of pigs can host and support the growth of xenografted human tumors and has the potential to be an effective animal model for cancer therapy. Wild-type and immunodeficient pigs were injected subcutaneously in the left ear with human melanoma cells (A375SM cells) and in the right ear with human pancreatic carcinoma cells (PANC-1). All immunodeficient pigs developed tumors that were verified by histology and immunohistochemistry. Nonaffected littermates did not develop tumors. Immunodeficient pigs, which do not reject xenografted human tumors, have the potential to become an extremely useful animal model for cancer therapy because of their similarity in size, anatomy, and physiology to humans.

Introduction

Preclinical research on animal models is essential in developing and evaluating cancer therapeutics [170]. Syngeneic, xenograft, and genetically engineered mouse models have been developed to study cancer and cancer drug development [171]. Mouse xenograft models are used extensively in preclinical studies because of their relatively good correlation with human clinical data, as compared to other animal models [172-174]. However, studies on these mouse models often fail to accurately predict the response to and the effect of anticancer agents in human patients [172-174]. Ninety percent of new anticancer drugs that showed antitumor efficacy in mouse-based preclinical studies failed in human clinical studies [173, 174]. Several methods of overcoming this shortfall have been proposed, including genetically engineered transgenic mouse models and orthotopic xenograft models [175, 176], but these have yet to demonstrate significant improvements in translatability [175].Thus, there is a tremendous demand for more sophisticated animal models, which may improve the translation efficiency from preclinical to clinical studies.

Pigs are large animals with similar anatomy and physiology to humans and have been used in many research areas [177]. The higher sequence homology of pigs with human xenobiotic receptors may allow more accurate prediction of pharmacodynamic and pharmacokinetic properties of drugs compared with mice [178]. Several attempts have been made to establish porcine tumor models in pigs as a treatment model for human cancers, for example, investigating spontaneous myelogenous leukemias [179], developing transplantable hematologic tumors [180], and genetically inducing tumorigenesis [181].

A xenograft model of human tumors in pigs would be an excellent model. Xenograft models of human tumors are often used in severe combined immunodeficiency (SCID) mice, which have severe lymphopenia due to defects in a DNA-dependent protein kinase gene that prevents variable–diversity–joining [V(D)J] gene region recombination [182]. The severe lymphopenia prevents SCID mice from rejecting human tumors. SCID-associated severe lymphopenia is also known in other species, notably humans. Several genetic defects have been identified in humans as causing SCID, including defects in adenylate kinase 2, adenosine deaminase, purine nucleoside phosphorylase, interleukin (IL)-2 receptor γ, Janus kinase 3, and the IL-7 receptor [183]. We recently identified pigs that are severely immunocompromised

(SCID-like pigs) (research paper not published yet). Yorkshire pigs bred for increased feed efficiency were noted to exhibit SCID-like symptoms. Further analysis of these pigs showed extremely decreased levels of lymphocytes in circulation and significantly atrophied thymus and lymph nodes. The mode of inheritance appears to be simple autosomal recessive, although the actual mutation remains to be elucidated. In the present study, we show evidence that these pigs can be used as human xenograft tumor models. As proof of concept, human melanoma cells (A375SM, amelanotic melanoma) and human pancreatic carcinoma cells (PANC-1) were transplanted subcutaneously into immunodeficient pigs, and the tumor-forming ability of the neoplastic cells was evaluated.

Materials and Methods

Reagents and cells

PANC-1 cells and A375SM cells were purchased from ATCC (Manassas, VA). Dulbecco's Modified Eagle's Medium (DMEM) and penicillin (10,000 units/mL)/streptomycin (10,000 μg/mL) were purchased from Life Technologies (Grand Island, NY). Fetal bovine serum (FBS), hematoxylin, eosin, Tris–hydrochloride, and ethylenediaminetetraacetic acid (EDTA) were purchased from Sigma-Aldrich (St. Louis, MO). Antimitochondrial clone 113-1 (mouse anti-human mitochondrial antibody) was purchased from Millipore (Temecula, CA). Bond Polymer Refine Red detection kit, Bond Primary Antibody Diluent, and alkaline phosphatase-conjugated Poly-AP anti-mouse antibody were purchased from Leica Microsystems (Buffalo Grove, IL). Fatal-plus (pentobarbital sodium) was obtained from Vortech Pharmaceuticals (Dearborn, MI). Banamine (flunixin meglumine) was obtained from Merck Animal Health/Intervet (Summit, NJ). Excenel (ceftiofur HCl) was obtained from Pfizer Animal Health (New York, NY). Second Bite Medicated feed with Tiamulin (35 g/ton) and chlortetracycline (400 g/ton) was purchased from Key Feeds, Fourth and Pomeroy Associates (Clay Center, KS).

Pig care

Six littermate pigs (6 weeks of age, two male and four female) were obtained from Iowa State University from a boar and a sow that have been identified as carriers of the immunodeficiency gene. Pigs were identified at 2 weeks of age as likely to be immunodeficient or immunocompetent based on lymphocyte counts: values were 1.08, 1.22, and 1.81×10^3

lymphocytes/μL for pigs expected to be immunodeficient (n=3, one male, two female) and 3.08, 4.13, and 5.18×10^3 lymphocytes/μL for presumed immunocompetent pigs (n=3, one male, two female). Pigs were transported to the Kansas State University at 6 weeks of age. Pigs were housed in a clean environment in raised pens upon arrival; however, neither the previous housing nor transportation was aseptic. Two days after arrival, blood samples were collected from the pigs to confirm the status of each pig by immunophenotyping. After confirmation of the immune status, the immunodeficient pigs were separated from the immunocompetent pigs in two different rooms in a clean environment in raised pens. Pigs were kept on a medicated diet and monitored daily for health status; ceftiofur HCl (2.2 mg/kg) and flunixin meglumine (1.1 mg/kg) were administered intramuscularly as indicated by veterinary consultation.

Xenograft tumor injection

A375SM cells and PANC-1 cells were cultured in the DMEM with 10% FBS and 1% penicillin/streptomycin. PANC-1 and A375SM cells were lifted, counted, and concentrated to 40 million cells/mL in PBS. Pigs were anesthetized by administration of isoflurane gas vaporized into oxygen (1–5%) and delivered via a face mask. 100 μL (4 million cells) of the PANC-1 cell suspension was injected subcutaneously into the right ear by tenting the skin of the ear near the base; 100 μL (4 million cells) of the A375SM cell suspension was injected subcutaneously into the left ear by tenting the skin of the ear near the base. After injecting, the pigs were removed from anesthesia and observed until reaching sternal recumbency.

After tumor injection, the pigs were monitored daily for tumor growth. Both right and left ears were visually inspected and palpated to determine presence of tumors daily. Once tumors were identified, calipers were used to measure the tumor size.

Histopathology and immunohistochemistry

Immunocompromised pigs were monitored for signs of respiratory disease, which often occurs because of the immunocompromised status. When a serious disease presented, the pigs were euthanized using Fatal-plus (days 6, 14, and 22). Unaffected littermates were euthanized with the last immunocompromised pig at day 22. At euthanasia, ear tissue was collected and fixed in 10% buffered formalin, processed routinely for sectioning, and then stained with

hematoxylin and eosin (H&E). H&E sections were evaluated for histological evidence of tumors. For immunohistochemical analysis, unstained paraffin-embedded tissue was probed with anti-human mitochondrial antibody. Tissues were stained using the Leica Bond-Max automatic stainer (Leica Microsystems) with the Bond Polymer Refine Red detection kit. Tissues were pretreated for 20 min with Tris–EDTA (pH 9.0) for antigen retrieval. The primary antibody was diluted 1:100 using Bond Primary Antibody Diluent. Tissues were then stained with the primary antibody for 15 min followed by a secondary antibody (Powervision Poly-AP Anti-Mouse) for 25 min. Antibody-probed tissues were then counterstained with hematoxylin. Antibody-probed sections were evaluated for positive staining, indicating the presence of human cells.

Results

Pig observations

No visible tumor growth was noted at day 6 when the first immunodeficient pig (pig 1) was euthanized. On day 13, a small, firm, very slightly raised, elongated white mass was identified visually and by palpation on the left ear (amelanotic melanoma) of pig 2, but was too small to measure with the caliper. Pig 2 was euthanized on day 14. On day 14, a similar small, firm, raised, elongated white mass was identified on the left ear of pig 3, but was too small to measure with the caliper. On day 20, gross photographs were taken of the mass (Figure 5-1). On day 22, pig 3 was euthanized. At postmortem examination, the tumor in the left ear (melanoma) was dissected free from the skin and measured 10.3×5.5 mm. No grossly discernible tumors were observed in the right ears (pancreatic carcinoma) of any of the immunodeficient pigs. No grossly discernible tumors were observed in either ear in the wild-type pigs.

Histopathology and immunohistochemistry

Histology and immunohistochemistry revealed the presence of tumors in all injection sites for both tumors in SCID-like pigs. Pig 1 showed small tumors in both the right ear (Figure 5-2A) and the left ear (Figure 5-3A) histologically, indicating the lack of rejection of both the PANC-1 and the ASM375 cells. These tumors were verified by strong positive cytoplasmic staining with anti-human mitochondrial antibody (Figure 5-2 B,C and Figure 5-3B,C). Pig 2 also showed tumors in both the right ear (Figure 5-2D) and the left ear (Figure 5-3D) histologically, which were verified by positive immunostaining (Figure 5-2 E,F and Figure 5-3 E,F). Pig 3 also

showed tumors in both the right ear and the left ear that were substantially larger than the tumors of pigs 1 and 2. These tumors were also identified histologically and verified by positive staining with anti-human mitochondrial antibody (Figure 5-2G-I and Figure 5-3G-I).

All six tumor sites showed characteristic histologic features of malignant neoplasia, including bizarre and atypical mitotic figures and prominent anisocytosis and anisokaryosis (Figure 5-4). No tumors were identified histologically in the ears of wild-type pigs (Figure 5-5), consistent with expected rejection of human origin cells by pigs with intact immune systems. Full histopathological descriptions of the tumors of each immunodeficient pig are as follows

Pig 1

Right ear- Focally within the subcutis is a small, unencapsulated, well-demarcated neoplasm composed of nests and packets of neoplastic cells on a fine fibrovascular stroma. Neoplastic cells are polygonal, with variably distinct cell borders and moderate-to-large amounts of pale eosinophilic vacuolated cytoplasm. Nuclei are round to oval to irregular and vesicular, with generally 1–3 prominent magenta nucleoli. Anisocytosis and anisokaryosis are moderate, and mitoses are 8 in 10 high-power fields (hpf) and occasionally bizarre. At the periphery of the neoplasm, adjacent to a small vessel, are small numbers of lymphocytes.

Left ear - Within the deep dermis, subcutis, and skeletal muscle, there is an unencapsulated, moderately demarcated and infiltrative neoplasm composed of nests and short streams of neoplastic cells on a scant fibrovascular stroma. Neoplastic cells are polygonal to spindloid, with indistinct cell borders and a small-to-moderate amount of vacuolated eosinophilic cytoplasm. Nuclei are oval to irregular, with finely stippled chromatin and 1–2 variably prominent nucleoli. Anisocytosis and anisokaryosis are mild, and mitoses are 4 in 10 hpf.

Pig 2

Right ear- Within the subcutis and skeletal muscle, there is an unencapsulated, moderately demarcated and mildly infiltrativeneoplasm composed of nests and packets of neoplastic cells on a fine fibrovascular stroma. Neoplastic cells are polygonal, with variably distinct cell borders and moderate-to-large amounts of pale eosinophilic vacuolated cytoplasm. Nuclei are round to oval to irregular and vesicular, with one generally prominent magenta nucleolus. Anisocytosis and anisokaryosis are mild to moderate, and mitoses are 1 in 10 hpf. The neoplasm is surrounded by small numbers of lymphocytes and rare plasma cells.

Left ear- Within the deep dermis and subcutis, and extending into the adjacent skeletal muscle, is an unencapsulated, moderately demarcated and mildly infiltrative neoplasm composed of nests and short streams of neoplastic cells within a moderate amount of fibrovascular stroma. Neoplastic cells are polygonal to spindloid, with indistinct cell borders and a small amount of vacuolated eosinophilic cytoplasm. Nuclei are round to oval to irregular, with finely stippled chromatin and 1–2 variably prominent nucleoli. Anisocytosis and anisokaryosis are moderate, and mitoses are 4–7 per hpf and often bizarre.

Pig 3

Right ear-Within the dermis, subcutis, and skeletal muscle, there is anunencapsulated, poorly demarcated and infiltrative neoplasm composed of nests and packets of neoplastic cells on a fine fibrovascular stroma. Neoplastic cells are polygonal, with variably distinct cell borders and a small to moderate of pale eosinophilic-to-amphophilic vacuolated cytoplasm. Nuclei
are round to oval to irregular and vesicular, with one-tomultiple variably prominent nucleoli. Anisocytosis and anisokaryosis are moderate, and mitoses are <1 in 10 hpf.

Left ear- The deep dermis and subcutis contain an unencapsulated, moderately demarcated neoplasm composed of densely packed nests and short streams of neoplastic cells within a moderate amount of fibrovascular stroma. Neoplastic cells are polygonal to spindloid, with indistinct cell borders and a small amount of vacuolated eosinophilic cytoplasm. Nuclei are round to oval to irregular, with finely stippled chromatin and 1–2 variably prominent nucleoli. Anisocytosis and anisokaryosis are moderate, and mitoses are 2–5 per hpf and often bizarre.

Discussion

A large-animal model of human tumors that closely mimics the size, anatomy, and physiology of humans would be of great value to cancer research. Here we have demonstrated that a naturally occurring immunodeficient line of pigs is capable of hosting xenograft human cells and developing active human tumors. It is possible that immunodeficient pigs fail to reject human xenograft tumors due to their low levels of lymphocytes, but immunodeficient pigs do not fail to produce all lymphocytes. Preliminary results indicate that the lymphocytes present in immunodeficient pigs do not express CD3, CD4, CD8, CD21, or CD79a. This may indicate that the remaining cells are natural killer (NK) cells that may not be functional due to lack of T-cell-associated cytokine stimulation. Therefore, there may be no functional lymphocytes that would

be able to reject the human tumor xenograft. Further studies are being done on the lymphocyte profiles in the immunodeficient pigs.

The melanoma model described here is orthotopic; the subcutaneous model of pancreatic adenocarcinoma, however, is not orthotopic. For this study, the proof of concept that immunodeficient pigs would not reject tumors was demonstrated using an easily monitored tumor location. In the future, orthotopic models of pancreatic cancer may be explored in these pigs to determine their suitability for investigating this devastating human cancer.
One of the major problems with current animal models for human tumors is the low translatability to clinical settings [174]. This is often due to the limited similarity in anatomy and physiology of common tumor models such as SCID mice [172, 174]. Because pig anatomy and physiology are very similar to that of humans, the immunodeficient pig tumor model could be used for testing multiple types of cancer therapy, including chemotherapy, radiotherapy, and surgical reduction, with more realistic results. Therefore, this model has the potential to be a valuable human cancer model for preclinical cancer research, with a high rate of translatability to the clinical settings.

The usefulness of this model may not be limited to cancer therapy. Since the immunodeficient pigs do not reject xenografts, they may be a useful model for other disease states as well. For example, human liver cell xenografts could be grown in pigs and then infected with hepatitis B or C for testing various antiviral medications. Similarly, the pigs could be reconstituted with primitive human hematopoietic stem cells (e.g., cord blood) to generate a pig chimera with a human immune system, a useful model for studies such as human immunodeficiency virus antiviral therapies. Thus, a pig model that does not reject human xenografts is a unique animal model with potential uses in a variety of preclinical applications for human health.

Figure 5-1 Antemortem visual evidence of tumor growth in pig 3 (day 20)

A. Photograph indicated a large growth on the left ear, B. Same photograph as in (A), with the growth outlined for visual reference.

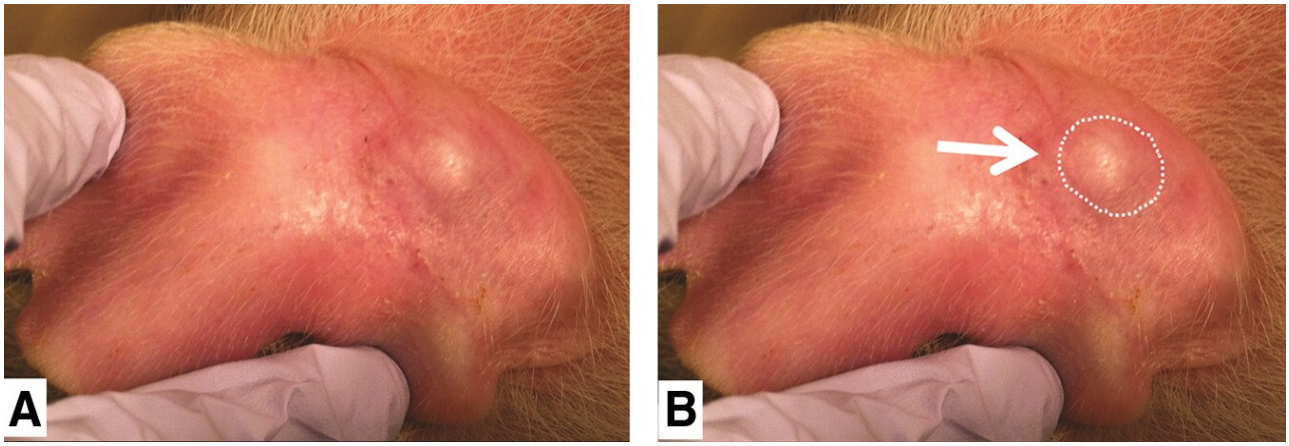

Figure 5-2 Right ear with pancreatic carcinoma cells from pigs euthanized at day-6,14,22 post-transplantation

A. There is a focal, well-demarcated, unencapsulated neoplasm composed of nests and packets of neoplastic cells within the subcutis. B, C Strong positivity to anti-human mitochondrial antibody is evident within the cytoplasm of neoplastic cells. D Within the subcutis and skeletal muscle, there is an unencapsulated, moderately demarcated, and mildly infiltrative neoplasm composed of nests and packets of neoplastic cells. E, F Strong positivity to anti-human mitochondrial antibody is evident within the cytoplasm of neoplastic cells. G Within the dermis, subcutis, and skeletal muscle, there is an unencapsulated, poorly demarcated, and infiltrative neoplasm composed of nests and packets of neoplastic cells. H, I Strong positivity to anti-human mitochondrial antibody is evident within the cytoplasm of neoplastic cells. (A, D, G) H&E stain; (B, C, E, F, H, I) anti-humanmitochondrial antibody immunohistochemistry. H&E, hematoxylin and eosin.

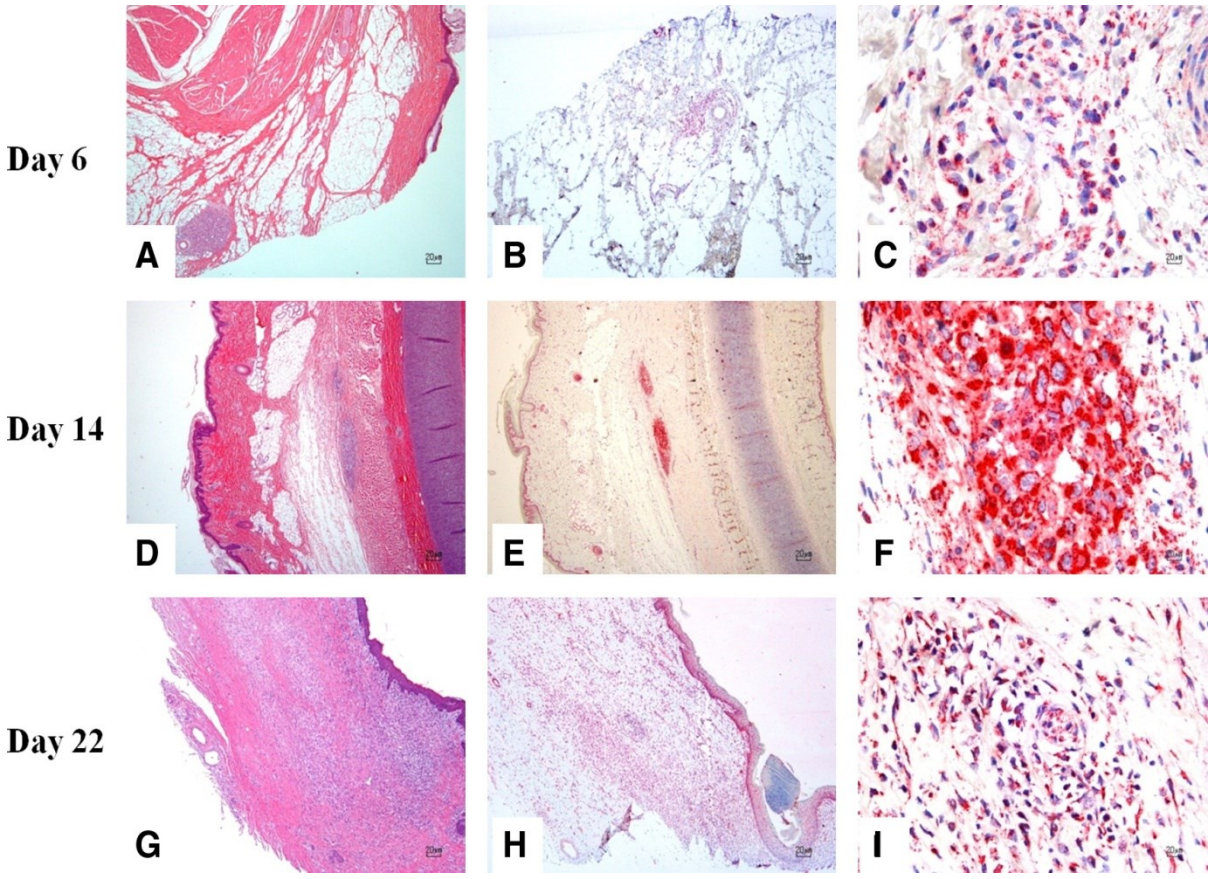

Figure 5-3 Left ear with melanoma cells from pigs euthanized at day 6, 14, and 22 post-transplantation

(A) Within the deep dermis, subcutis, and skeletal muscle, there is an unencapsulated and infiltrative neoplasm composed of nests and short streams of neoplastic cells. (B, C) Strong positivity to anti-human mitochondrial antibody is evident within the cytoplasm of neoplastic cells. (D) Within the deep dermis and subcutis, there is an unencapsulated and infiltrative neoplasm composed of nests and short streams of neoplastic cells within a moderate amount of fibrovascular stroma. (E, F) Strong positivity to anti-human mitochondrial antibody is evident within the cytoplasm of neoplastic cells. (G)Within the deep dermis and subcutis, there is an unencapsulated, moderately demarcated, and infiltrative neoplasm composed of nests and short streams of neoplastic cells within a moderate amount of fibrovascular stroma. (H, I) Strong positivity to anti-human mitochondrial antibody is evident within the cytoplasm of neoplastic cells.(A, D, G) H&E stain;(B, C, E, F, H, I) anti-human mitochondrial antibody immunohistochemistry.

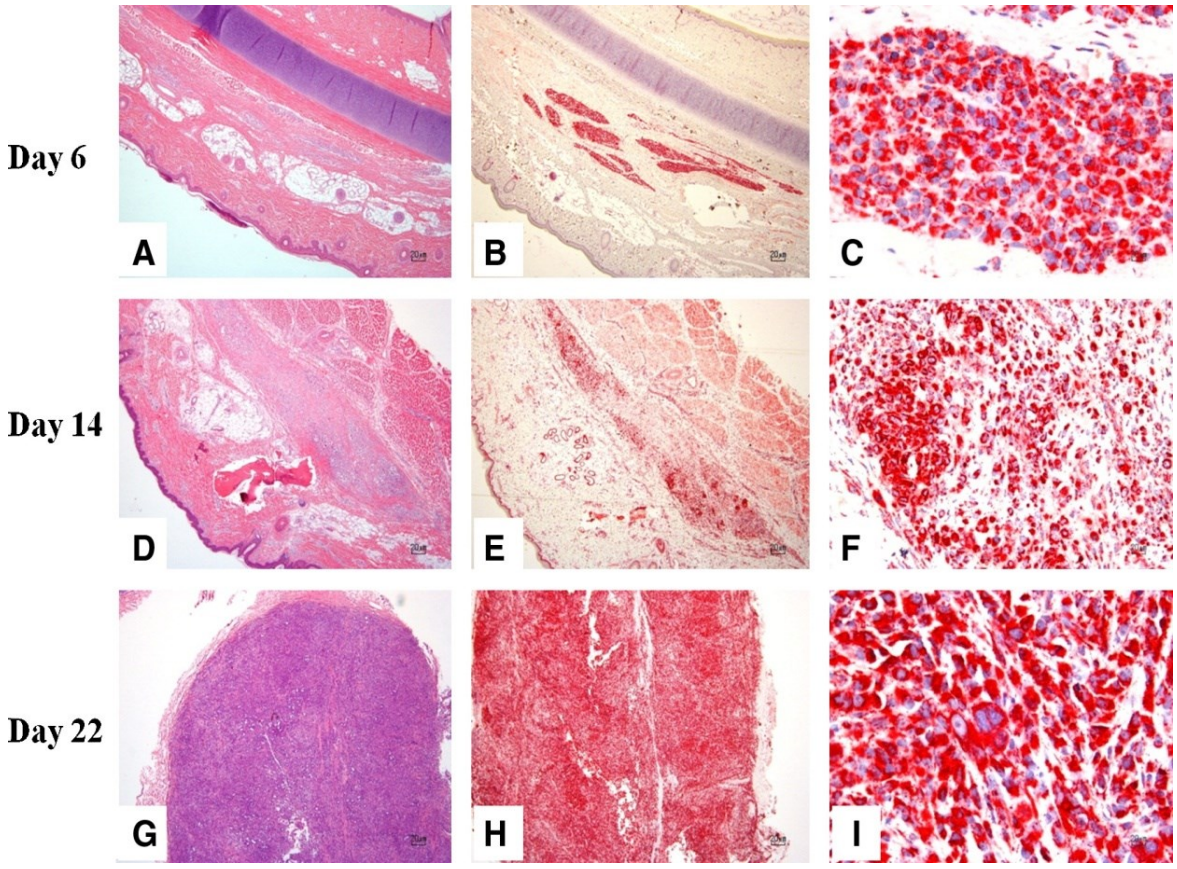

Figure 5-4 Photomicrographs of the left ear of pig 3 demonstrating histologic features of neoplasia

(A) Note multiple mitotic figures. (B) Note significant cellular and nuclear pleomorphism. H&E stain.

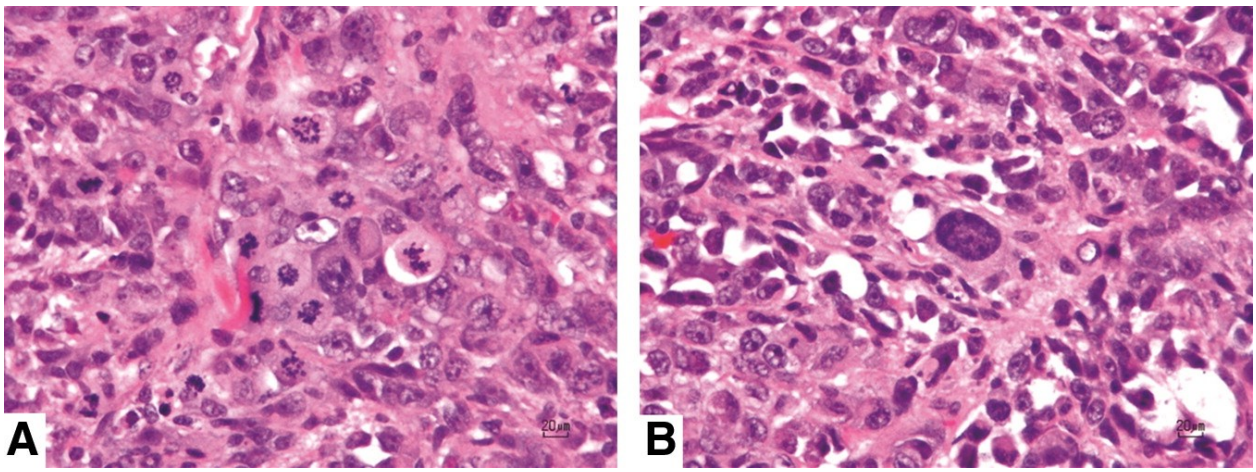

Figure 5-5 Wild type pigs ears histological analysis

Right ear (A) and left ear (B) from control pigs at day 22. No tumors were identified at the site of injection ofhuman-origin neoplastic cells. H&E stain.

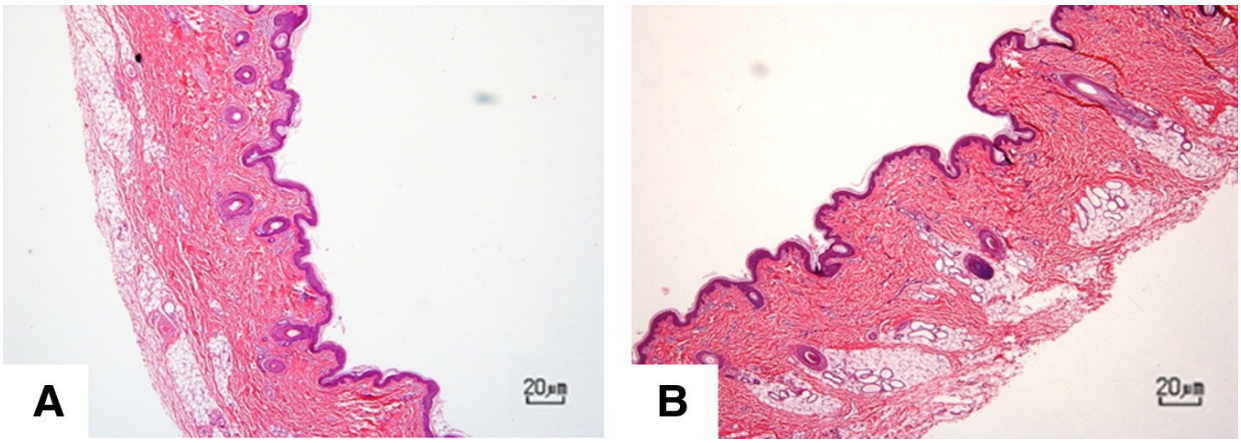

References

1. *World health organization Cancer key facts*. 2008 [cited; Available from: http://www.who.int/mediacentre/factsheets/fs297/en/.
2. Hanahan, D. and R.A. Weinberg, *Hallmarks of cancer: the next generation.* Cell. **144**(5): p. 646-74.
3. Hornberg, J.J., et al., *Cancer: a Systems Biology disease.* Biosystems, 2006. **83**(2-3): p. 81-90.
4. Weinberg, R.A., *The biology of Cancer*. 2 ed. 2013: Garland sciences.
5. Hanahan, D. and L.M. Coussens, *Accessories to the crime: functions of cells recruited to the tumor microenvironment.* Cancer Cell. **21**(3): p. 309-22.
6. DeVita, V.T., Jr. and S.A. Rosenberg, *Two hundred years of cancer research.* N Engl J Med. **366**(23): p. 2207-14.
7. Mukherjee, S., *The Emperor of All Maladies: A Biography of Cancer*. 2011.
8. Fischbach, M.A., J.A. Bluestone, and W.A. Lim, *Cell-based therapeutics: the next pillar of medicine.* Sci Transl Med. **5**(179): p. 179ps7.
9. Studeny, M., et al., *Mesenchymal stem cells: potential precursors for tumor stroma and targeted-delivery vehicles for anticancer agents.* J Natl Cancer Inst, 2004. **96**(21): p. 1593-603.
10. Aboody, K.S., et al., *Development of a tumor-selective approach to treat metastatic cancer.* PLoS One, 2006. **1**: p. e23.
11. Keung, E.Z., P.J. Nelson, and C. Conrad, *Concise review: genetically engineered stem cell therapy targeting angiogenesis and tumor stroma in gastrointestinal malignancy.* Stem Cells. **31**(2): p. 227-35.
12. Aboody, K.S., et al., *Neural stem cells display extensive tropism for pathology in adult brain: evidence from intracranial gliomas.* Proc Natl Acad Sci U S A, 2000. **97**(23): p. 12846-51.
13. Muthana, M., et al., *Use of macrophages to target therapeutic adenovirus to human prostate tumors.* Cancer Res. **71**(5): p. 1805-15.
14. Eisenstein, S., et al., *Myeloid-derived suppressor cells as a vehicle for tumor-specific oncolytic viral therapy.* Cancer Res. **73**(16): p. 5003-15.
15. Su, W., et al., *Human Embryonic Stem Cell-Derived Endothelial Cells as Cellular Delivery Vehicles for Treatment of Metastatic Breast Cancer.* Cell Transplant.
16. Dranoff, G., *Cytokines in cancer pathogenesis and cancer therapy.* Nat Rev Cancer, 2004. **4**(1): p. 11-22.
17. *Using mesenchymal stem cells to home in and deliver anti-tumor therapy with interferon-beta.* Cancer Biol Ther, 2004. **3**(12): p. 1192.
18. Seo, K.W., et al., *Anti-tumor effects of canine adipose tissue-derived mesenchymal stromal cell-based interferon-beta gene therapy and cisplatin in a mouse melanoma model.* Cytotherapy. **13**(8): p. 944-55.
19. Sims, T.L., Jr., et al., *Neural progenitor cell-mediated delivery of interferon beta improves neuroblastoma response to cyclophosphamide.* Ann Surg Oncol, 2008. **15**(11): p. 3259-67.
20. Aboody, K.S., J. Najbauer, and M.K. Danks, *Stem and progenitor cell-mediated tumor selective gene therapy.* Gene Ther, 2008. **15**(10): p. 739-52.

21. Li, X., et al., *In vitro effect of adenovirus-mediated human Gamma Interferon gene transfer into human mesenchymal stem cells for chronic myelogenous leukemia.* Hematol Oncol, 2006. **24**(3): p. 151-8.
22. Duan, X., et al., *Murine bone marrow-derived mesenchymal stem cells as vehicles for interleukin-12 gene delivery into Ewing sarcoma tumors.* Cancer, 2009. **115**(1): p. 13-22.
23. Elzaouk, L., K. Moelling, and J. Pavlovic, *Anti-tumor activity of mesenchymal stem cells producing IL-12 in a mouse melanoma model.* Exp Dermatol, 2006. **15**(11): p. 865-74.
24. Gao, P., et al., *Therapeutic potential of human mesenchymal stem cells producing IL-12 in a mouse xenograft model of renal cell carcinoma.* Cancer Lett. **290**(2): p. 157-66.
25. Barti-Juhasz, H., et al., *Bone marrow derived mesenchymal stem/stromal cells transduced with full length human TRAIL repress the growth of rhabdomyosarcoma cells in vitro.* Haematologica. **96**(3): p. e21-2.
26. Choi, S.A., et al., *Therapeutic efficacy and safety of TRAIL-producing human adipose tissue-derived mesenchymal stem cells against experimental brainstem glioma.* Neuro Oncol. **13**(1): p. 61-9.
27. Kim, S.M., et al., *Gene therapy using TRAIL-secreting human umbilical cord blood-derived mesenchymal stem cells against intracranial glioma.* Cancer Res, 2008. **68**(23): p. 9614-23.
28. Kim, S.M., et al., *Effective combination therapy for malignant glioma with TRAIL-secreting mesenchymal stem cells and lipoxygenase inhibitor MK886.* Cancer Res. **72**(18): p. 4807-17.
29. Lee, H.J., et al., *A therapeutic strategy for metastatic malignant fibrous histiocytoma through mesenchymal stromal cell-mediated TRAIL production.* Ann Surg. **257**(5): p. 952-60.
30. Menon, L.G., et al., *Human bone marrow-derived mesenchymal stromal cells expressing S-TRAIL as a cellular delivery vehicle for human glioma therapy.* Stem Cells, 2009. **27**(9): p. 2320-30.
31. Moniri, M.R., et al., *TRAIL-engineered pancreas-derived mesenchymal stem cells: characterization and cytotoxic effects on pancreatic cancer cells.* Cancer Gene Ther. **19**(9): p. 652-8.
32. Nesterenko, I., et al., *Evaluating the effect of therapeutic stem cells on TRAIL resistant and sensitive medulloblastomas.* PLoS One. **7**(11): p. e49219.
33. Zhang, B., et al., *The inhibitory effect of MSCs expressing TRAIL as a cellular delivery vehicle in combination with cisplatin on hepatocellular carcinoma.* Cancer Biol Ther. **13**(12): p. 1175-84.
34. Xu, G., et al., *Adenoviral-mediated interleukin-18 expression in mesenchymal stem cells effectively suppresses the growth of glioma in rats.* Cell Biol Int, 2009. **33**(4): p. 466-74.
35. Xin, H., et al., *Targeted delivery of CX3CL1 to multiple lung tumors by mesenchymal stem cells.* Stem Cells, 2007. **25**(7): p. 1618-26.
36. Xin, H., et al., *Intratracheal delivery of CX3CL1-expressing mesenchymal stem cells to multiple lung tumors.* Mol Med, 2009. **15**(9-10): p. 321-7.
37. Azrak, R.G., et al., *Therapeutic synergy between irinotecan and 5-fluorouracil against human tumor xenografts.* Clin Cancer Res, 2004. **10**(3): p. 1121-9.
38. Friedlos, F., et al., *Mustard prodrugs for activation by Escherichia coli nitroreductase in gene-directed enzyme prodrug therapy.* J Med Chem, 1997. **40**(8): p. 1270-5.

39. Greco, O. and G.U. Dachs, *Gene directed enzyme/prodrug therapy of cancer: historical appraisal and future prospectives.* J Cell Physiol, 2001. **187**(1): p. 22-36.
40. Altaner, C. and V. Altanerova, *Stem cell based glioblastoma gene therapy.* Neoplasma. **59**(6): p. 756-60.
41. Matuskova, M., et al., *HSV-tk expressing mesenchymal stem cells exert bystander effect on human glioblastoma cells.* Cancer Lett. **290**(1): p. 58-67.
42. Ryu, C.H., et al., *Valproic acid enhances anti-tumor effect of mesenchymal stem cell mediated HSV-TK gene therapy in intracranial glioma.* Biochem Biophys Res Commun. **421**(3): p. 585-90.
43. Choi, S.A., et al., *Human adipose tissue-derived mesenchymal stem cells: characteristics and therapeutic potential as cellular vehicles for prodrug gene therapy against brainstem gliomas.* Eur J Cancer. **48**(1): p. 129-37.
44. Basel, M.T., et al., *A cell-delivered and cell-activated SN38-dextran prodrug increases survival in a murine disseminated pancreatic cancer model.* Small. **8**(6): p. 913-20.
45. Seo, G.M., et al., *A self-contained enzyme activating prodrug cytotherapy for preclinical melanoma.* Mol Biol Rep. **39**(1): p. 157-65.
46. Kim, S.W., et al., *Complete regression of metastatic renal cell carcinoma by multiple injections of engineered mesenchymal stem cells expressing dodecameric TRAIL and HSV-TK.* Clin Cancer Res. **19**(2): p. 415-27.
47. Rachakatla, R.S., et al., *Combination treatment of human umbilical cord matrix stem cell-based interferon-beta gene therapy and 5-fluorouracil significantly reduces growth of metastatic human breast cancer in SCID mouse lungs.* Cancer Invest, 2008. **26**(7): p. 662-70.
48. Scott, A.M., J.D. Wolchok, and L.J. Old, *Antibody therapy of cancer.* Nat Rev Cancer. **12**(4): p. 278-87.
49. Frank, R.T., et al., *Neural stem cells as a novel platform for tumor-specific delivery of therapeutic antibodies.* PLoS One, 2009. **4**(12): p. e8314.
50. Willmon, C., et al., *Cell carriers for oncolytic viruses: Fed Ex for cancer therapy.* Mol Ther, 2009. **17**(10): p. 1667-76.
51. Sonabend, A.M., et al., *Oncolytic adenoviral therapy for glioblastoma multiforme.* Neurosurg Focus, 2006. **20**(4): p. E19.
52. Ahmed, A.U., et al., *A comparative study of neural and mesenchymal stem cell-based carriers for oncolytic adenovirus in a model of malignant glioma.* Mol Pharm. **8**(5): p. 1559-72.
53. Schnarr, K., et al., *Gold nanoparticle-loaded neural stem cells for photothermal ablation of cancer.* Adv Healthc Mater. **2**(7): p. 976-82.
54. Matsui, M., et al., *Targeted delivery of oligomannose-coated liposome to the omental micrometastasis by peritoneal macrophages from patients with gastric cancer.* Cancer Sci. **101**(7): p. 1670-7.
55. Knoop, K., et al., *Image-guided, tumor stroma-targeted 131I therapy of hepatocellular cancer after systemic mesenchymal stem cell-mediated NIS gene delivery.* Mol Ther. **19**(9): p. 1704-13.
56. Shrestha, T.B., et al., *Stem cell-based photodynamic therapy.* Photochem Photobiol Sci. **11**(7): p. 1251-8.
57. Dranoff, G., S. Grupp, and C. June, *Adoptive Cellular Therapy*, in *Cancer Immunology and Immunotherapy*, Springer Berlin Heidelberg. p. 149-172.

58. van der Zee, J., *Heating the patient: a promising approach?* Ann Oncol, 2002. **13**(8): p. 1173-84.
59. Kumar, C.S.S.R. and F. Mohammad, *Magnetic nanomaterials for hyperthermia-based therapy and controlled drug delivery.* Advanced Drug Delivery Reviews. **63**(9): p. 789-808.
60. Giovanella, B.C. and B. Mondovi, *Selective heat sensitivity of cancer cells: Introduction.* Recent Results Cancer Res, 1977(59): p. 1-6.
61. Dewey, W.C., *Interaction of heat with radiation and chemotherapy.* Cancer Res, 1984. **44**(10 Suppl): p. 4714s-4720s.
62. Tschoep-Lechner, K.E., et al., *Gemcitabine and cisplatin combined with regional hyperthermia as second-line treatment in patients with gemcitabine-refractory advanced pancreatic cancer.* Int J Hyperthermia. **29**(1): p. 8-16.
63. Zhao, C., C. Dai, and X. Chen, *Whole-body hyperthermia combined with hyperthermic intraperitoneal chemotherapy for the treatment of stage IV advanced gastric cancer.* Int J Hyperthermia. **28**(8): p. 735-41.
64. Hurwitz, M.D., et al., *Hyperthermia combined with radiation for the treatment of locally advanced prostate cancer: long-term results from Dana-Farber Cancer Institute study 94-153.* Cancer. **117**(3): p. 510-6.
65. Hurwitz, M.D., et al., *Hyperthermia combined with radiation in treatment of locally advanced prostate cancer is associated with a favourable toxicity profile.* Int J Hyperthermia, 2005. **21**(7): p. 649-56.
66. Zhu, J., et al., *[Hyperthermia combined with chemotherapy in the treatment of advanced non-small cell lung cancer: an initial study]*. Zhongguo Fei Ai Za Zhi, 2005. **8**(4): p. 326-8.
67. Ben-Yosef, R., et al., *Hyperthermia combined with radiation therapy in the treatment of local recurrent breast cancer.* Isr Med Assoc J, 2004. **6**(7): p. 392-5.
68. Gofrit, O.N., et al., *Combined local bladder hyperthermia and intravesical chemotherapy for the treatment of high-grade superficial bladder cancer.* Urology, 2004. **63**(3): p. 466-71.
69. Wust, P., et al., *Hyperthermia in combined treatment of cancer.* Lancet Oncol, 2002. **3**(8): p. 487-97.
70. Hildebrandt, B., et al., *The cellular and molecular basis of hyperthermia.* Crit Rev Oncol Hematol, 2002. **43**(1): p. 33-56.
71. Orgill, D.P., S.A. Porter, and H.O. Taylor, *Heat injury to cells in perfused systems.* Ann N Y Acad Sci, 2005. **1066**: p. 106-18.
72. Song, C.W., et al., *Improvement of tumor oxygenation status by mild temperature hyperthermia alone or in combination with carbogen.* Semin Oncol, 1997. **24**(6): p. 626-32.
73. Subjeck, J.R., et al., *Heat shock proteins and biological response to hyperthermia.* Br J Cancer Suppl, 1982. **5**: p. 127-31.
74. Ito, A., et al., *Antitumor effects of combined therapy of recombinant heat shock protein 70 and hyperthermia using magnetic nanoparticles in an experimental subcutaneous murine melanoma.* Cancer Immunol Immunother, 2004. **53**(1): p. 26-32.
75. Li, Z., A. Menoret, and P. Srivastava, *Roles of heat-shock proteins in antigen presentation and cross-presentation.* Curr Opin Immunol, 2002. **14**(1): p. 45-51.

76. Srivastava, P., *Roles of heat-shock proteins in innate and adaptive immunity.* Nat Rev Immunol, 2002. **2**(3): p. 185-94.
77. Jordan, A., et al., *Presentation of a new magnetic field therapy system for the treatment of human solid tumors with magnetic fluid hyperthermia.* Journal of Magnetism and Magnetic Materials, 2001. **225**(1â€“2): p. 118-126.
78. Jordan, A., et al., *Inductive heating of ferrimagnetic particles and magnetic fluids: physical evaluation of their potential for hyperthermia. 1993.* Int J Hyperthermia, 2009. **25**(7): p. 499-511.
79. Kumar, C.S. and F. Mohammad, *Magnetic nanomaterials for hyperthermia-based therapy and controlled drug delivery.* Adv Drug Deliv Rev. **63**(9): p. 789-808.
80. Chatterjee, D.K., P. Diagaradjane, and S. Krishnan, *Nanoparticle-mediated hyperthermia in cancer therapy.* Ther Deliv. **2**(8): p. 1001-14.
81. Kottitz, R., P.C. Fannin, and L. Trahms, *Time domain study of Brownian and NÃ©el relaxation in ferrofluids.* Journal of Magnetism and Magnetic Materials, 1995. **149**(1â€“2): p. 42-46.
82. Pakhomov, A.B., Y. Bao, and K.M. Krishnan, *Effects of surfactant friction on Brownian magnetic relaxation in nanoparticle ferrofluids.* Journal of Applied Physics, 2005. **97**(10): p. 10Q305-3.
83. Mornet, S., et al., *Magnetic nanoparticle design for medical diagnosis and therapy.* Journal of Materials Chemistry, 2004. **14**(14): p. 2161-2175.
84. Huber, D.L., *Synthesis, properties, and applications of iron nanoparticles.* Small, 2005. **1**(5): p. 482-501.
85. Gordon, R.T., J.R. Hines, and D. Gordon, *Intracellular hyperthermia. A biophysical approach to cancer treatment via intracellular temperature and biophysical alterations.* Med Hypotheses, 1979. **5**(1): p. 83-102.
86. Xie, J., et al., *Iron oxide nanoparticle platform for biomedical applications.* Curr Med Chem, 2009. **16**(10): p. 1278-94.
87. Jordan, A., et al., *The effect of thermotherapy using magnetic nanoparticles on rat malignant glioma.* J Neurooncol, 2006. **78**(1): p. 7-14.
88. Jordan, A., et al., *Effects of magnetic fluid hyperthermia (MFH) on C3H mammary carcinoma in vivo.* Int J Hyperthermia, 1997. **13**(6): p. 587-605.
89. Huang, H.S. and J.F. Hainfield, *Intravenous magnetic nanoparticle cancer hyperthermia.* Int J Nanomedicine. **8**: p. 2521-32.
90. Balivada, S., et al., *A/C magnetic hyperthermia of melanoma mediated by iron(0)/iron oxide core/shell magnetic nanoparticles: a mouse study.* BMC Cancer. **10**: p. 119.
91. Shecterle, L.M. and J.A. St Cyr, *Whole body hyperthermia as a potential therapeutic option.* Cancer Biother, 1995. **10**(4): p. 253-6.
92. Habash, R.W., et al., *Thermal therapy, part 2: hyperthermia techniques.* Crit Rev Biomed Eng, 2006. **34**(6): p. 491-542.
93. Hildebrandt, B., et al., *Current status of radiant whole-body hyperthermia at temperatures >41.5 degrees C and practical guidelines for the treatment of adults. The German 'Interdisciplinary Working Group on Hyperthermia'.* Int J Hyperthermia, 2005. **21**(2): p. 169-83.
94. Jia, D. and J. Liu, *Current devices for high-performance whole-body hyperthermia therapy.* Expert Rev Med Devices. **7**(3): p. 407-23.

95. Sminia, P., et al., *Effect of hyperthermia on the central nervous system: a review.* Int J Hyperthermia, 1994. **10**(1): p. 1-30.
96. Vertree, R.A., et al., *Whole-body hyperthermia: a review of theory, design and application.* Perfusion, 2002. **17**(4): p. 279-90.
97. Kraybill, W.G., et al., *A phase I study of fever-range whole body hyperthermia (FR-WBH) in patients with advanced solid tumours: correlation with mouse models.* Int J Hyperthermia, 2002. **18**(3): p. 253-66.
98. Jia, D., et al., *Inhibition of B16 murine melanoma metastasis and enhancement of immunity by fever-range whole body hyperthermia.* Int J Hyperthermia. **27**(3): p. 275-85.
99. Ueno, S., P. Lovsund, and P.A. Oberg, *Effects of alternating magnetic fields and low-frequency electric currents on human skin blood flow.* Med Biol Eng Comput, 1986. **24**(1): p. 57-61.
100. *Do weak alternating magnetic fields have biological effects?* Public Health, 1982. **96**(4): p. 189-90.
101. Maier-Hauff, K., et al., *Intracranial Thermotherapy using Magnetic Nanoparticles Combined with External Beam Radiotherapy: Results of a Feasibility Study on Patients with Glioblastoma Multiforme.* Journal of Neuro-Oncology, 2007. **81**(1): p. 53-60.
102. Dilnawaz, F., et al., *Dual drug loaded superparamagnetic iron oxide nanoparticles for targeted cancer therapy.* Biomaterials. **31**(13): p. 3694-706.
103. Chen, Y., et al., *Nanoparticles modified with tumor-targeting scFv deliver siRNA and miRNA for cancer therapy.* Mol Ther. **18**(9): p. 1650-6.
104. Sugahara, K.N., et al., *Tissue-penetrating delivery of compounds and nanoparticles into tumors.* Cancer Cell, 2009. **16**(6): p. 510-20.
105. Sugahara, K.N., et al., *Coadministration of a tumor-penetrating peptide enhances the efficacy of cancer drugs.* Science. **328**(5981): p. 1031-5.
106. Gao, J., H. Gu, and B. Xu, *Multifunctional magnetic nanoparticles: design, synthesis, and biomedical applications.* Acc Chem Res, 2009. **42**(8): p. 1097-107.
107. Salloum, M., R. Ma, and L. Zhu, *An in-vivo experimental study of temperature elevations in animal tissue during magnetic nanoparticle hyperthermia.* Int J Hyperthermia, 2008. **24**(7): p. 589-601.
108. Salloum, M., et al., *Controlling nanoparticle delivery in magnetic nanoparticle hyperthermia for cancer treatment: experimental study in agarose gel.* Int J Hyperthermia, 2008. **24**(4): p. 337-45.
109. Shinkai, M. and A. Ito, *Functional magnetic particles for medical application.* Adv Biochem Eng Biotechnol, 2004. **91**: p. 191-220.
110. Arbab, A.S., et al., *Magnetic resonance imaging and confocal microscopy studies of magnetically labeled endothelial progenitor cells trafficking to sites of tumor angiogenesis.* Stem Cells, 2006. **24**(3): p. 671-8.
111. De Palma, M., et al., *Tumor-targeted interferon-alpha delivery by Tie2-expressing monocytes inhibits tumor growth and metastasis.* Cancer Cell, 2008. **14**(4): p. 299-311.
112. Ganta, C., et al., *Rat umbilical cord stem cells completely abolish rat mammary carcinomas with no evidence of metastasis or recurrence 100 days post-tumor cell inoculation.* Cancer Res, 2009. **69**(5): p. 1815-20.
113. Nakamizo, A., et al., *Human bone marrow-derived mesenchymal stem cells in the treatment of gliomas.* Cancer Res, 2005. **65**(8): p. 3307-18.

114. Rachakatla, R.S., et al., *Development of human umbilical cord matrix stem cell-based gene therapy for experimental lung tumors.* Cancer Gene Ther, 2007. **14**(10): p. 828-35.
115. Studeny, M., et al., *Bone marrow-derived mesenchymal stem cells as vehicles for interferon-beta delivery into tumors.* Cancer Res, 2002. **62**(13): p. 3603-8.
116. Wolf, D., et al., *Re: Mesenchymal stem cells: potential precursors for tumor stroma and targeted-delivery vehicles for anticancer agents.* J Natl Cancer Inst, 2005. **97**(7): p. 540-1; author reply 541-2.
117. Loebinger, M.R., et al., *Magnetic resonance imaging of mesenchymal stem cells homing to pulmonary metastases using biocompatible magnetic nanoparticles.* Cancer Res, 2009. **69**(23): p. 8862-7.
118. Kim, S.K., et al., *Human neural stem cells target experimental intracranial medulloblastoma and deliver a therapeutic gene leading to tumor regression.* Clin Cancer Res, 2006. **12**(18): p. 5550-6.
119. Ziu, M., et al., *Glioma-produced extracellular matrix influences brain tumor tropism of human neural stem cells.* J Neurooncol, 2006. **79**(2): p. 125-33.
120. Aboody, K.S., et al., *Targeting of melanoma brain metastases using engineered neural stem/progenitor cells.* Neuro Oncol, 2006. **8**(2): p. 119-26.
121. Ehtesham, M., et al., *The use of interleukin 12-secreting neural stem cells for the treatment of intracranial glioma.* Cancer Res, 2002. **62**(20): p. 5657-63.
122. Rachakatla, R.S., et al., *Attenuation of mouse melanoma by A/C magnetic field after delivery of bi-magnetic nanoparticles by neural progenitor cells.* ACS Nano. **4**(12): p. 7093-104.
123. Ourednik, J., et al., *Neural stem cells display an inherent mechanism for rescuing dysfunctional neurons.* Nat Biotechnol, 2002. **20**(11): p. 1103-10.
124. Riemer, J., et al., *Colorimetric ferrozine-based assay for the quantitation of iron in cultured cells.* Anal Biochem, 2004. **331**(2): p. 370-5.
125. Shevchenko, A., et al., *Mass spectrometric sequencing of proteins silver-stained polyacrylamide gels.* Anal Chem, 1996. **68**(5): p. 850-8.
126. Tang, S.J., et al., *Phosphoglycerate kinase 1-overexpressing lung cancer cells reduce cyclooxygenase 2 expression and promote anti-tumor immunity in vivo.* Int J Cancer, 2008. **123**(12): p. 2840-8.
127. Wang, J., et al., *Characterization of phosphoglycerate kinase-1 expression of stromal cells derived from tumor microenvironment in prostate cancer progression.* Cancer Res. **70**(2): p. 471-80.
128. Nakano, H., et al., *TRAF5, an activator of NF-kappaB and putative signal transducer for the lymphotoxin-beta receptor.* J Biol Chem, 1996. **271**(25): p. 14661-4.
129. Gibbs, P.E. and M.D. Maines, *Biliverdin inhibits activation of NF-kappaB: reversal of inhibition by human biliverdin reductase.* Int J Cancer, 2007. **121**(11): p. 2567-74.
130. Wu, K. and B. Bonavida, *The activated NF-kappaB-Snail-RKIP circuitry in cancer regulates both the metastatic cascade and resistance to apoptosis by cytotoxic drugs.* Critical reviews in immunology, 2009. **29**(3): p. 241-254.
131. Melle, C., et al., *Identification of specific protein markers in microdissected hepatocellular carcinoma.* J Proteome Res, 2007. **6**(1): p. 306-15.
132. Selga, E., V. Noe, and C.J. Ciudad, *Transcriptional regulation of aldo-keto reductase 1C1 in HT29 human colon cancer cells resistant to methotrexate: role in the cell cycle and apoptosis.* Biochem Pharmacol, 2008. **75**(2): p. 414-26.

133. Maines, M.D., et al., *THE OXIDOREDUCTASE, BILIVERDIN REDUCTASE, IS INDUCED IN HUMAN RENAL CARCINOMA - pH AND COFACTOR-SPECIFIC INCREASE IN ACTIVITY.* The Journal of Urology, 1999. **162**(4): p. 1467-1472.
134. Cho, J.A., et al., *Hyperthermia-treated mesenchymal stem cells exert antitumor effects on human carcinoma cell line.* Cancer, 2009. **115**(2): p. 311-23.
135. *Hyperthermia on mesenchymal stem cells (MSCs) can sensitize tumor cells to undergo cell deathâ€* International Journal of Hyperthermia, 2008. **24**(8): p. 638-648.
136. Multhoff, G., *Activation of natural killer cells by heat shock protein 70. 2002.* Int J Hyperthermia, 2009. **25**(3): p. 169-75.
137. Fierro, M.T., et al., *In vitro and in vivo susceptibility of human leukemic cells to lymphokine activated killer activity.* Leukemia, 1988. **2**(1): p. 50-4.
138. Kubes, J., et al., *Immunological response in the mouse melanoma model after local hyperthermia.* Physiol Res, 2008. **57**(3): p. 459-65.
139. Philip, P.A., et al., *Consensus report of the national cancer institute clinical trials planning meeting on pancreas cancer treatment.* J Clin Oncol, 2009. **27**(33): p. 5660-9.
140. Solinas, G., et al., *Tumor-associated macrophages (TAM) as major players of the cancer-related inflammation.* J Leukoc Biol, 2009. **86**(5): p. 1065-73.
141. Strik, H.M., et al., *Models of monocytic invasion into glioma cell aggregates.* Anticancer Res, 2006. **26**(2A): p. 865-71.
142. Baek, S.K., et al., *Photothermal treatment of glioma; an in vitro study of macrophage-mediated delivery of gold nanoshells.* J Neurooncol. **104**(2): p. 439-48.
143. Aderem, A. and D.M. Underhill, *Mechanisms of phagocytosis in macrophages.* Annu Rev Immunol, 1999. **17**: p. 593-623.
144. Raynal, I., et al., *Macrophage endocytosis of superparamagnetic iron oxide nanoparticles: mechanisms and comparison of ferumoxides and ferumoxtran-10.* Invest Radiol, 2004. **39**(1): p. 56-63.
145. Zhang, Y., N. Kohler, and M. Zhang, *Surface modification of superparamagnetic magnetite nanoparticles and their intracellular uptake.* Biomaterials, 2002. **23**(7): p. 1553-1561.
146. Doi, C., et al., *Cytotherapy with naive rat umbilical cord matrix stem cells significantly attenuates growth of murine pancreatic cancer cells and increases survival in syngeneic mice.* Cytotherapy. **12**(3): p. 408-17.
147. Basel, M.T., et al., *Cell-delivered magnetic nanoparticles caused hyperthermia-mediated increased survival in a murine pancreatic cancer model.* Int J Nanomedicine. **7**: p. 297-306.
148. Appenheimer, M.M., et al., *Impact of fever-range thermal stress on lymphocyte-endothelial adhesion and lymphocyte trafficking.* Immunol Invest, 2005. **34**(3): p. 295-323.
149. *How is the immune response affected by hyperthermia and heat shock proteins?* International Journal of Hyperthermia, 2005. **21**(8): p. 713-716.
150. Chen, T., et al., *Chemokine-containing exosomes are released from heat-stressed tumor cells via lipid raft-dependent pathway and act as efficient tumor vaccine.* J Immunol. **186**(4): p. 2219-28.
151. Fuggetta, M.P., et al., *In vitro effect of hyperthermia on natural cell-mediated cytotoxicity.* Anticancer Res, 2000. **20**(3A): p. 1667-72.

152. Ito, A., H. Honda, and T. Kobayashi, *Cancer immunotherapy based on intracellular hyperthermia using magnetite nanoparticles: a novel concept of â€œheat-controlled necrosisâ€□ with heat shock protein expression.* Cancer Immunology, Immunotherapy, 2006. **55**(3): p. 320-328.
153. Manjili, M.H., et al., *Cancer immunotherapy: stress proteins and hyperthermia.* Int J Hyperthermia, 2002. **18**(6): p. 506-20.
154. Milani, V. and E. Noessner, *Effects of thermal stress on tumor antigenicity and recognition by immune effector cells.* Cancer Immunol Immunother, 2006. **55**(3): p. 312-9.
155. Segal, B.H., et al., *Heat shock proteins as vaccine adjuvants in infections and cancer.* Drug Discovery Today, 2006. **11**(11â€“12): p. 534-540.
156. *Tumour infiltrating host cells and their significance for hyperthermia.* International Journal of Hyperthermia. **26**(3): p. 247-255.
157. *American cancer society prostate cancer key statistics*. 2013 [cited; Available from: http://www.cancer.org/cancer/prostatecancer/detailedguide/prostate-cancer-key-statistics.
158. Quinn, D.I., et al., *Docetaxel and atrasentan versus docetaxel and placebo for men with advanced castration-resistant prostate cancer (SWOG S0421): a randomised phase 3 trial.* Lancet Oncol. **14**(9): p. 893-900.
159. Scher, H.I., et al., *Increased survival with enzalutamide in prostate cancer after chemotherapy.* N Engl J Med. **367**(13): p. 1187-97.
160. Lim, W.A., *Designing customized cell signalling circuits.* Nat Rev Mol Cell Biol. **11**(6): p. 393-403.
161. Walters, J., et al., *A constitutively active and uninhibitable caspase-3 zymogen efficiently induces apoptosis.* Biochem J, 2009. **424**(3): p. 335-45.
162. Pop, C., et al., *Mutations in the procaspase-3 dimer interface affect the activity of the zymogen.* Biochemistry, 2003. **42**(42): p. 12311-20.
163. Bok, R.A., et al., *Patterns of protease production during prostate cancer progression: proteomic evidence for cascades in a transgenic model.* Prostate Cancer Prostatic Dis, 2003. **6**(4): p. 272-80.
164. Storr, S.J., et al., *The calpain system and cancer.* Nat Rev Cancer. **11**(5): p. 364-74.
165. Ke, S.H., et al., *Optimal subsite occupancy and design of a selective inhibitor of urokinase.* J Biol Chem, 1997. **272**(33): p. 20456-62.
166. Kelly, J.C., et al., *Profiling of calpain activity with a series of FRET-based substrates.* Biochim Biophys Acta, 2009. **1794**(10): p. 1505-9.
167. Yoshida, E., et al., *Enhancement of the expression of urokinase-type plasminogen activator from PC-3 human prostate cancer cells by thrombin.* Cancer Res, 1994. **54**(12): p. 3300-4.
168. Thomas, P. and T.G. Smart, *HEK293 cell line: a vehicle for the expression of recombinant proteins.* J Pharmacol Toxicol Methods, 2005. **51**(3): p. 187-200.
169. Chen, R., et al., *Mammalian glycophosphatidylinositol anchor transfer to proteins and posttransfer deacylation.* Proc Natl Acad Sci U S A, 1998. **95**(16): p. 9512-7.
170. Rothenberg, M.L., D.P. Carbone, and D.H. Johnson, *Improving the evaluation of new cancer treatments: challenges and opportunities.* Nat Rev Cancer, 2003. **3**(4): p. 303-9.
171. Richmond, A. and Y. Su, *Mouse xenograft models vs GEM models for human cancer therapeutics.* Dis Model Mech, 2008. **1**(2-3): p. 78-82.

172. Kelland, L.R., *Of mice and men: values and liabilities of the athymic nude mouse model in anticancer drug development.* Eur J Cancer, 2004. **40**(6): p. 827-36.
173. Sausville, E.A. and A.M. Burger, *Contributions of human tumor xenografts to anticancer drug development.* Cancer Res, 2006. **66**(7): p. 3351-4, discussion 3354.
174. Teicher, B.A., M. Liu, and D. Hicklin, *Human Tumor Xenograft Efficacy Models*, in *Tumor Models in Cancer Research*. 2011, Humana Press. p. 99-124.
175. Garber, K., *Realistic rodents? Debate grows over new mouse models of cancer.* J Natl Cancer Inst, 2006. **98**(17): p. 1176-8.
176. Sharpless, N.E. and R.A. Depinho, *The mighty mouse: genetically engineered mouse models in cancer drug development.* Nat Rev Drug Discov, 2006. **5**(9): p. 741-54.
177. Schook, L., et al., *Swine in biomedical research: creating the building blocks of animal models.* Anim Biotechnol, 2005. **16**(2): p. 183-90.
178. Swanson, K.S., et al., *Genomics and clinical medicine: rationale for creating and effectively evaluating animal models.* Exp Biol Med (Maywood), 2004. **229**(9): p. 866-75.
179. Duran-Struuck, R., et al., *Myelogenous leukemia in adult inbred MHC-defined miniature swine: a model for human myeloid leukemias.* Vet Immunol Immunopathol. **135**(3-4): p. 243-56.
180. Cho, P.S., et al., *Establishment of transplantable porcine tumor cell lines derived from MHC-inbred miniature swine.* Blood, 2007. **110**(12): p. 3996-4004.
181. Adam, S.J., et al., *Genetic induction of tumorigenesis in swine.* Oncogene, 2007. **26**(7): p. 1038-45.
182. Finnie, N.J., et al., *DNA-dependent protein kinase defects are linked to deficiencies in DNA repair and V(D)J recombination.* Philos Trans R Soc Lond B Biol Sci, 1996. **351**(1336): p. 173-9.
183. Notarangelo, L.D., *Primary immunodeficiencies.* J Allergy Clin Immunol. **125**(2 Suppl 2): p. S182-94.